No. 86 – December 1996

Report by the Director General

R. GIACCONI

In the first week of December, several important events will occur in Chile. It is planned that instruments of ratification and approval will be exchanged between the Government of Chile and ESO for the new Agreement which will then come into force. A foundation ceremony will take place on Cerro Paranal in the presence of high Chilean authorities, honoured guests and the ESO Council. A time capsule will be walled into the foundations of unit telescope 1. Finally, the Council will meet and decide on important budgetary matters regarding the ESO budget for the year to come.

Taking the last point first, ESO is making excellent progress in carrying out the VLT programme within the schedule and cost anticipated, which have not changed in the last several years. Thanks to the outstanding efforts of the VLT team, led by Professor Massimo Tarenghi, and all other elements of the ESO organisation, we are sufficiently advanced that we believe there remain no major technical issues to the successful completion of the project except for integration, commissioning and operation. The ESO Science and Technology Committee visited the Ansaldo factory in Milano during their 41st meeting on October 30 and 31, where they attended a demonstration of the VLT telescope structure smoothly pointing under software control. Since 1995 we have also improved on our cash flow situation, showing a positive balance as early as 2001 rather than 2003, as foreseen at the end of 1995.

However, the announcement in August 1996 by the German Government of their intention to decrease contributions to all scientific international organisations in 1997, 1998, 1999 and 2000 has created a substantial problem for ESO and changes the situation considerably. Since the other member states did not wish to alter the percentage of contributions because of a reduced German support, the decision was made by the ESO Council to reduce all contributions by the same proportional amount as requested by Germany. This results in a very substantial shortfall in contributions in the period 1997–2003, amounting to 7.4%.

In attempting to cope with this financial crisis we must take into account several factors:

The construction and commissioning of the VLT/VLTI is an activity which extends over several years. We have therefore adopted as our operating guideline a detailed technical, managerial, personnel and financial plan for our activities from 1996 to 2003. Within this plan, peak VLT capital expenditures occur in 1997 because of the advanced state of delivery of contracts and procurements already committed (85%). Any attempt to substantially shift VLT expenditures results in very severe damage to the project and increases its costs without substantially improving the total fiscal profile in the 1997–2000 period.

The ESO Executive has come to the conclusion that the only feasible alternative is a multi-year, multi-faceted plan to reduce ESO costs in this period.

Certain items which have small technical impact can be deferred to improve cash flow and interest payments. Small delays in the VLT/VLTI could be tolerated (3–6 months) to avoid overtime payments. Some reduction in activities could be foreseen at ESO Headquarters in Garching. However, it is clear that the bulk of the saving must occur in the area of personnel cost.

Here, the situation is also quite difficult since the ESO Council and Executive had already embarked in a containment of personnel costs over the last few years. Some small reduction on head counts could still be made but most of the savings can occur only by further reducing yearly increases below inflation growth levels.

A plan along these lines was discussed with the Committee of Council in Basel on October 22, and was proposed by the Executive to the Finance Committee which met on November 6 and 7 in Garching and approved it. The plan, if approved by Council, will result in an appropriate decrease of expenditures at ESO over the period 1997–2003. It retains the basic technical content of VLT/VLTI and La Silla operations. It requires substantial sacrifices and co-operation by the staff who will hopefully understand that at the moment, the only alternative to salary growth containment is a reduction in staff complement.

The Executive believes that further reductions could not be sustained without irreparable long-term damage to ESO and the VLT. Containment of personnel costs, in particular, can only be sustained till the point where salaries are no longer competitive and result in loss of experienced staff and demotivation of the remainder.

Returning now to a happier subject, the ratification and approval by the Chilean Government and by ESO of the Interpretative, Supplementary and Modifying Agreement to the Convention of 1963 has important consequences for the scientific communities in ESO Member States and Chile.

It gives ESO a certainty of stability for our future activities in Chile and the operations of the VLT observatory for many decades. At the same time, Chilean astronomers will have direct access to this new and powerful tool for astronomical observations by means of guaranteed observing time.

Now that the Agreement is coming into force, it is important that Chilean and European Scientific Communities at large are informed of some details of the Agreement regarding observing time:

To this purpose, some items of Article 11 of the Agreement, which are directly relevant to the subject, are reproduced in full below.

Article Eleven

1. The Chilean Scientist shall continue to have access to the instruments of observing of ESO on the basis of competitive projects, on equal conditions with the astronomers of the member countries of ESO. There are no limits to the percentage of time which can be acquired in this way.

2. In recognition of the role of Chile as the host country and to assist in the development of astronomy in Chile, ESO is prepared to make observing time available to scientifically meritorious Chilean proposals, independent of the competitive pressure, up to the fractions of observing time specified in this Article.

3. Consequently, Chilean scientists who present meritorious projects, shall have the right to obtain additional time up to 10% of observing time in each and every telescope installed or to be installed by ESO, without prejudice to the statements in paragraphs four and five of the present Article.

4. Chilean scientists who present meritorious projects shall have the right to obtain up to 10% of the observing time of the VLT/VLTI telescopes (defined in Article Two), it being understood that at least one half of this 10% shall be dedicated to projects of Chilean astronomers in co-operation with astronomers of ESO member countries. This percentage shall be acquired over a period of five years starting from the beginning of the functioning of the first telescope as agreed upon between the parties through an exchange of Notes. In case of an increase in the request for observing time by Chilean scientists for projects of special scientific merit, the Director General of ESO may assign additional observing time for these projects, within the fraction of observing time devoted to co-operative projects.

5. The percentage of time indicated for the telescopes presently functioning, 10%, shall be established on the basis of total time available to ESO and in accordance with the distribution by the Observing Programmes Committee of ESO (OPC). In the case of telescopes presently in operation, for which a Member State of ESO contributed financially, in total or in part, in addition to its ordinary contribution, the Organisation shall make its best efforts to ensure that a similar percentage to that mentioned in the second paragraph shall be granted.

6. Any proposal whose principal investigator is a Chilean scientist or is a foreign scientist affiliated to a Chilean institution included in a list to be approved by the Joint Committee mentioned in Article Nine, shall be considered as a Chilean proposal.*

*7. The proposals for observation submitted by Chilean scientists, which respond to the regular calls for competition, shall be qualified in accordance with ANNEX A** for all of the telescopes installed or to be installed.*

8. Those proposals from Chilean scientists which have obtained a classification higher than 3.0, within the percentage specified in this Article, shall be accepted. The Chilean scientists whose proposals are accepted shall be subject to the same rules and shall have the same facilities and obligations as the scientists of ESO member States.

9. It is understood that the limiting value specified as 3.0 is a part of the current scheme of evaluation. In case there are changes in the scale of evaluation, the corresponding limiting value on the new scale shall be equivalent to the one specified here, which shall be determined by the parties.

10. Meritorious projects shall be selected by the ESO Observing Programmes Committee (OPC) in which a Chilean scientist shall be incorporated as a full member. Similarly, a Chilean scientist shall be incorporated as a full member in the Scientific Technical Committee of ESO (STC) and a Chilean scientist as a full member in the Users' Committee (UC).

---

* This Joint Committee will consist of three representatives of the Chilean Government and three representatives of ESO.

** ANNEX A provides the evaluation system for the applications.

TELESCOPES AND INSTRUMENTATION

VLT Status Report

M. TARENGHI, ESO

The VLT Programme is now in an advanced stage. Nearly all major contracts for the Unit Telescopes have been concluded and the remaining contracts will be signed in the next few months. Some of the first parts for UT #1 have already been delivered and others are in or nearing their test periods prior to delivery to ESO. Activities in Europe and on Paranal are reaching the final stages, in particular for the first Unit Telescope (UT #1).

The first enclosure on Paranal is almost completed and the acceptance testing is planned for January 1997. The remaining enclosures are in an advanced erection phase, see Figure 1 (cover page) and Figure 2. In parallel, SKANSKA completed the final adjustment and casting of the embedded beams and rings within the specified tolerances, and in a very smooth operation the first rotating platform was installed in the coudé station of UT #1.

The erection of the main structure of UT #1 on Paranal has started (see Fig. 3). The azimuth tracks have already been aligned; the cable wrap, the oil pumping station and the oil recovery system have been installed. Even though some manufacturing problems by subcontractors have caused delays in the delivery of the base frame, AES is confident that they will be able to keep to the contractual delivery date.

Figure 1 was obtained mid-October 1996 and shows the four enclosures at different stages of integration. No. 1 is complete, no. 2 is in the final stages of the implementation of the aluminium cladding, no. 3 is ready for enclosure cladding and no. 4 is in the final stages of steel erection which was completed the following day with the positioning of the roof using the 350-ton crane situated next to the dome.

Back in Europe, all four primary mirror blanks have been delivered by SCHOTT and are of excellent quality. Two completed mirrors are being stored by REOSC and the third one is in the process of being polished according to schedule.

Installation and testing are the key activities in Europe. The integration of the main structure and the acceptance testing in Milan, planned for November 1996, are nearing completion (Figs. 4 and 5). ESO computers and control electronics have already been installed and are ready for the ESO tests in Milan.

Figure 2 shows details of enclosure no. 2 and in the background enclosure no. 1. Clearly visible are the openings foreseen to optimise the ventilation during the night to avoid any contribution from dome seeing.

The first M1 Cell – M3 Tower unit is now being integrated for the European acceptance testing, which is planned for early January 1997. The M2 Unit contract also achieved a major milestone. The first Beryllium blank was completed and nickel-plated. It has been accepted by the subcontractor and has been transported to Europe. The Electromechanical Unit is also in an advanced stage and is now being integrated for the acceptance and dynamic tests with a dummy mirror starting January 1997.

The first Nasmyth adapter/rotator was completed and delivered to ESO for extensive tests on hardware and software (see Fig. 6). The first M3 mirror cell is nearing completion and is planned to be delivered to ESO in November 1996.

Work is also progressing in all other areas, well in line with the VLT integration schedule, and ESO will enter the integration period of the UT #1 in the middle of next year.

An important highlight of the last months was the development in the VLTI Programme. The VLTI “New Plan” was submitted to STC and Council in

Figure 3 was taken inside enclosure no. 1 and shows the 2 azimuth tracks of the first telescope structure already in place and going for the final adjustment. The inner part shows the cable wrap in place and the beginning of the installation of the necessary connections. At the bottom of the hole the coudé rotating platform has already been installed.

Figure 5 shows a different view of the telescope structure of the first telescope, and clearly visible is the dummy simulating the mass and other characteristics of the mirror cell and associated mirror. This piece in steel and concrete was extensively used to test the procedure of mounting and dismounting the mirror cell.

Figure 4 was taken in Milan in October 1996 during the final integration of the telescope structure. The telescope is fully equipped with all subsystems and associated electronics.

Figure 6 shows the first of the 12 adapter/rotators in the Garching assembly hall during integration and testing. The Beryllium arm that will explore the focal plane has not yet been integrated. On the left-hand side, one can see the electronic test rack used to collect all parameters for final analysis and performance of the machine.

May and June 1996 and its implementation was decided in the form of an ESO-MPI-INSU agreement. The updated agreement has already been sent to INSU and MPG, and their signatures are expected in the next few weeks. The first stage of this plan will provide the coherent combination of two Unit Telescopes in the thermal infrared by the year 2000, and of two Auxiliary Telescopes in the near-infrared by the year 2002.

To conclude, excellent technical progress continues to be made, and cost and technical performance are satisfactory. Significant management effort is being continuously applied to maintain the schedule, in particular with regard to the subsystems which have remained on the critical path.

Massimo Tarenghi
e-mail: mtarengh@eso.org

The Secondary Mirror Units of the VLT: Design Overview and Manufacturing Status

S. STANGHELLINI, ESO

Introduction

The M2 Unit, with the secondary mirror and its mechanics, plays a central role in the on-line active control of the optical train of the VLT. The secondary mirror has a diameter of 1116 mm; it is slightly undersized as required for IR observation, and it defines the telescope pupil. The complete mechanical unit is located in the shadow of the secondary mirror, as seen from the telescope focus. The unit is also equipped with a deployable sky baffle.

As part of the active optics loop of the telescope, the M2 Unit will correct two optical aberrations: the defocus and the decentring coma. Both of these are linked to the deformation of the telescope tube and of the optical train under the effect of gravity and thermal espansion. In addition, it has fast steering mirror capability to correct tracking errors outside the bandwidth of the main telescope drives and to perform field chopping during infrared observations.

The design of the M2 Unit and the manufacturing of the aspherical secondary mirror represent a considerable technical challenge. This is, amongst others, linked to the dynamic performance requested from the secondary mirror and to the general requirements of the VLT programme.

After having performed feasibility and development studies, ESO issued in 1993 a call for tender for the procurement of the M2 Unit, with a light-weighted mirror of Beryllium or Silicon Carbide, materials both judged suitable for a mirror with the required performance. In September 1994, following difficulties with the procurement of the initially selected Silicon Carbide blank, ESO awarded a contract to the German company Dornier Satellitensysteme GmbH for the procurement of the four M2 Units and of the first secondary mirror in Beryllium. Dornier retains the overall system responsibility and subcontracted the mirror design and manufacture to REOSC Optique. In June 1996, ESO awarded a contract to REOSC Optique for the procurement of three additional Beryllium mirrors.

Major Mechanical Requirements and Design

The position of the secondary mirror must be controlled in five degrees of freedom. The mirror accuracy and stability requirements are linked to the optical design of the telescope and to the optical error budget. A stiff M2 Unit mechanical design and very limited cross talk between the kinematic functions are required. During tilt and chopping it must also be ensured that no reaction force is transmitted to the telescope spiders which, being optimised for low beam obstruction and wind cross-section, act as a flexible support. To avoid any excitation of the spiders, the tilt and chopping mechanism is equipped with a reaction force compensation device.

Of particular importance is also the reproducibility of the zero position of the mirror when the tilt and chopping mechanism is not in operation to ensure accurate blind pointing of the telescope.

The final design developed by Dornier is shown in Figure 1. The complete mechanical and electronic units are located inside a welded plate steel structure interfacing the spiders and creating a rigid, closed environment for the mechanisms and the electronics. In kinematic terms, the design includes a separate-stage architecture with focusing, centring and chopping stages in cascade.

Focusing Stage

Focusing is performed by moving M2 in steps along the telescope tube axis when a pre-defined focus error budget is exceeded, as detected by the image analyser. An accuracy of 1 µm is demanded. The focus drive of the M2 Unit acts on a focus trolley sliding on linear guides and moves together with

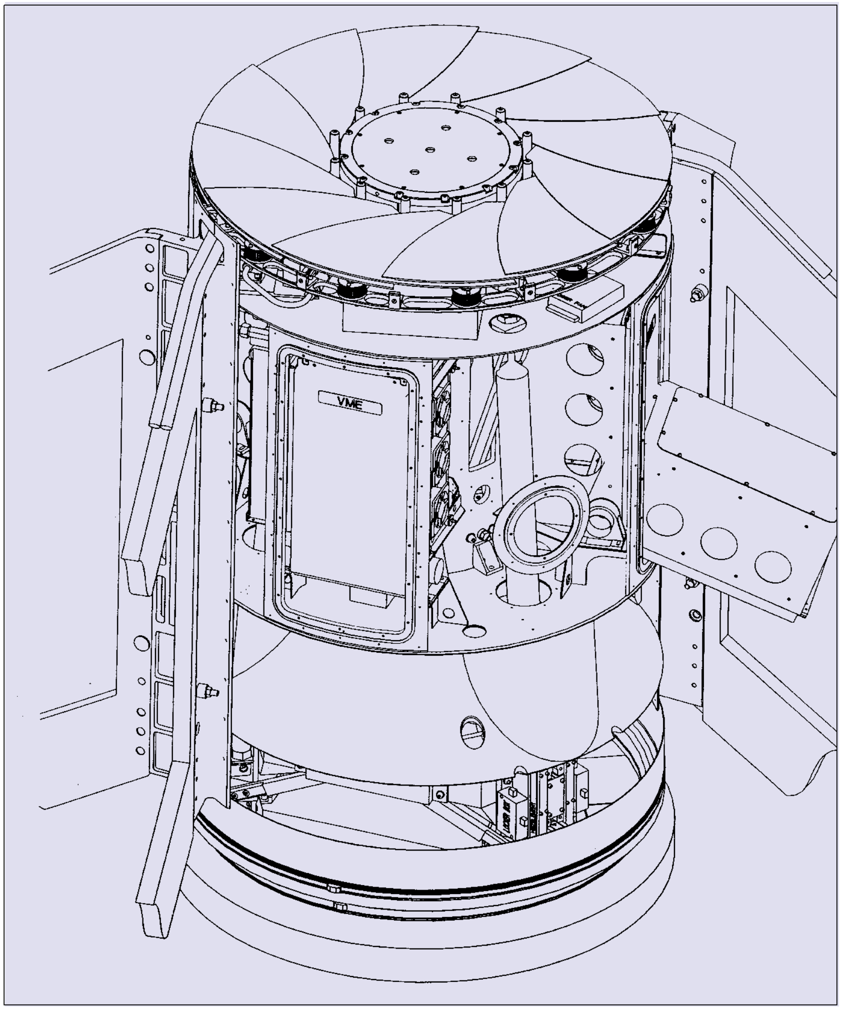

Figure1: M2 Unit design (without covers).

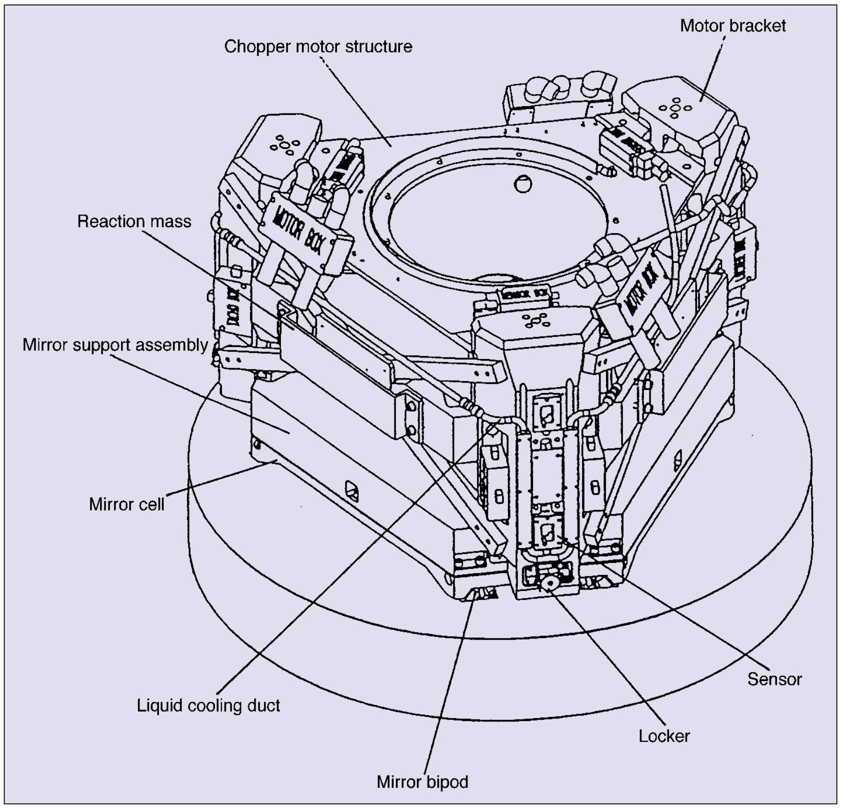

Figure 2: Chopper assembly.

the centring stage, the tilt and chopping stage, and the mirror. The linear bearings, optimised for stiffness, low friction and hysteresis, are carefully prestressed by means of cylindrical wedges. Strain gauges are permanently installed on the bearing races to monitor the prestress and to allow checks and maintenance during the operational life of the M2 Unit. The focusing drive can be removed on line and replaced as a single unit.

Centring Stage

Centring is performed by moving the M2 around its centre of curvature which is located 4.5 m behind the mirror vertex. Similarly to defocus, the decentring coma, which is an aberration caused by the misalignment of two optical systems, is generated by mechanical flexures. Centring errors will be corrected by moving M2 in steps (accuracy 0.3 arcsec) according to the error measured by the image analyser.

The mechanical design is based on two oppositely mounted eccentrics, one fixed to the focusing stage and the other fixed to the chopping assembly. The movement along the centre of curvature of the mirror is imposed by a pantograph realised with three centring bars equipped with flexures and oriented towards the centre of curvature of the mirror. To obtain the desired stroke, the two eccentrics are moved in opposite directions, while to obtain the desired direction of the centring motion, the two eccentrics are rotated in the same sense. Thus the entire chopper structure moves on the surface of an ideal sphere centred on the centre of curvature of the mirror.

Field stabilisation and Chopping

The tilt of the mirror is used for “field stabilisation”, which is the correction of the residual tracking error of the telescope in continuous mode by means of the M2. It is driven by the signal obtained from the autoguider or from the instrument. The system, required to operate up to 10 Hz, will allow correction of atmospheric image motion and of wind buffeting.

Chopping is kinematically identical to field stabilisation. A maximum chopping frequency of 5 Hz with a throw of 0.5 arcmin, and a duty cycle $\geq$ 80 % are specified. The chopping axis of the M2 rotates to take into account the field rotation due to the Alt-Az mount of the VLT.

The tilt and chopping stage is shown in Figure 2. It consists of a fixed structure, the mirror support assembly and the reaction mass. The mirror support assembly is equipped with three linear motors, which are able to develop 450 N peak force, mounted directly above the three supports of the secondary mirror. A similar arrangement is used for the reaction mass. The moving assemblies tilt around a mechanical pivot. During operation the reaction forces from the mirror assembly and from the reaction mass, driven in opposition of phase, are equal

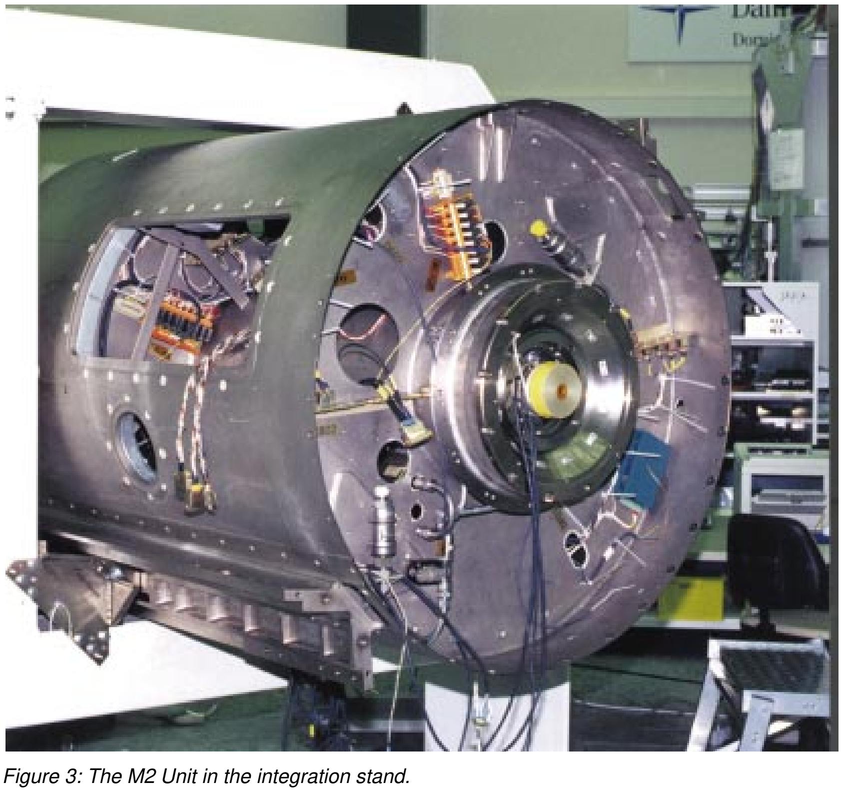

Figure 3: The M2 Unit in the integration stand.

in magnitude and opposite in direction so as to achieve a net zero force and moment on the structure. This requires the coincidence of the pivot with the centre of mass of the moving assembly, obtained by design first, and by adjustment later. The system uses optical incremental encoders with 8 nm resolution, mounted together with the tachometers in a small sensor assembly, optimised to eliminate resonant frequencies below 2000 Hz. A low value of the inertia of the moving masses was achieved through the use of Beryllium for the mirror, and Titanium for the mirror support assembly.

Control Electronics

The M2 Unit contains its own Local Control Unit (LCU) This demands careful use of the space inside the unit, but minimises the cables and the connectors to be routed along the telescope spiders. The LCU electronic cabinets can be accessed through openings in the mechanical housing.

The control system of the tilt and chopping stage uses two independent servo-loops, controlling two of the motors (masters), while the third one (slave) is commanded in such a way that the reaction force which is applied on the pivot is kept equal to zero. Each of the two servos consists of a speed loop within a position loop. The reaction mass is controlled in a similar way to eliminate dynamic reactions to the telescope spiders.

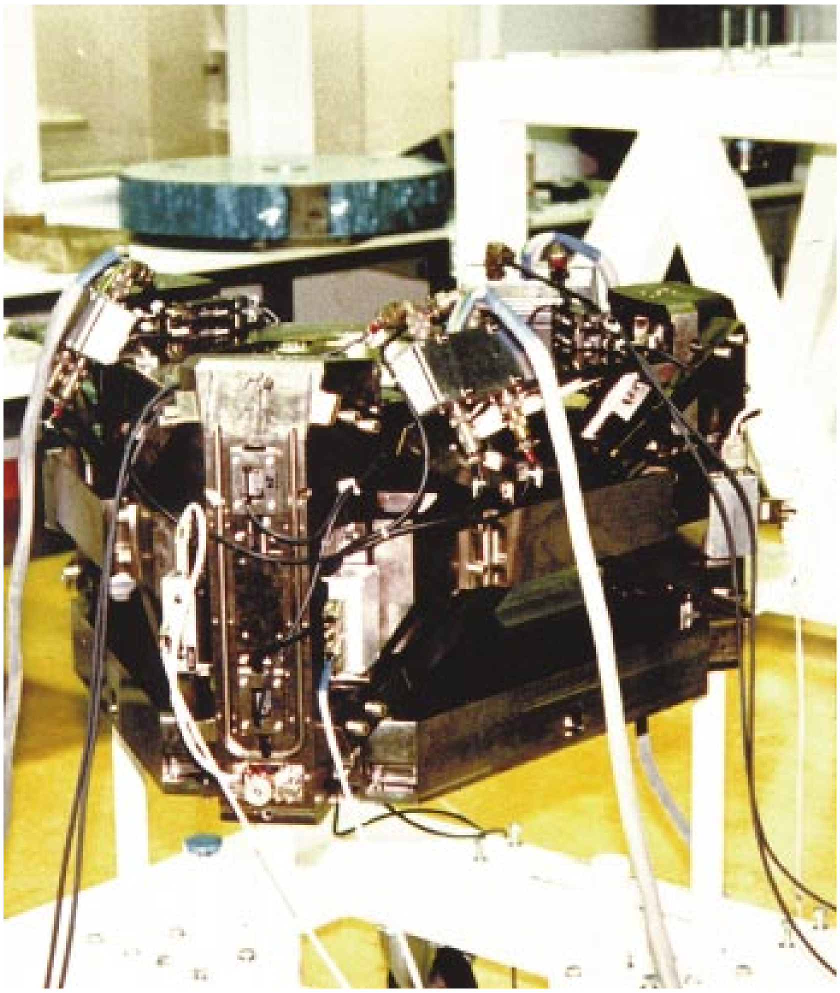

Figure 4: Tilt and Chopping stage during integration (dummy M2 in the background).

Thermal Control

The thermal control of the M2 Unit combines active and passive control methods:

• Active temperature control of the M2 Unit surface (housing and sky baffle) by means of electrical heaters and passive radiation/convection to the ambient air. The inner surface of the thermal skin is equipped with thermistor controlled heater mats and is coated externally with a low-emissivity foil.

• De-coupling of the interior temperature of the M2 Unit from the ambient air is achieved by means of insulation.

• Active temperature control of the electronic boxes is achieved by liquid coolant and, when necessary, by auxiliary heaters and fans. The fan arrangement is mounted on a vibration absorber and has been tested for vibrations.

• Liquid cooling of the chopping motors. The power dissipated is less than 12 W/motor.

• Minimised heat exchange between chopper and mirror by means of active temperature control of the parts opposite to the mirror back side. The mirror temperature and the mentioned parts will be maintained within ±3°K from the ambient temperature.

Secondary Mirror Characteristics and Manufacturing Process

The secondary mirror is a convex hyperbolic mirror of 1116 mm useful optical diameter, whose centre of curvature is located 4.5 m behind the vertex. The deviation between the best fitting sphere and the mirror surface is approximately 70 μm. The micro-roughness of the optical surface is $\leq$ 2 nm RMS.

The specification of the optical quality is based on the concept of Central Intensity Ratio which compares the performance of the telescope to an ideal diffraction-limited telescope in well-defined atmospheric conditions. The required optical quality makes use of the active correction capability of the VLT and calls for a CIR of 0.98 at λ = 500 nm.

The mechanical characteristics of the mirror are of no less importance than the optical ones. The mirror must be stiff and light to limit the actuators forces and power dissipation, to achieve a high closed-loop bandwidth and to minimise the stresses. In its final design the first eigenfrequency of the mirror assembly is around 400 Hz, while the final mass of the mirror is 42 kg.

To achieve these performances, the blank, exhibiting an open back flat structure, is made of light-weighted, Nickel-plated Beryllium. The optical figuring is done on the nickel layer. The support system uses three flexural bipods located at approximately two thirds of the radius and screwed onto the blank in reinforced areas. The mirror cell is made of Titanium.

The manufacturing technology can be considered to represent the state of the art for large Beryllium optics. The requirements set on the secondary mirror, especially in mechanical terms, led to select a structural grade Beryllium (I-220H), rather than an optical one. Starting from Beryllium powder obtained by impact grinding in order to overcome the anisotropy of Beryllium, a billet of 1.2 m diameter is produced by Hot Isostatic Pressing (HIP). The billet exhibits a density $\geq$ 99.7% of the nominal density. After radiographic inspection, the blank is light-weighted and the interfaces for the supports are generated by machining.

The procedure of grinding to the aspherical shape includes also a certain number of thermal annealing cycles for the removal of internal stresses and to

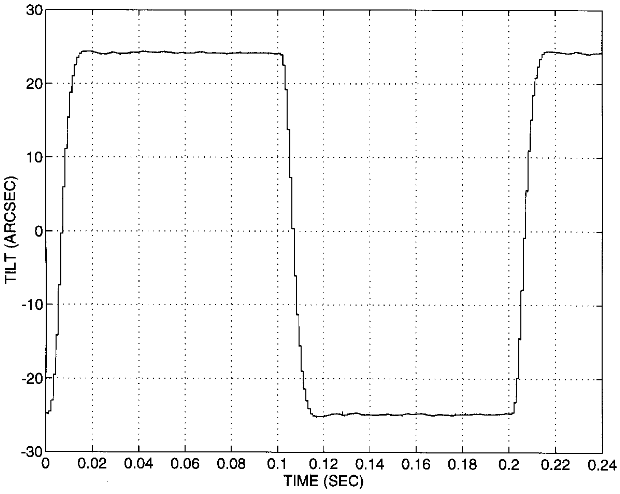

Chopping ± 25 arcsec @ 5 Hz
Jitter = 0.08″ RMS, Settling time < 20 msec

Figure 5: Chopping preliminary performance.

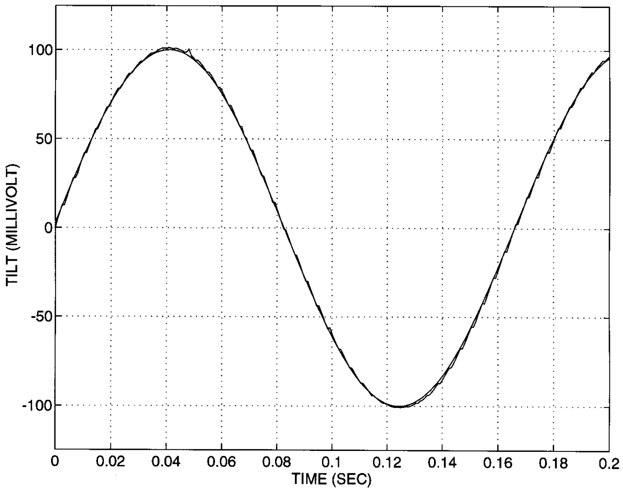

Field stabilisation @ 6 Hz (Tilt command superimposed on actual tilt)
Relative tracking error < 1.31 % (electronic noise of test set-up)

Figure 6: Field stabilisation preliminary performance.

stabilise the mirror. The blank is then electroless nickel plated. Due to the large surface of the structural pockets and ribs at the back of the blank, a thinner layer of nickel is put on the back face than on the front face to avoid unnecessary weight increase. The minimum thickness of Nickel on the front surface is dictated by the polishing process. The blank is slightly oversized to avoid edge effects during polishing. After polishing, the edge of the mirror is cut by electromachining. This generates also a sharp edge, necessary for reducing infrared emissivity.

In all manufacturing processes, great care has been used to avoid any figure change induced by the release of internal stresses or by the removal of material, thus guaranteeing the long-term stability of the blank. To this purpose, a large number of thermal cycles were foreseen at each manufacturing stage and also during polishing.

Status of Manufacturing and Integration

The Final Design Review (FDR) of the M2 unit was performed at Dornier premises in November 1995. At that time, in less than sixteen months from the start of the activity, a breadboard of the tilt and chopping stage had been designed, manufactured and assembled, and preliminary tests had been started. The tests, performed with a dummy secondary mirror, showed that the specified performance can be achieved. The compensation system of the chopping stage showed its ability to reduce the forces leaked to the spiders to below 5 N. A further reduction is expected by means of the final tuning with the real mirror. Since then the chopper has been refurbished and the system is approaching its final testing. Figures 5 and 6, elaborated at ESO by E. Manil, show the performance of the chopper already achieved during the preliminary tests.

The rest of the electromechanical unit is well advanced in the integration and testing phase. The mechanical structure is mounted in a dedicated stand which serves for integration and testing. The thermal skin, the heaters, the insulation and the liquid cooling loop are mounted. The focusing system was tested at unitary level and is assembled. The linear guides have been adjusted and their precision checked. The centring stage with the two eccentric drives has been singularly tested and is undergoing integration in the unit. The chopper is completing the unitary tests and it will be mounted soon on the M2 unit. The electronics is largely manufactured and the cabling has been assembled with the help of a full-scale model.

The acceptance of the first Beryllium blank by REOSC, although slightly delayed, is a remarkable milestone considering the difficulty and the criticality of most of the processes involved in the manufacturing of a blank of such size. The blank exhibits a very low internal stress, excellent micro-yield strength, is coated on both sides with low-stress Nickel closely matching the thermal expansion coefficient of the Beryllium. All these characteristics, extremely important for the polishability and for the long-term stability of the blank, were obtained through a carefully-controlled manufacturing process.

The shape of the blank differs from the final asphere by about 7 μm peak to valley. Although critical tasks still lie ahead before the figuring is completed, the present results are both exciting and technically promising. It is worth noting here that this is one of the largest Beryllium blanks ever produced.

After its completion and optical verification, the mirror will be shipped from REOSC to Dornier where it will be integrated in the M2 Unit for final testing, before being shipped to Chile.

Stefano Stanghellini
e-mail: sstanghe@eso.org

All VLT Primary Mirror Blanks Delivered

P. DIERICKX, ESO

The last of the four VLT primary mirror blanks was formally delivered by SCHOTT Glaswerke on September 30, thereby closing eight years of a very fruitful collaboration between SCHOTT and ESO.

On ESO's part, the preparation of the contract, signed in September 1988, is the work of D. Enard and R. Fischer. The SCHOTT contract was set on a fixed-price basis, whereby the production of the 8-m blanks has probably been the highest risk area for the entire VLT programme. The collaboration went on fairly smoothly – at least for ESO. The formidable difficulty of producing a usable 8-m Zerodur casting should however not be underestimated.

Zerodur is a glass ceramic with approximately 70% of crystalline phase (quartz mixed crystal) and 30% of residual glass phase. The crystalline phase has a negative coefficient of thermal expansion (CTE), while the coefficient of the glass phase is positive; the final properties are adjusted by means of a thermal cycle (ceramisation) with the aim to reach near-zero overall expansion coefficient. Typical values of the CTE for large Zerodur mirrors are lower than 0.05×10^{-6} °K^{-1} (-0.003×10^{-6} for the NTT blank, -0.017×10^{-6} to -0.043×10^{-6} for the VLT blanks), with homogeneities in the range of 0.02–0.01×10^{-6}.

The fabrication process starts with a casting at 1400 °C. After cooling down to room temperature, the result is a glassy substrate which is machined to the approximate size, then ceramised and thereafter machined to final shape.

To execute the contract, SCHOTT built a dedicated 50,000 m^2 facility, with a 70-ton melting tank, 3 annealing and ceramisation furnaces, a spinning table, a grinding machine. Essential handling and storage equipment included a handling tool with 18 suction cups, an impressive mirror turning device, a mirror "shelf" and a dedicated support system for quality control measurements.

The melting tank entered into operation in 1991 and all castings, including, but not limited to, the 4 VLT blanks, were produced between 1991 and 1993. During these two years, the melting tank was permanently kept at a temperature (with 20 to 60 tons of glass) in excess of 1400 °C. The countdown for casting started 3 to 4 weeks prior to the casting itself, a most spectacular process in every respect; the most visible part is the process itself (Dante would have loved it), but the most important one is the flawless training, co-ordination and operation of the casting team. There, in addition to the technological dimension, enters the human one.

The spin-casting process (Figs. 1 and 2) was successfully validated on a series of 1–4-m-class castings. The first attempts at producing the VLT mirror blanks were, however, unsuccessful: the mirror blanks broke during the annealing process, as a result of internal stresses

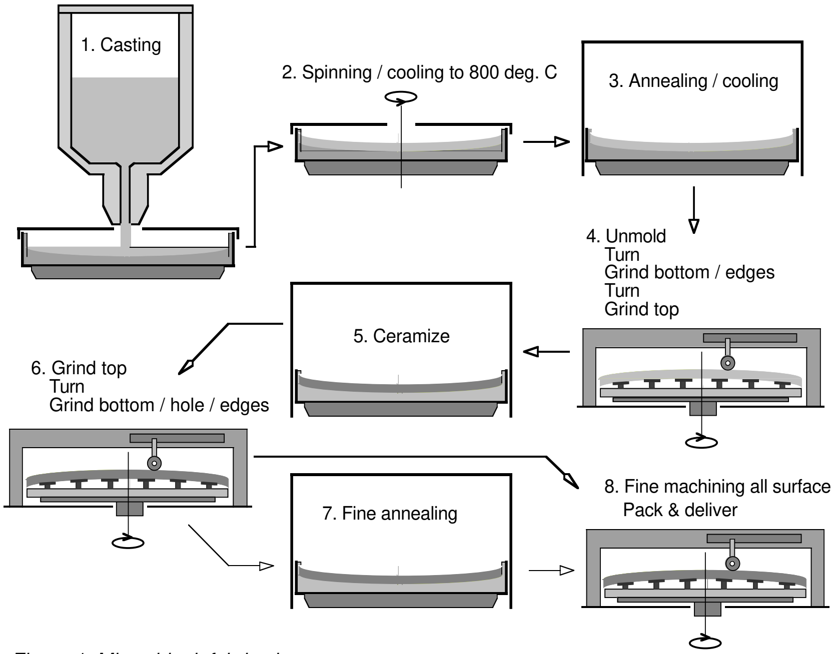

Figure 1: Mirror blank fabrication process.

Figure 2: 8-m blank being spun.

Figure 3: Turning the blank convex side up.

generated over the cooling cycle. The culprit: a sub-millimetre thin crystalline layer building up at the contact area between the bulk of the substrate and the mold. This layer, having a coefficient of thermal expansion different from the one of the glassy Zerodur, would eventually lead to breakage during cooling at temperatures in the range of 200 to 300 °C.

A major effort was made by the manufacturer in modelling and controlling the cooling cycle – a tremendous task since the properties of the material change with temperature. The blanks were actively supported, and particular attention was paid to the homogeneity of the temperature distribution during cooling. The challenge is to bring a melt of about 50 tons of glass from 950 °C to room temperature in a fully-controlled and homogeneous way.

Eventually, the molds were modified as well, and a particular separation agent (SCHOTT proprietary information) had to be used at the interface between the mold and the glass. The last produced blanks had crystalline layers of about 0.3 mm thickness, small enough in order not to generate inadmissible tensile stresses in the substrates.

Producing large mirror blanks requires more than controlling melting, casting and annealing processes. Substantial engineering effort had to be put in the areas of handling, machining and, of course, human safety. In spite of all precautions taken to limit internal stresses upon cooling down, residual stresses in the blank coming out of the annealing and cooling furnace are still dangerously high. In addition, inclusions which had fallen from the melting tank or risen from the mold into the substrate, together with possible damages such as surface cracks, require complex tooling and careful preparation of unmolding and handling. The blank is brought from the furnace onto a turning device, which turns the convex surface up (Fig. 3). The blank is brought onto the grinding machine and surface damages as well as critical inclusions are promptly machined out.

The enumeration of the difficulties could lead to the conclusion that, would the blanks indeed be feasible, the level of quality (residual stresses, homogeneity) at the very end of the process would not likely meet the highest standard. The credit for demonstrating that this assumption is wrong must be attributed to the team of SCHOTT Glaswerke.

Indeed, the homogeneity, inclusion content and dimensional accuracy fully meet the specifications – and in many

TABLE 1. Data for the four VLT primary mirror blanks.

Characteristic	Specified	Blank 1	Blank 2	Blank 3	Blank 4	
Geometrical dimensions						
Diameter	8200±2	8201.52	8201.74	8201.72	8201.74	mm
Dia. centre hole	1000±0.5	999.81	999.93	999.87	999.72	mm
Concentricity	±1	0.01	0.01	0.01	0.01	mm
Thickness	177+2–0	177.9	177.7	177.5	177.7	mm
Concave surface						
Curvature	28975	28975	28975	28975	28975	mm
Profile tolerance	2	0.12	0.08	0.08	0.06	mm
Convex surface						
Curvature	28977	28977	28977	28977	28977	mm
Profile tolerance	2	0.05	0.07	0.06	0.07	mm
Material properties						
Density	2.53	2.534	2.534	2.534	2.535	
CTE	$0 \pm 0.15\ 10^{-6}$	$-0.043\ 10^{-6}$	$-0.032\ 10^{-6}$	$-0.040\ 10^{-6}$	$-0.017\ 10^{-6}$	K^{-1}
Homogeneity	$<0.05\ 10^{-6}$	$0.009\ 10^{-6}$	$0.011\ 10^{-6}$	$0.024\ 10^{-6}$	$0.028\ 10^{-6}$	K^{-1}
Young's modulus	91000	90000	90000	90400	90300	Mpa
Poisson's ratio	0.24	0.243	0.243	0.243	0.24	
Internal quality						
Inclusions in critical volume						
Mean size	< 5	< 0.5	< 0.5	< 0.6	< 0.6	mm
Maximum size	< 8	2.3	3.5	1.1	1.6	mm
Average number	< 0.5	< 0.01	< 0.01	< 0.01	< 0.01	cm^{-3}
Maximum in 10 cm^3	≤ 8	< 4	< 4	< 4	≤ 4	
Stress birefringence caused by inclusions						
in critical volume	≤ 25	≤ 21	<12	0	0	nm
outside critical volume	≤ 50	≤ 30	<12	≤ 27	0	nm
Permanent stress at outer edge (compressive)						
Mean value	≥ –10	–6.2	–9.3	–6.5	–8.0	nm/cm
Maximum value	≥ –20	–7.0	–10.4	–8.3	–9.5	nm/cm

Figure 4: Preparation for the measurement of residual stresses (birefringense measurements).

areas exceed them by a substantial factor (Table 1). Residual stresses were found to be extremely low (Fig. 4). The contract was executed in time, within specifications and budget.

All four blanks are now at REOSC; two of them have been completely processed into finished mirror assemblies, tested and found to comply with the specifications (Fig. 5). They are now in storage prior to their departure to Chile. The third one is under polishing (currently about half a wave RMS wavefront error) and should be completed during the first quarter of 1997. The last one will remain in storage until early 1998, when REOSC will mount axial interfaces and start grinding.

In the light of the achievements realised so far, it is particularly interesting to review the documentation of the mid-80's, when the currently built telescopes (Keck, Gemini, Subaru, LBT, SST – renamed Hobby/Eberly) were in their conceptual design phase. At that time, possible diameters for monolithic mirrors rapidly narrowed to the 8-m range, with the argument that the extrapolation of the mirror technology to the 8-m range represented an ambitious but realistic step beyond the 4-m-class telescopes of the 60's–70's. Key issues were the technology for the blank production, but also the difficulty of handling very large mirrors. The developments undertaken and the results obtained by SCHOTT may lead to the impression that larger monolithic mirrors might be theoretically feasible, e.g. in the 10–12-m range. This may be true from a pure technological point of view, but the experience gathered so far indicates that there would most likely be a noticeable discontinuity in the cost-scaling law above a limit which looms around 8.4 m, essentially set by handling and above all transport constraints.

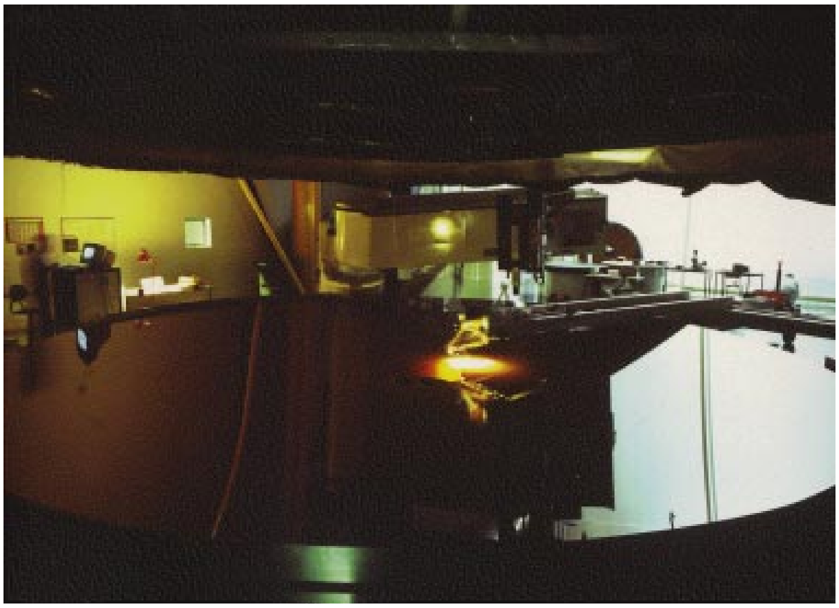

Figure 5: Primary Mirror undergoing acceptance tests at REOSC.

Philippe Dierickx
e-mail: pdierick@eso.org

ISAAC Takes Shape

J.-L. LIZON, Integration Group, Instrumentation Division, ESO, Garching

Description

ISAAC (Infrared Spectrometer and Array Camera) is one of the two VLT instruments being developed by ESO and is planned to be installed at one of the UT1 Nasmyth foci in 1998. Its scientific capabilities include both 1–5 μm imaging over a field of up to 2.5 × 2.5 arcmin and long-slit spectroscopy at nominal resolving powers of p 500 and p 5000. In order to optimise its performance over the full wavelength range, it contains two separate cameras optimised for the 1–2.5 μm and 2–5 μm regions which can be used to directly image either the telescope focal plane or the intermediate spectrum produced by a grating spectrometer. Further details of the instrument design and performance can be found under Very Large Telescope (VLT) Observatory on ESO's WWW Home Page.

ISAAC Integration and First Tests

Our main purpose here is to report on the status of the instrument integration and results of the first tests performed in Garching. As can be seen from the ac-

▲
Figure 1: One of the two ISAAC cameras comprising the array detector unit (not shown); the objective wheel and two filter wheels. In common with most moving functions, the wheels are driven by 5-phase stepper motors and spring loaded worm gears acting on the large toothed rings.

Figure 2: The partly assembled instrument showing the cryogenic optical assembly with one of the cameras mounted (only the detector unit visible at the top right) provisionally supported in the vacuum vessel.

companying photographs, the scientific requirements of achieving excellent image quality over a moderately large field at an 8-m telescope leads to a rather large instrument. This is a general feature of the major VLT instruments. What makes ISAAC a particular challenge, however, is that its complete optical and detector assemblies must operate at cryogenic temperatures and under vacuum. This poses a range of difficult design and integration problems. Although designed to be as compact as possible (e.g. by employing a novel spectrometer collimator consisting of 3 off-axis hyperbolic, diamond-turned mirrors) the vacuum tank housing the instrument is still p 1.5 m in diameter. The cryogenically cooled optical assembly is only slightly smaller and weighs p 300 kg. Although shrinking significantly on cool-down it must not distort the optical alignment and must be supported such that it meets stringent flexure requirements but with minimum thermal conductivity to the vacuum vessel. Its various motor-driven moving functions must also operate reliably and with high precision but without conventional lubrication and with a minimum of power dissipation. Despite its large size and weight, the cryogenic system has been designed to achieve cooling times which are comparable to many much smaller instruments currently in operation. Nevertheless, every modification required during the integration phase carries a large time penalty resulting from the need to close, evacuate, cool, warm-up and open the instrument.

The accompanying photographs illustrate several phases in the integration process. Figure 1. shows one of the two camera assemblies comprising the infrared array detector (up to 1024 × 1024 pixel format); objective wheel for changing the magnification and two filter/polariser wheels. The wheels are driven by 5-phase stepper motors and worm gears acting on the outer toothed rings. As with all ISAAC functions, the cameras have been assembled and performance tested as units in a separate, rotatable, cryogenic test chamber in order to minimise problems at the system integration level. Figure 2 shows the cast aluminium optical support structure mounted in the vacuum vessel and with some of the functions installed. At the top right, one of the detector units can be seen but the camera itself is buried inside the housing. The supporting system is provisional – the whole optical assembly is finally supported by two stainless steel spiders attached to the front and back which allow for the instrument shrinkage and are attached close to the centre of gravity to minimise flexure. Figure 3 shows the integration at a more advanced stage with the installation of additional functions including the large slit/mask wheel prominent at the front. Also visible are the two closed-cycle coolers at the top and bottom which maintain the instrument at p 80 K and the infrared detectors at temperatures down to p 30 K. Figure 4 is a rear view of the complete instrument enclosed in its vacuum vessel. The unit to the right is the permanently-mounted magnetic bearing, turbo-molecular pump used to evacuate the vessel. The two closed-cycle coolers are mounted on bellows and supported by the long bar to minimise vibrations. Figure 5 shows the instrument from the front during optical testing through its entrance window with a laser interferometer. In the background can be seen the instrument attachment flange mounted on the Nasmyth adapter simulator used for flexure and other tests. Partially visible on the right is the cryogenic test facility used to test the individual functions.

Some Early Results

So far the tests of ISAAC seem to confirm that its overall design is sound. After only a few thermal cycles, evacuation of the vessel already takes less than 15 hours and is expected to become progressively faster as the residual outgassing decreases. The cryogenic optical assembly cools to 80 K in only 26 hours using its integrated, continuous-flow liquid-nitrogen pre-cooling system and can be warmed up in less than 12 hours with the instrument-mounted heaters. Most importantly, the optics not only survives cooling but its optical quality remains essentially unchanged relative to room temperature. This is a great relief, despite our confidence in the design, considering that the spectrometer chain includes a large-lens collimator (16 cm diameter BaF2), the three-mirror collimator, grating mount, a 4-lens objective and several diamond-turned aluminium mirrors. The spectrometer collimator was of

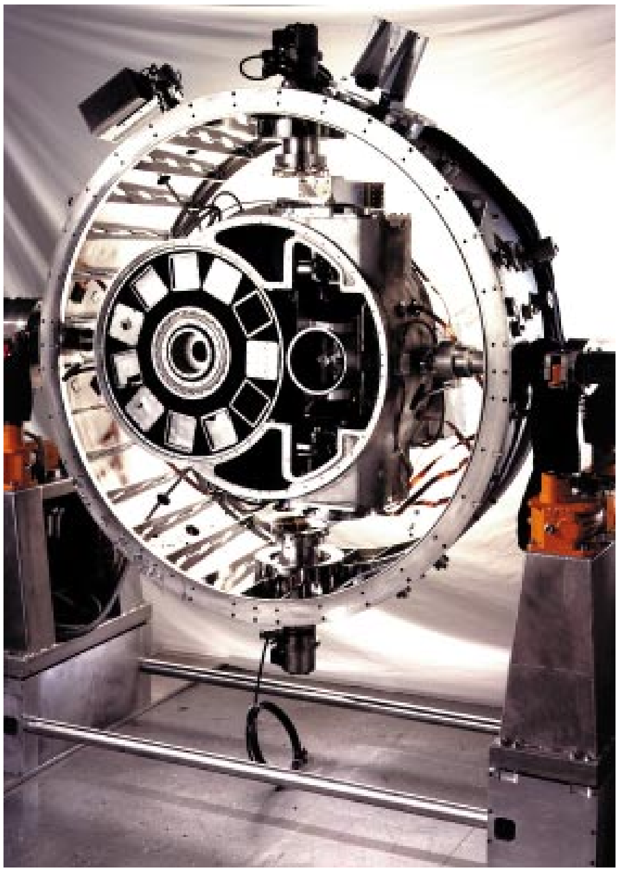

Figure 3: Almost completely assembled instrument with the large slit/ mask wheel clearly visible at the front.

▲ Figure 4: Rear view of ISAAC fully integrated in its vacuum vessel. The closed-cycle coolers at the top and bottom are mounted on bellows and connected by the long bar to minimise vibrations. Also visible to the right is the permanently mounted magnetic bearing turbomolecular pump used to evacuate the vessel.

particular concern because its 3 mirrors are attached to and hence sensitive to any thermal distortion of the large optical support structure. The supporting spiders also perform as designed to provide rigidity of the complete instrument at the few μm level when cold. All of the moving functions operate smoothly and the vibrations introduced by the closed-cycle coolers are at an acceptable level, not only for the instrument itself but also to meet the more demanding requirements imposed by the VLTI. Readers with experience in building cryogenic instruments would be surprised if there had been no problems at all. In fact, achieving some of the above has required considerable effort, and not all aspects are yet fully acceptable. In particular, maintaining a low enough operating temperature using the closed-cycle coolers alone has proved difficult. It is now clear that this was due both to reduced cooling power when operating two coolers over long gas lines from a single compressor and additional parasitic heat loads. Most of the additional heat load has now been traced to unplanned thermal contacts, which have been removed, and a higher than expected emissivity of the radiation shield which has been temporarily solved using superinsulation. In parallel, the first detector system and control software have been prepared and are almost ready to be installed for the first complete system test during the next few weeks.

Acknowledgements

Although only the integration aspects have been illustrated here, this development would not have been possible without the combined efforts of the ISAAC team which is headed by Alan Moorwood as PI and includes staff in the Instrumentation, VLT and Data Management Divisions. I am particularly grateful to Armin Silber and Ralf Büttinghaus for their help with the integration and to Ralf for actually manufacturing many of the mechanical pieces. Credit for the optical performance reported here is due largely to the efforts of Bernard Delabre and Anton van Dijsseldonk while Gotthard Huster was responsible for most of the mechanical design.

J.-L. Lizon
e-mail: jlizon@eso.org

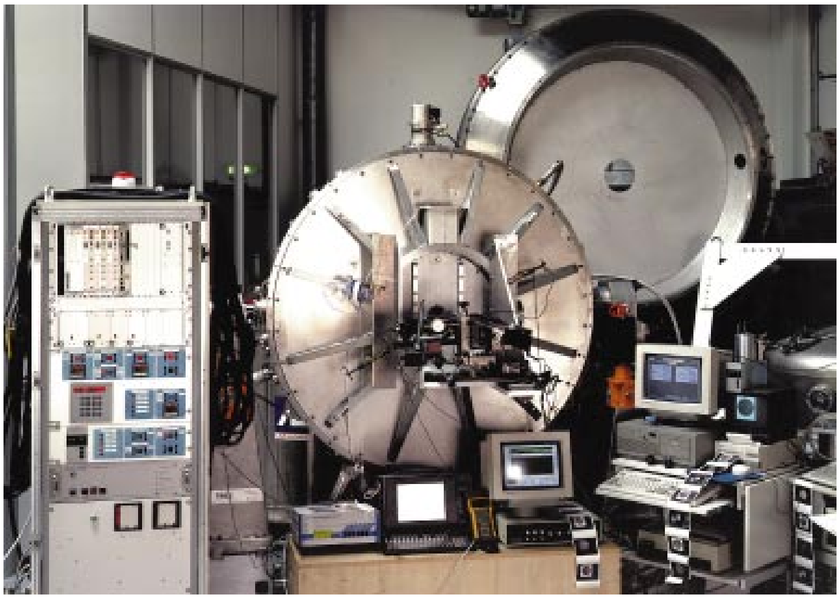

Figure 5: Front view of ISAAC during optical testing through the entrance window with a laser interferometer. In the background can be seen the ISAAC adapter flange mounted on the Nasmyth simulator used for flexure and other tests. Partly visible to the right is the cryogenic test facility used for testing the individual functions.

The ESO Infrared Detector High-Speed Array Control and Processing Electronics IRACE

M. MEYER, G. FINGER, H. MEHRGAN, J. STEGMEIER, A.F.M. MOORWOOD

Abstract

The ESO Infrared Detector High Speed Array Control and Processing Electronics, IRACE, is designed as a modular system which supports readout and data processing of arrays with four, and eventually more, output channels. In addition, the system can handle several separate arrays by routing the data to multiple processing chains. Detector front-end(s) are galvanically isolated from the data processing and system administration by fiberoptic links. The multiprocessor system(s) for on-line data handling are based on the IMS T9000 transputer, the most advanced European-produced processor. A key component of the whole system is a 1 Gigabit/s fiberoptic link. The link not only transmits data, but the architecture of the system allows distribution of data to the multiprocessor system(s) in a flexible and simple way. We present here the principles of the system operation, the achieved readout and on-line processing speeds and present first measurement results with a 1024 × 1024 pixel IR array.

Introduction

The electronic part of the data-acquisition system IRACE consists of the detector front-end and a data-acquisition computer or multiprocessor system for more demanding applications. The low-noise detector front-end and the data-acquisition computer are galvanically isolated, to avoid ground loops. An additional advantage of fiberoptics is the ability to transmit data over huge distances at high speed, e.g. between telescope and control room.

The ESO IR data-acquisition system IRACE is primarily built for the VLT instrument ISAAC, which will be equipped with a 4-output channel 256 × 256 or, if available, 32-output channel 1024 × 1024 pixel InSb array in its long-wavelength channel from 2.5 to 5 μm and a MCT 1024 × 1024 array for the short wavelength channel from 1 to 2.5 μm. The data transmission between detector front-end and data-acquisition computer system requires a high speed link, e.g. for double-correlated sampling in the L filter (3.8 μm) with a scale of 0.23″/pixel, we expect a flux of 1.84E06 photons/s/pixel (based on measurements with the ESO IRAC1 camera at the 2.2-m telescope). That gives a data rate of p 4E08 bits/s or 180 GByte/h for 16 bit ADC's

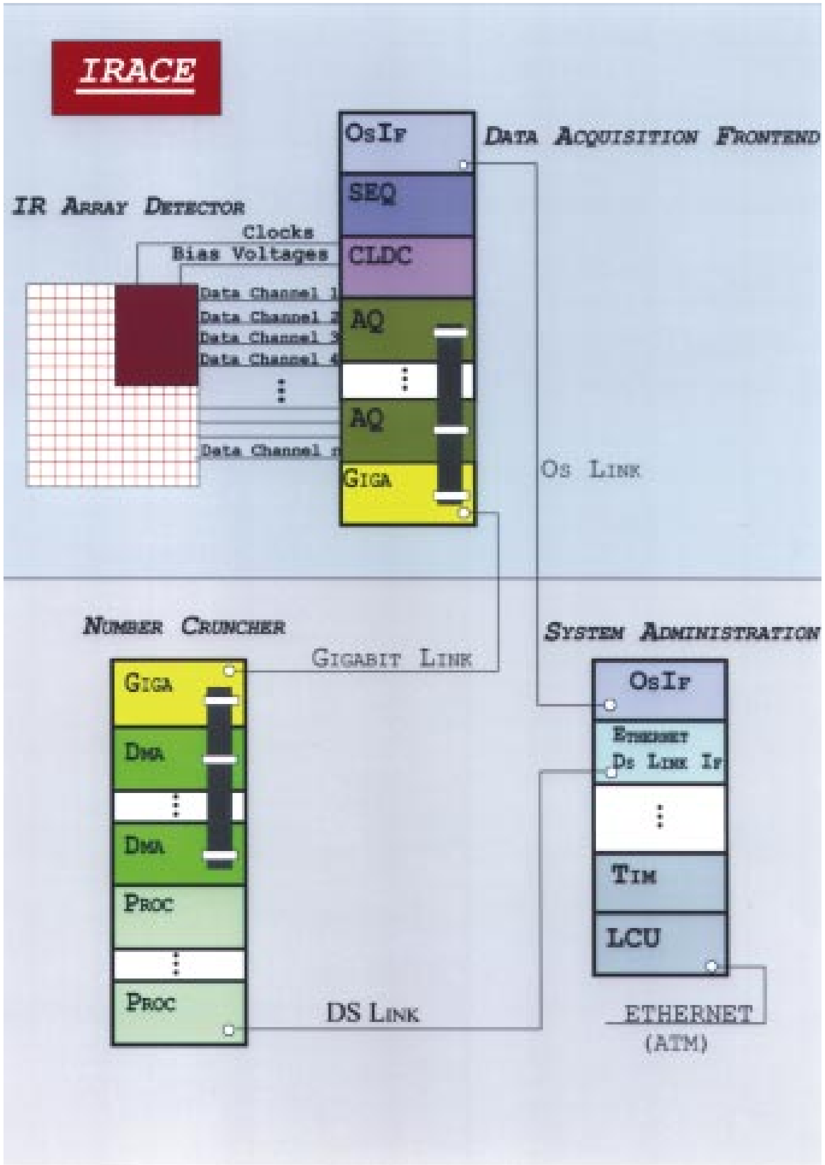

Figure 1: IRACE Block Diagram.

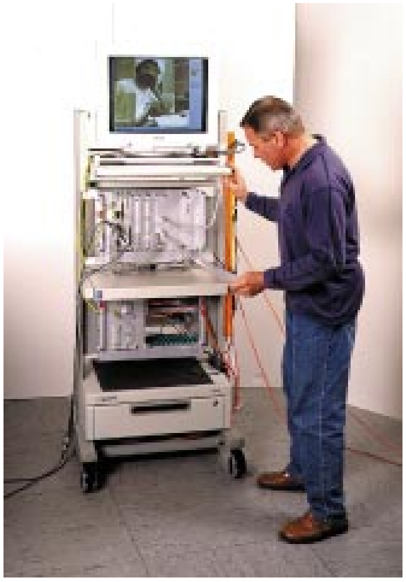

Figure 2: IRACE.

and an array with 32 parallel output channels. This shows that pre-processing of the incoming data is absolutely necessary. But even in the low background bands J, H and K multiple, non-destructive sampling and linear regression analysis gives the best results at short readout times per frame with correspondingly high frame and data rates. To process in real time the continuous stream of data, a multiprocessor system based on T9000 transputers and C104 packet switches was developed. The system is scaleable to the processing needs and the use of OCCAM as programming language, and the INMOS software tools are very convenient for multiprocessor system programming.

The IRACE System

Figure 1 shows a block diagram of IRACE and Figure 2 a photograph of the system, which consists of four main groups:

- The IR array detector with differential drivers on the detector data lines
- The Data Acquisition Front-end
- The Number Cruncher
- The System Administration

The IR array detector is located inside a vacuum vessel and the analogue signals are fed out over differential line drivers to the data terminal. Two additional terminals on the vessel supply the clock and bias voltages.

The data-acquisition front-end is a VME-size crate located on the vacuum vessel. It contains the clock pattern sequencer (SEQ), the clock and bias generator (CLDC), the acquisition modules (AQ), the fiberoptic link interface to the system administration (OsIf) and the fiberoptic high-speed data link (GIGA). The front-end is a T8 transputer system, programmed and set up by OsIf, a T8 protocol fiberoptic link. The sequencer is FIFO based and supports 48 bit wide words with a cycle time > 33 ns. The module with the level converters for the clocks and the bias generators (CLDC) provides 16 clocks and 16 biases. All voltage levels are set by software and can be inspected with a telemetry system at any time, even during detector readout. The differential analogue data lines are fed into a four-channel analogue to digital converter board (AQ) with preamplifiers and anti-aliasing filters. The digitised data leave AQ to a high speed bus (p 100 MByte/s) and enter the transmitter side of the Gigabit fiberoptic link (GIGA). The data leave the front-end over a high-speed fiberoptic link with 1Gbit/s. Front-end and array detector are galvanically completely floating, so it is possible to choose a ground point on the instrument without danger of creating ground loops.

The System Administration and the Number Cruncher reside in another VME crate. This crate may be installed

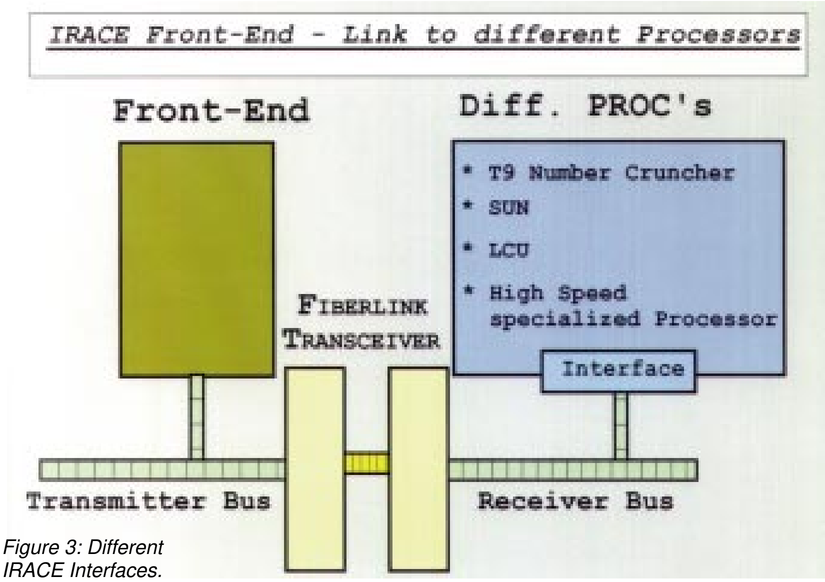

Figure 3: Different IRACE Interfaces.

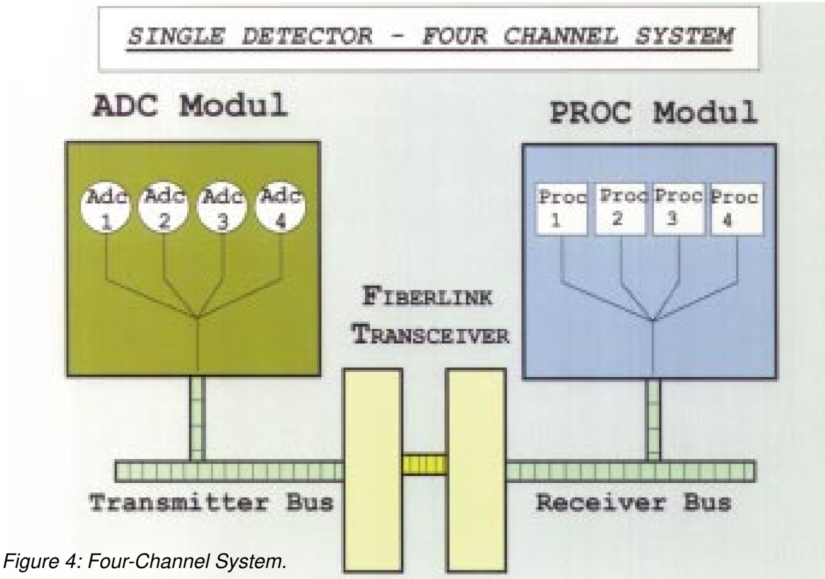

Figure 4: Four-Channel System.

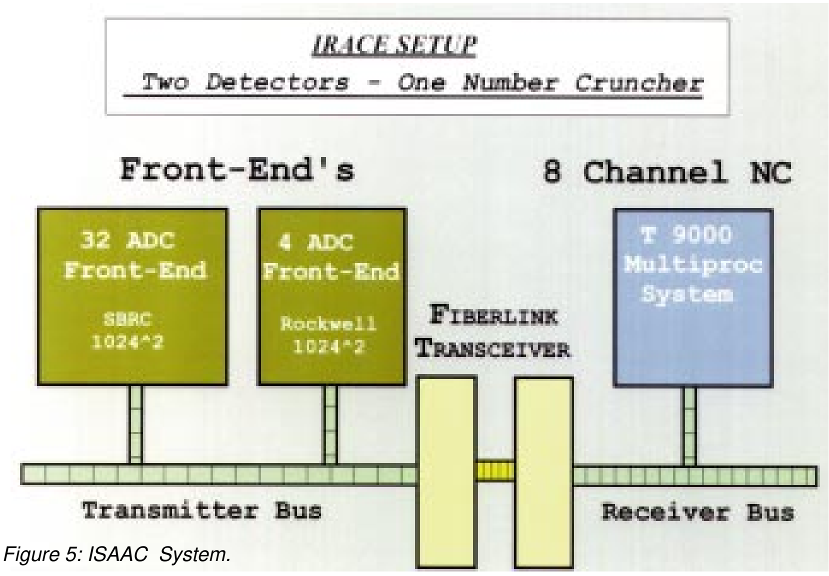

Figure 5: ISAAC System.

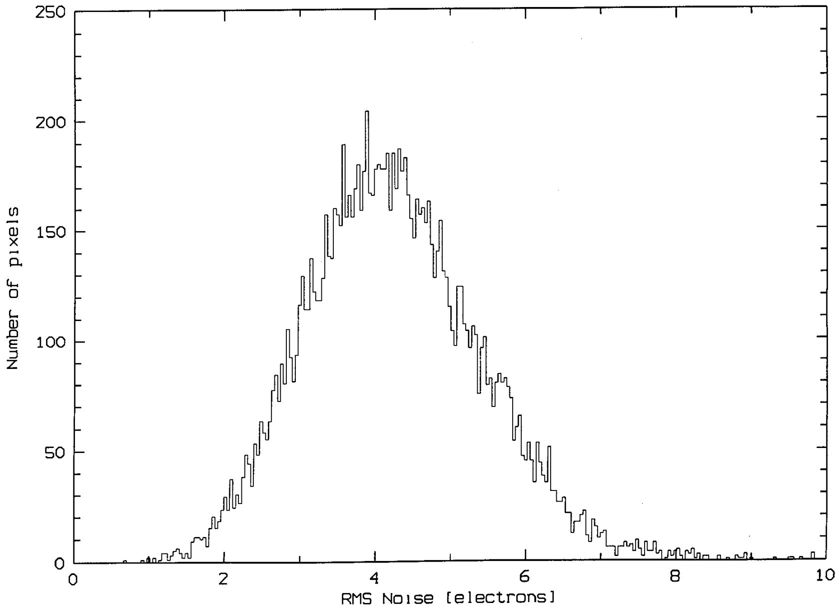

Figure 6: Noise Histogram of the HAWAII 1024 × 1024 MCT array.

in a remote location; the only physical connection to the front end is by the fiberoptic links. Link lengths up to 2 km are possible. The System Administration consists of the Ethernet (or possibly an ATM) interface to the host workstation, the local control unit (LCU), the time reference system (TIM), the T8 Os fiberoptic link to the front-end (OsIf), and an Ethernet DS link interface to the number cruncher. All downloading, commands and housekeeping operations are done over this system.

The number cruncher system gets the data from the receiver of the Gigabit fiberoptic transceiver (GIGA). The fiberoptic link receiver puts the data onto a high-speed bus with identical protocol and function as the bus on the front-end side. Dma controllers (DMA) on this bus transport and interface the incoming data to the multiprocessor system (PROC). While data are being processed in real time, intermediate and averaged images are sent to the LCU and to the host workstation. It is possible to have an optional connection on the number cruncher to an array of SCSI disks for raw data taking and a fast on line display.

Functionally there are two blocks, the detector control block and the data-acquisition chain. The detector control block consists of sequencer and clock/bias driver which are responsible for the set-up of the detector itself. The acquisition chain starts at the ADC's of AQ and includes the high-speed fiberoptic link and the number cruncher. The only direct link between the two blocks is the conversion signal produced by the sequencer. The two blocks can be seen as independent systems which simplifies testing and maintenance because both blocks can run independently.

A completely new method was developed for the data-acquisition chain to fulfil the high-speed requirements of the new IR arrays with multiple outputs (up to 32 at present) and the corresponding high data rates. This system is centred around a 1 Gigabit/s fiberoptic link. The fiberoptic link can be interfaced to different platforms. For applications where number crunching is not required, the gigabit link can be directly interfaced to the LCU or any processor system (Fig. 3). The multiprocessor system built for ISAAC is based on T9000 transputers and C104 packet routing switches. The number cruncher is a modular design and can be tailored to the needs of the application and the required speed of readout and data processing.

The gigabit link connects the ADC's to the number cruncher system. The link not only transmits data but also distributes the data directly to the input processors of the number cruncher system. In Figure 4, the data of a 4-channel detector (like the Rockwell HAWAII 1024 × 1024 in ISAAC) are routed to a four-channel number cruncher front-end. Each quadrant is routed to one input processor. For detectors with multiple output channels (like the SBRC ALADDIN 32-channel 1024 × 1024 InSb array) more computing power is required. In this case the ADC module consists of 32 ADC's. On the processor side, an 8-input channel front-end has to be implemented with each input processor this is processing 4 detector channels.

Two detectors are installed in ISAAC; a 4-channel Rockwell 1024 × 1024 for the wavelength range from 1 to 2.5 μm and a SBRC 1024 × 1024 for the 2.5 to 5 μm region. Only one arm of the instrument is active for a given observation. IRACE is able to process the two different detectors with only one number cruncher, because the system can be dynamically configured to the active detector system (Fig. 5).

Supported Data Processing Modes and Achieved Readout Speeds

The following readout modes have been implemented:

- Uncorrelated sampling
- Double-correlated sampling
- Triple-correlated sampling
- Multiple non-destructive readout with linear fitting of the integration ramp
- On-chip tip tilt correction with destructive readout
- On-chip tip tilt correction with non-destructive readout

TABLE 1. Readout speed of IRACE.

READ MODE	READ + PROCESSING TIME per PIXEL and CHANNEL TIME (ns)	READOUT TIME 4 Channel IRACE 4 Channel HAWAII TIME (ms)	READOUT TIME 8 Channel IRACE 32 Channel ALADDIN TIME (ms)
RAW	300	80 + Reset	40 + Reset
RAW + SUM	300	80 + Reset	40 + Reset
DOUBLE	600	160 + Reset	80 + Reset
DOUBLE + SUM	600	160 + Reset	80 + Reset
NON-DESTRUCTIVE	750	200 + Reset	100 + Reset

Reset = 2 ms
Non-Destructive Readout includes time for linear fit of consecutive reads.

• Raw data taking with high storage of individual readouts to local SCSI disk array

Processing Time for Different Read Modes per Pixel and Channel

In Table 1, the read and processing time of IRACE is shown. Column 1 describes the read mode, column 2 shows the read and processing times for a single pixel in one channel, Column 3 the possible time for readout of a 4-channel detector like the Rockwell 1024 × 1024 HAWAII array and Column 4 shows the time for readout with an 8-channel IRACE system as used with the SBRC ALADDIN 1024 × 1024 InSb array. The fastest readout speed per pixel which is possible with the HAWAII detector was measured to be 3 µs/pixel corresponding to an array readout time of 800 ms. IRACE is a factor of four faster than the analogue bandwidth of this array. In the case of the ALADDIN 1024^2 array with 32 parallel outputs and 3µs/pixel, an 8-channel system just matches the speed requirements of 100 ms for the most demanding processing task of multiple non-destructive readout.

For a window of 256 × 256 pixels applying multiple non-destructive readouts and a least-square fit of the integration ramp, the obtained noise histogram is shown in Figure 6. The noise histogram peaks at 4 electrons rms. The conversion of ADU's to electrons was calibrated by the usual shot noise method. To compare this noise figure with the common definition of readout noise per single readout as defined for double correlated sampling, it has to be divided by the square root of 2 and corresponds to an rms noise of 2.8 electrons. This is the best noise figure ever reported for IR arrays

We could also demonstrate the IRACE system performance to detect a very faint thermal target. Figure 7 shows the K prime image of a thermal bar pattern at ambient temperature taken with a good quadrant of the HAWAII engineering grade array. The temperature difference of the bars is 4.0 10^{-2} K. A cryogenic neutral-density filter was used to attenuate this pattern by a factor of 10^{-2} to simulate the low background in the spectroscopic mode of ISAAC. The image is a raw difference with the target shifted in position. The bar pattern at the bottom edge of the image is at the detection limit. The contrast of the pattern corresponds to a signal of 6 electrons per pixel integrated in a two-minute exposure. The detected photon-generated current is 5 10^{-2} electrons/sec which well demonstrates the performance of IRACE.

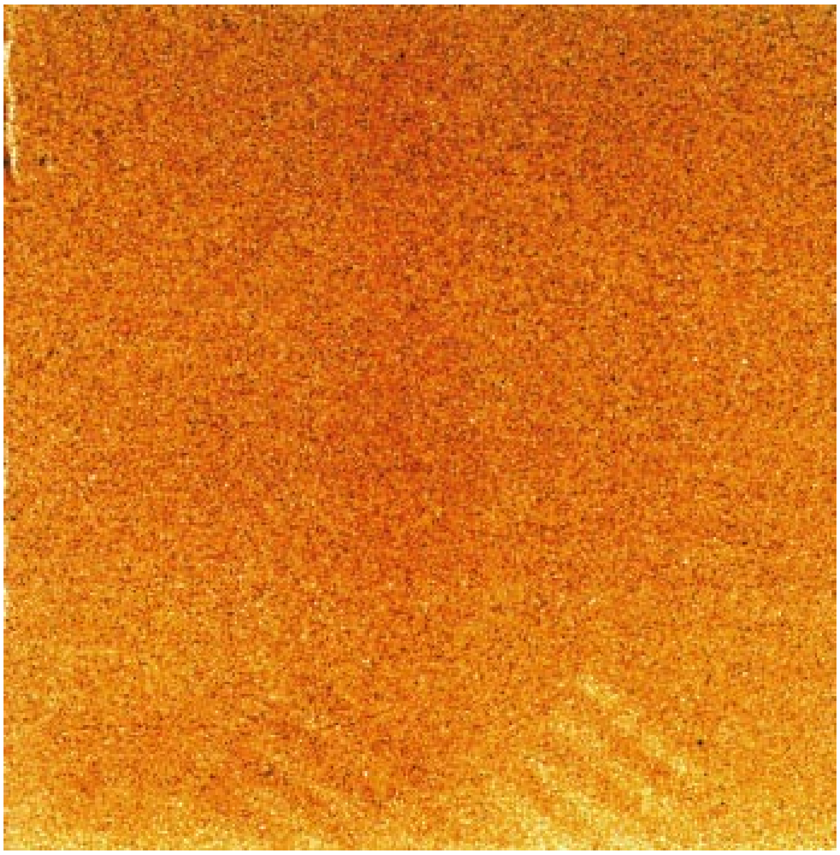

Figure 7: Faint thermal target at bottom edge of the image taken with one quadrant of the HAWAII 1024 × 1024 MCT array. The contrast of the thermal target corresponds to a signal of 6 electrons during an integration time of 2 minutes.

Conclusions

The ESO Infrared Detector High Speed Array Control and Processing Electronics IRACE is a flexible and modular system for high-speed and low-noise data acquisition. With its huge and scaleable computing power, it fulfils the requirements for future detector developments. A big advantage is the use of T9000 transputers with their inherent communication capabilities and large memory sizes. The system is completely programmable in the high-level language OCCAM, which simplifies parallel processing. First test results with a 1024 × 1024 IR array detector have yielded a read noise of 4 e^- and detection of a signal corresponding to only 6 e^- during an integration time of 2 minutes. We conclude that the astronomical performance of ISAAC will be limited by detector and/or background noise and not by the IRACE acquisition system.

Acknowledgements

The IRACE team gratefully acknowledges the excellent support of H. Kasten, G. Fischer, G. Nicolini and E. Pomaroli, who contributed substantially to the success of this completely in-house-produced system.

Manfred Meyer
e-mail: mmeyer@eso.org

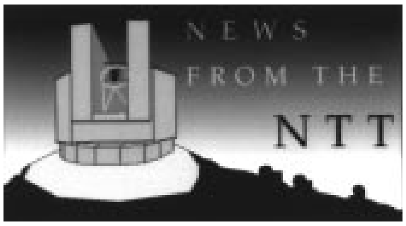

The NTT upgrade project has the following goals:

1. *Establish a robust operating procedure for the telescope to minimise down time and maximise the scientific output.*
2. *Test the VLT control system in real operations prior to installation on UT1.*
3. *Test the VLT operations scheme and the data flow from proposal preparation to final product.*

J. SPYROMILIO, ESO

Last time I wrote for *The Messenger* the NTT news, we had just completed basic functionality tests for all critical systems and were looking forward to the integration phase of the NTT upgrade. At that time, the primary mirror was still in the 3.6-m aluminising plant and the telescope immobilised. I am glad to inform you that we are still proceeding exactly on schedule and I see no problems in returning the NTT to the community as promised on July 1st 1997. In the two months that have passed since the last update was written, a lot of progress has been made.

The telescope, although still not fully integrated (there remains work to be finished on the rotators), has pointed to 1.5 arcsecond (RMS) accuracy. This was the result of a single iteration of the new VLT pointing modelling software, and we expect to do better after the NTT re-alignment process and the telescope servos are tuned. As expected, since the pointing model is integral to the NTT tracking software, the tracking also seems to be very good. However, we have not, at the time of writing, attacked the "NTT font" error found in the VLT-TCS test in December 1996 (see Figure 3 in Wallander et al., *The Messenger*, 83, 7, 1996).

The detailed state of the system is as follows. The telescope altitude and azimuth axes point and track, but the servos still need tuning. The telescope start-up is not as yet reliable and occasionally we get telescope oscillations. This problem, although as yet not fully understood, is being tackled as this article is being written. I expect that when the axes servos are tuned, this intermittent problem will not recur. The rotators are in a comparable state with some effort remaining in tuning the servo parameters. The primary, secondary and tertiary mirror control is working well with minor improvements pending. The new VLT-TCCD guide probe cameras are now functioning and are being used for autoguiding and image analysis tests. The VLT autoguiding software was tested for the first time this week (30 October) and is now working in an engineering mode. That is to say, commands are sent to the control tasks via a terminal without any of the graphical user interfaces or automatic guide-star selection mechanisms which are envisaged. These are expected to be tested in the next few weeks. Image analysis is still in a rudimentary state but no show-stoppers can be seen. The ACE CCD controllers have arrived on La Silla and are being tested. SUSI integration is expected to start within the next couple of weeks. EMMI follows shortly thereafter.

It is worth noting an amusing incident which occurred during the telescope integration. It demonstrates just how close the NTT and VLT control systems are.

Accidentally, we compiled and linked the workstation part of the system without the NTT flag set. Since the telescope pointing and tracking is handled directly at the VME level, no problems were found, with stars appearing as expected in the centre of the field. However, when we looked at the sidereal time on the workstation it was 2 minutes 48 seconds off. This is the difference in sidereal time between Paranal and La Silla. The tracking and pointing is handled at the VME level and the site parameters were correctly set there, as that part of the code had not been recompiled. We were in fact running the workstations in the NTT as if the telescope were on Paranal! The only difference between NTT and VLT, at the workstation level, is the longitude and latitude of the telescope being controlled.

The Immediate Future

In the first week of November the tertiary mirror will be removed for aluminisation. This will complete the re-coating of all telescope mirrors. While the tertiary is out, the mechanical and optical axes of the telescope will be tested for alignment. In this process, not only do we hope to improve the telescope alignment, but also to test the VLT alignment procedure and tools. Here again is an indication of the complete immersion of the NTT project in the VLT world. Most of the month of November will be spent aligning the telescope and fixing problems we found while testing the basic functionality of the system.

As mentioned above, the new ACE CCD controllers will be installed in SUSI and EMMI in early November. The refurbished camera of the red arm, a new RILD mirror and an improved grism wheel will be installed in EMMI. SUSI got a new M4 last May but, as for EMMI, she will be sporting new software and in fact also new electronics for moving the two motors.

In December, we plan to begin the re-commissioning of the telescope and instruments. At the same time the first data-flow modules are expected to be delivered by the Data Management Division. Beta testing of the phase II proposal preparation will take place in November and we expect that the first observing blocks will be built at that time. In December, these observing blocks will be delivered to the mountain as part of the commissioning of the telescope and will be passed to the control system for execution. This functionality is based on the usage of the VLT sequencer tool. The VLT control is designed to be an integrated system. All functions, whether in the instrument, detector or the telescope may be driven directly from the sequencer. The sequencer language is tcl, a very common scripting language used at many observatories already. The ability to co-ordinate and automate all tasks taking place within the dome is critical to the planned operations scheme. In this context, the sequencer is already being used extensively for maintenance monitoring of functions within the NTT.

In January, the NTT will receive the data flow hardware. An on-line archive workstation will arrive with 22 Gb of disk space. This will allow us to have immediate access to data taken during the last 4 or so days of operation. The data taken from the instrument workstation will be directly sent to this place for safe storage. From there they are forwarded to the pipeline workstation. Both these machines will live in the NTT control room. The data will be delivered to the astronomer on CD-ROMs, which will be prepared at a further workstation located at the computer centre in the administration building.

The commissioning of the VLT data-flow system will also start in January. This system has been extensively discussed in previous issues of *The Messenger* and forms the essence of the operations scheme of the VLT. In February/March, we plan to start with some first scientific exposures. These will be executed in service mode and are strictly shared risk.

The Not So Immediate Future

Exciting developments are also foreseen for the second half 1997 for the NTT. We are currently planning to upgrade the EMMI red arm CCD controller. The new FIERA controller, a prototype of which underwent functionality tests in Garching in November and came through with flying colours, is planned to arrive at the

NTT in the third quarter of 1997 (for specifications see Beletic, *The Messenger*, 83, 4, 1996). FIERA will deliver an order-of-magnitude improvement over ACE in readout speed and depending on the detectors used, possibly a further improvement over the already low noise figures. In the last quarter of 1997, the NTT will get two new instruments. SOFI (Son OF ISAAC), a derivative of the first instrument to be installed on UT1 of the VLT, is an infrared camera/spectrograph delivering both narrow- and wide-field imaging and intermediate-resolution spectroscopy. At the same time, SUSI II, or as she is affectionately known within the NTT team, SUSANA (SUperb Seeing At Nasmyth A), equipped with a 4k CCD mosaic and FIERA, will also be installed replacing SUSI.

The NTT will thus remain truly the New Technology Telescope it was always envisaged to be, with cutting-edge instrumentation and capabilities. Stay tuned for exciting results. All of these developments are in the spirit of using the NTT as a test bed for the VLT. SOFI uses many common functions with ISAAC, and SUSANA is a derivative of the VLT test camera to be used in the commissioning and science verification phases of Paranal.

Staff Movements

The NTT team bids farewell to Roland Gredel who is taking over the duties of 3.6-m+CAT team leader. Many thanks Roland and good luck with your new responsibilities.

Jason Spyromilio
e-mail: jspyromi@eso.org

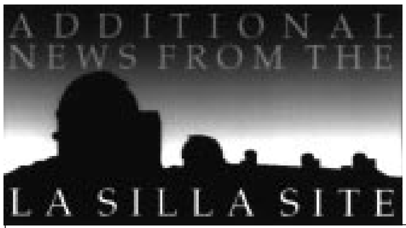

The La Silla News Page

The editors of the La Silla News Page would like to welcome readers of the sixth edition of a page devoted to reporting on technical updates and observational achievements at La Silla. We would like this page to inform the astronomical community of changes made to telescopes, instruments, operations, and of instrumental performances that cannot be reported conveniently elsewhere. Contributions and inquiries to this page from the community are most welcome (P. Bouchet, R. Gredel, C. Lidman).

A New CCD for EFOSC2 at the ESO-MPI 2.2-m

T. AUGUSTEIJN

A new CCD (#40) has recently been installed in EFOSC2 at the ESO-MPI 2.2-m telescope. This thinned CCD has a very high quantum efficiency in the blue and UV through "UV flooding" of the backside. The new CCD for EFOSC2 is a 2048 × 2048 array of 15-micron pixels, which corresponds to 0.262 arcsec on the sky. The field of view with the new CCD is currently limited to a circular area with a 7.7 arcmin diameter. This limitation is caused by the diagonal mirror in the DISCO adapter used to divert light to the guide probe.

The efficiency of the new system was measured by observing several photometric and spectrophotometric standard stars on several nights. In Figure 1 we show the relative increase in efficiency with respect to the old CCD(#19) by plotting the ratio of the observed count rate as a function of wavelength of the new CCD with respect to that of the old. In this figure the triangles connected by a dashed line correspond to measurements made with grism #1. The horizontal lines correspond to measurements made with broad-band filters. The circles are placed at the effective wavelength of each filter and the tick marks give the FWHM of each filter. From this one can see that the new CCD gives a seven-fold increase in sensitivity in the blue, a two-fold increase in the visual, and a three-fold increase in the red with respect to the old CCD!

Also shown in the figure, as squares connected by a dotted line, is the ratio of the quantum efficiencies of the two CCDs (measured in Garching before shipment to Chile). From the figure, it can be seen that the measurements made with the grism and the broad-band filters are reasonably consistent, but that there is a significant discrepancy in the blue with respect to the increase in efficiency expected on the basis of the quantum efficiencies measured originally. This difference probably reflects a decrease in the efficiency of the old CCD with respect to the original measurements and might explain the observed de-

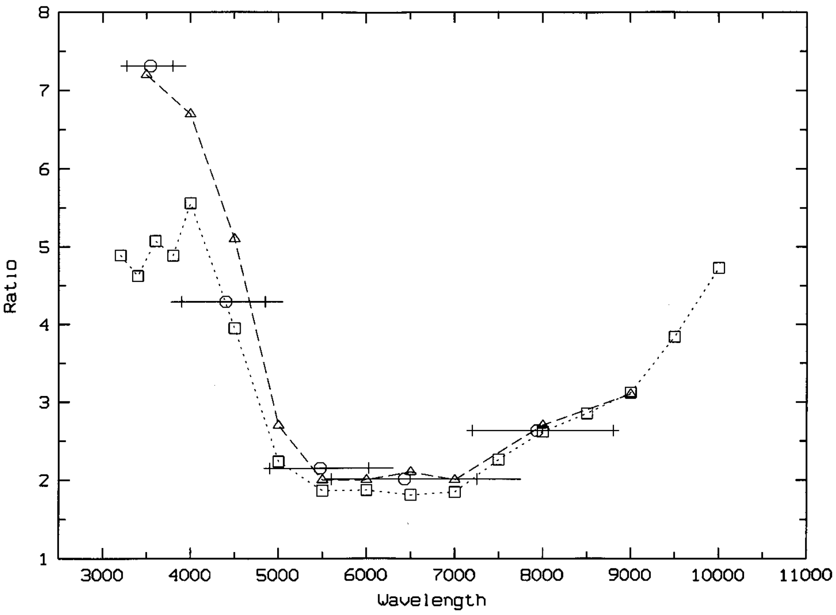

Figure 1: Ratio of observed fluxes of CCD #40 with respect to CCD #19 as a function of wavelength using grism #1 and broad-band filters.

crease in efficiency in the blue reported before. A possible reason for this apparent decrease is the degradation of the UV-coating of CCD #19 with time, a known phenomenon for this type of CCD.

A full report on the commissioning of the new CCD #40 mounted in EFOSC2 at the ESO-MPI 2.2-m telescope can be found on 2.2-m team WWW pages at the address:

http://www.ls.eso.org/lasilla/Telescopes/2p2T/2p2T.html.

Overhaul and Attempted Upgrade of DFOSC CCD

J. STORM

The DFOSC CCD and dewar spent the month of July in Garching and Copenhagen where the dewar underwent a major overhaul to improve its vacuum capabilities.

It was also planned to replace the CCD (W11-4) with a new LORAL/LESSER platinum flash-gate device in Copenhagen. Unfortunately the new devices which the Copenhagen CCD group had received all suffered from manufacturing defects which appeared after a few thermic cycles of the devices. As a result, none of these devices could be used for the DFOSC camera. Instead the surface of the current CCD was chemically cleaned and another attempt at UV-flooding the device was performed. Unfortunately the UV-flooding did not prove stable and it was necessary to remove the UV-flooding all together. Various possibilities of significantly improving the quantum efficiency of the camera, i.e. acquiring a new CCD, are being investigated. A test report describing the current status of the array is available from the 2p2team web pages:
http://www.ls.eso.org/lasilla/Telescopes/2p2T/2p2T.html

News regarding the replacement of the current CCD will also be posted in the 2p2team news section.

About the Spectroscopic Stability of EFOSC1

S. BENETTI

This report discusses the long-term spectrophotometric stability of EFOSC1. EFOSC1 is a focal reducer attached to the Cassegrain focus of the ESO 3.6-m telescope. It is equipped with CCD #26. An earlier report (see *The Messenger* 83, 12) discusses the photometric stability of EFOSC1.

During thirteen nights covering the period from 1992 to 1996, spectra of several spectrophotometric standards were taken with EFOSC1 and the B300 grism. In order to collect all the light coming from the star, all standards were observed with wide slits (5 or 10 arcsec). The extracted spectra were corrected to unit airmass using the standard atmospheric extinction table for La Silla. From each spectrum, a spectral response curve for the B300 grism was derived. Out of fourteen spectra, twelve were taken under photometric conditions.

During the period from 1993 to 1996, additional spectra of several spectrophotometric standards were taken under photometric conditions with the R300 grism. Response curves for the R300 grism were likewise derived.

The dispersions around the average (zero point) response curve (using only those observations obtained under photometric conditions) for the B300 and R300 grisms were computed. The dispersion around the B300 zero point curve is small, with variations of 8–9% for wavelengths larger than 3800 Å, and a variation of about 12% around 3800 Å. The dispersion for the R300 grism is also small, with a variation of about 8% up to ~ 8500 Å, increasing to 10% around 9000 Å and to 16% towards the very red end of R300 wavelength range. This increasing variation can be understood in terms of the low signal of the observations and the poor sampling of the standard stars at these wavelengths, and to fitting procedures.

In Figure 1, the mean response curves for B300 and R300 are shown. They are respectively the mean of the fourteen B300 and the seven R300 response curves. Before taking the mean, they were normalised with respect to the zero point response curve. For the B300 curves, the normalisation occurs at 5500 Å; for the R300 curves, the normalisation occurs at 6500 Å. After normalisation, the variation of the B300 curves with respect to the mean B300 response curve is much smaller (~ 3%). The dispersion around the mean R300 response curve is also ~ 3%, but increases towards the red end.

In summary, the spectroscopic stability of the system (telescope + EFOSC1 + CCD#26) from 1992 to 1996 has been analysed. No temporal trends have been found. These findings reflect the results published in the EFOSC1 photometric study. Once more EFOSC1 proves its reliability.

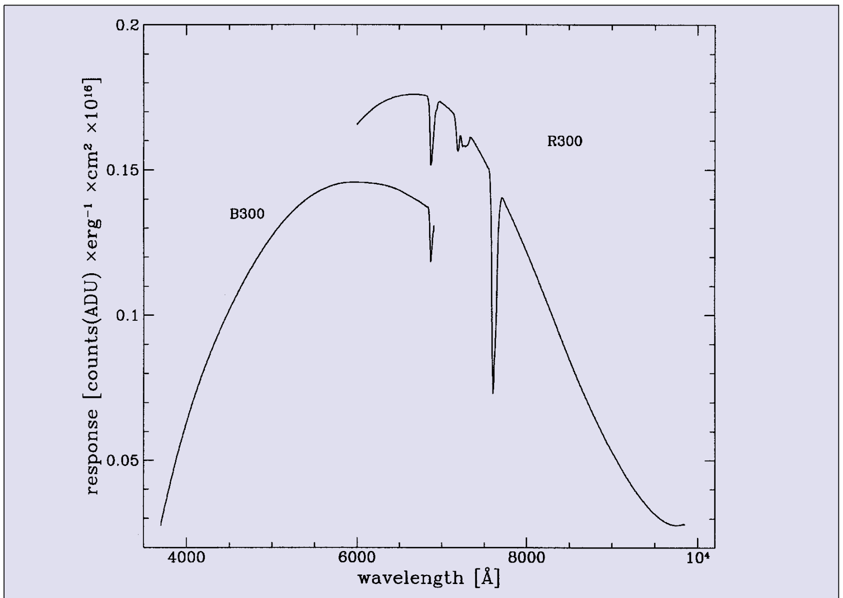

Figure 1: Spectral response curves of 3.6-m telescope + EFOSC1 + CCD#26 for B300 and R300 grisms (the conversion factor for CCD #26 is 4e⁻/ADU). The main atmospheric absorption bands have been tentatively modelled. These curves can be found in the EFOSC1, ESO-La Silla, WWW page (http: //www.ls.eso.org/lasilla/Telescopes/360cat/html/EFOSC1/efosc1.html) as fits files.

The Image Quality of the 3.6-m Telescope (Part IV) Better than 0.6″

S. GUISARD, ESO-La Silla

With this fourth article we will bring to a conclusion the first part of our study which started in September 1995. This part concerns the study and improvement of the image quality (IQ) at the Cassegrain focus of the 3.6-m telescope at Zenith. The second part, started a few months ago, studies the IQ at larger zenithal distance.

In this article we will explain how the IQ at zenith could be brought from 1.2″–1.3″ to less than 0.6″ during test time over the last twelve months. The goal was to obtain subarcsec images with good outside seeing (0.6″–0.7″) and to be able to go down to 0.8″ at the telescope during periods of outstandingly good external seeing (0.4″). Both objectives have been largely achieved. We first present the results of the August and October test nights. The parameters that contribute to the IQ in general have previously been detailed [1] and the most relevant ones with respect to the degradation of the IQ at the 3.6-m are reviewed here as well as the methods to minimise their effects. In the forthcoming months, changes will be made at the telescope to implement these improvements during regular observing time. The IQ that one can expect in the future is presented at the end of this article.

1. Results from the August and October Test Nights

For these nights (August 30, and October 8 and 18, 1996), the IQ measurements were made as usual [1] except that:

- the focal plane of the telescope was shifted 166 mm down to compensate for 0.6″ d80% (the diameter of the circle containing 80% of the light) of spherical aberration.
- forced ventilation on the mirror has been used.

The IQ values are summarised in Table 1. This table can be compared to the table published in an earlier article [1]. Of particular interest are the very good results obtained during the last October night, where images (30 to 120 seconds exposure) with IQ as good as 0.58″ were taken.

Calculations show that for all these nights the IQ was limited by outside seeing, remaining optical quality and pixel size, and not by dome and mirror seeing. Relative to the October nights, the degraded optical quality of the August night is explained by the aberration hysteresis which we are studying at the moment and which prevented us from getting the same results as the last night.

TABLE 1.

	30/08/1996	08/10/1996	18/10/1996 beginning	18/10/1996 end
Average outside seeing	0.40″	1.12″	0.75″	0.43″
Average 3.6-m	0.73″	1.16″	0.83″	0.66″
Best value 3.6-m	0.67″	0.99″	0.75″	0.58″
Worse value 3.6-m	0.81″	1.34″	0.90″	0.78″
Number of measurements	22	27	19	22
Optical quality	0.55″	0.40″	~0.40″	~0.40″

2. Optical Quality

2.1 Spherical Aberration

The existence of spherical aberration at the Cassegrain focus was hypothesised in the last article [2], but was still waiting for confirmation. The most recent set of tests (August and October 1996) were all done with the position of focal plane 166 mm lower than the usual one and confirms that spherical aberration was present at the old focus position.

Another concern was the variability in the spherical aberration values measured (see [2], Table 4) despite the fact that spherical aberration is a "strong" aberration. Part of this variability is caused by the M1 mirror cell but still needs further investigation (part of the IQ study at large zenithal distance). A second cause is mirror seeing. This idea was proposed by Ray Wilson and has now been proved. The proof is outlined below in the section discussing mirror seeing.

Nevertheless, these two effects do not appear to fully explain the long-term variability of the spherical aberration as measured by Antares since 1991 [2].

Antares (a Shack-Hartmann wavefront analyser) and curvature sensing (intra- and extrafocal image analysis) measurements show that the residual spherical aberration at the new focus position (166 mm below the old one) is less than 0.15″ (d80%), whereas it was measured to be between 0.6″ and 0.8″ by Antares at the old focus position. We therefore confirm that the spherical aberration is a limiting factor of the IQ at the actual instrument position.

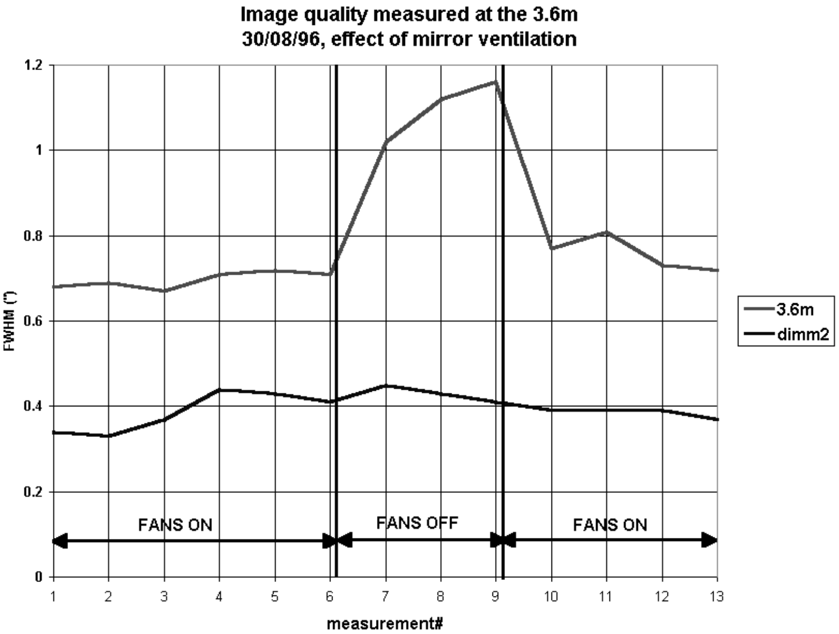

Figure 1.

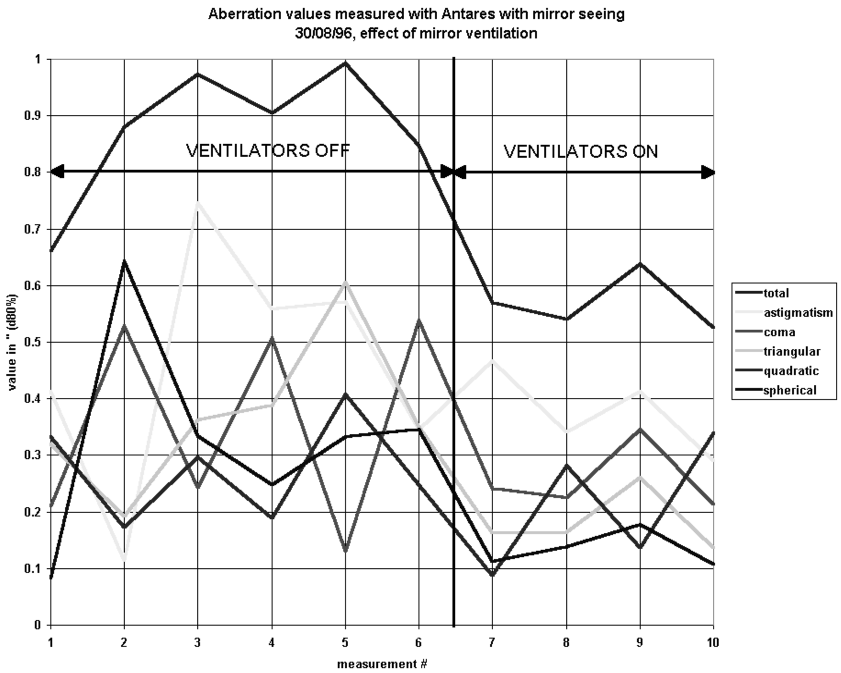

Figure 2.

2.2 Other Aberrations

As already written [2], triangular coma, astigmatism and quadratic astigmatism at zenith are now within the range of values we used to have before the October 1994 aluminisation (respectively <0.2″, <0.2″ and <0.1″ d80%). This improvement occurred after the June technical time. These aberration values have been confirmed with the curvature sensing method and Antares in August.

3. Mirror Seeing

3.1 Effect on IQ

For the first time it has been possible to prove the existence of mirror seeing, quantify its effect and remove it. This has only been possible thanks to the relocation of the mirror cover, done during June technical time [3]. This change allowed the installation of a very powerful ventilation system above the main mirror. This system was used for the first time during the August test night. Although the mirror temperature was 2 degrees higher than the ambient air, we were able to obtain good images (see Table 1). In fact the ventilation system eliminated all mirror seeing (estimated to 1.1″) during these nights. This was proved when the ventilation system was switched off (see Fig. 1). The IQ measured at the telescope increased from 0.7″ to 1.2″ in only a few minutes. It came back to 0.7″ a few minutes after the system was switched on again.

3.2 Effect on the Aberration Values Measured by Antares

The effect of mirror seeing is illustrated in Figure 2, and explains the variability and the size of the aberrations as measured by Antares. In the presence of mirror seeing, Antares gives high and noisy values. When the mirror seeing is removed (ventilation system on), the aberrations come back to the expected values and the noise in the measurements decreases.

4. Other Effects

• Dome seeing: a dome-seeing monitor was installed at the beginning of the year. Significant dome seeing has never been detected since then. The most recent test nights also showed no dome seeing, so we can say that we do not have a major dome-seeing problem at the 3.6-m. Previously, it was said that this was the major source of IQ loss. Recently, efforts to control the thermal environment of the telescope were initiated. This included a better floor cooling strategy, removal of heat sources, and the installation of cooled electronic racks [3], etc. Although we believe that dome seeing is not a problem, we will remain conscious of the thermal environment of the telescope. All temperature values will be available at any time via the new TCS–GUI (Telescope Control System – Graphical User Interface) system. The dome seeing monitor will remain installed so that dome-seeing measurements can be performed at any time.

• Guiding accuracy: a quick check of the guiding accuracy was done in August. A 5-minute exposure with 0.69″ IQ was obtained. In comparison with the 30-second images taken immediately before (0.69″ also), this demonstrates that the telescope guides accurately.

5. Expected IQ in the Future:

We have shown that during night tests we can obtain good images with the 3.6-m. In the coming months, two significant modifications to the telescope will occur so that the IQ obtained with the instruments also improves. These changes are:

• A special flange to lower the instruments to the new focal plane will be manufactured in order to remove spherical aberration. This implies that modifications to the instrument-handling tools and perhaps to the Cassegrain cage will be required.

• A 'clean' ventilation system shall be installed. The principal concern is that dust may quickly dirty the mirror and

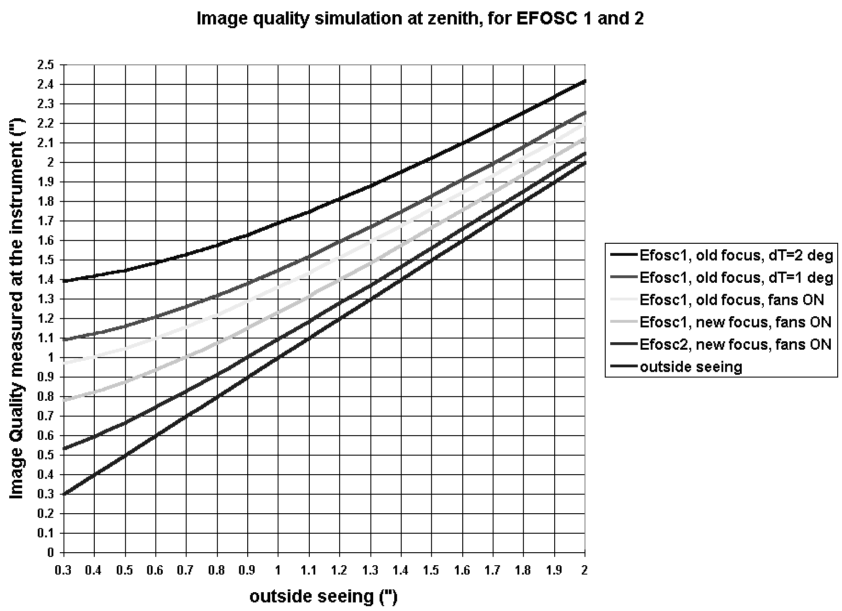

Figure 3.

may also fall down the Cassegrain hole onto the instrument optics or onto slits.

Figure 3 shows the expected IQ one should obtain with EFOSC 1 and 2 at zenith according to the outside seeing value, for different mirror-seeing conditions and focal-plane positions. The six curves represent, from top to bottom:

1. The IQ with EFOSC1 at the actual focus position, with the mirror 2 degrees hotter than the ambient air.
2. Same as 1 but with 1 degree mirror seeing only.
3. Same as 1 but without mirror seeing (or with the ventilation system on).
4. EFOSC 1 at the new focus position with the ventilation system on.
5. EFOSC 2 at the new focus position with the ventilation system on.
6. Outside seeing value.

The first two curves are in fact the IQ we now have. The ventilation system should bring down these curves close to the third one. Moving the instruments down shall also give a substantial improvement to the IQ of the order of 0.1″ to 0.2″ as demonstrated by curve 4. However, we see that the IQ will be mainly limited by EFOSC1 pixel size (0.6″). The installation of EFOSC 2 (0.19″/pixel) at the 3.6-m next year will improve further the IQ by 0.15″ to 0.25″, providing of course that the instrument does not degrade the images. This fifth curve is in fact the curve we measure now with the direct CCD (0.19″/pixel) at zenith during the night tests with the new focus position and the M1 ventilation system working.

6. The IQ Study Keeps On Going

Very good results have been obtained at zenith (Zd < 30 degrees). The second part of our study will now aim to achieve good image quality far from zenith (Zd p 60 degrees). This includes work on activating M2 to compensate for telescope flexure and improvements to the support of M1.

In the meantime, the shift of the focal plane and the ventilation system will be implemented so as to give the expected IQ with the instruments at the Cassegrain focus.

References

[1] S. Guisard, "The Image Quality of the 3.6-m Telescope: Part II", *The Messenger* No. **83**, March 1996.
[2] S. Guisard, "The Image Quality of the 3.6-m Telescope: Part III", *The Messenger* No. **85**, September 1996.
[3] J. Fluxa, G. Ihle, S. Guisard "Report on the Technical Time in June 1996", *The Messenger* No. **85**, September 1996.
[4] S. Guisard, "Report on the night test, 29th and 30th August 1996", 3.6-m+CAT Upgrade 3P6-PLA-032-008, September 1996.

Stephane Guisard
e-mail: sguisard@eso.org

Science with the VLT: High-Resolution Infrared Spectroscopy

G. WIEDEMANN, ESO

I. Introduction

Infrared astronomy has received an enormous boost ten years ago when the first small two-dimensional detectors became available. The 1987 Hilo conference on "Infrared Astronomy with Arrays" (Wynn-Williams & Becklin, 1987) marks the beginning triumph of IR arrays in astronomy. While 'imaging observers' greeted the new multi-pixel devices enthusiastically, their potential for spectroscopy was also immediately recognised. The VLT Working Group on Infrared Aspects (VLT Report No. 51, July 1986) had already emphasised the scientific potential of high-resolution (R p 10^5) spectroscopy in the 1–5 μm range and the large VLT-specific gain of this observational mode. The ESO VLT Instrumentation Plan, endorsed by the STC in March 1990, proposed the development of a dedicated high-resolution cryogenic echelle spectrometer or FTS and/or extending a 'visible' echelle spectrometer into the near-IR. Following the February 1992 ESO Workshop on High-Resolution Spectroscopy with the VLT, highest priority was given to a cryogenic echelle instrument at Nasmyth (rather than the combined focus previously considered) due to its large sensitivity gain relative to an FTS (Moorwood & Wiedemann, 1992; Ridgway & Hinkle, 1992), and the high scientific importance attached to the 2–5 μm region which cannot be competitively covered by an extended 'visible' spectrometer. Subsequently, a concept definition & preliminary design study for a cryogenic high-resolution IR echelle spectrograph (CRIRES) was prepared and presented to the STC Working Group "Scientific Priorities for the VLT" (ESO Scientific Report No. 15, December 1994). CRIRES has been ranked very high among the 'future' instruments in the VLT plan. High spectral resolution, coupled with the large wavelength coverage and the high sensitivity of a cooled echelle constitutes a unique observing capability, that cannot be substituted by other instrument combinations or observing strategies. Together with UVES, the VLT spectrograph for the optical and ultraviolet, CRIRES will open the possibility to obtain spectra with a resolution of R = 100,000 from the blue to 5 μm. The Scientific and Technical Committee (Resolution of 10 February 1995) recommended the continuation of the preliminary studies for CRIRES, in the context of clarifying possible instrument designs. The instrument concept has since been developed further with special consideration of technological advances in adaptive optics, IR detectors and optical components, and with regard to the evolution of scientific priorities of the VLT observatory.

Obviously, the demand for an extension of high-resolution spectroscopic capabilities at large telescopes into the IR (cf. ESO Workshop "High-Resolution Spectroscopy with the VLT", 1992; UCLA/Lick/NOAO/McDonald Workshop "High-Resolution Spectroscopy with Very Large Telescopes", Tucson, 1994) is being voiced increasingly at a time when technological improvements are indeed offering enhanced sensitivity and wavelength coverage of IR spectrometers.

This article summarises arguments for astronomical high-resolution spectroscopy in the infrared, illustrates some of the science priorities and provides a short description of the planned VLT instrument.

II. High-Resolution Spectroscopy in the Infrared

1. IR Source Brightness

'Cool' astronomical targets, whose study does not depend on particular visible or UV features, can be observed favourably in the infrared. In the era of photon detectors, the relevant Planck-function for the 'brightness', n_{ph} (photon flux in a velocity resolution element $\delta\lambda = \frac{\lambda}{R}$) of a blackbody at temperature T is:

$$n_{ph} = \frac{2c}{\lambda^3 \bullet R \bullet (\exp\frac{hc}{\lambda kT} - 1)} * A\Omega, \qquad [1]$$

where c is the speed of light, h and k are Planck's and Boltzmann's constants, respectively, and A Ω is the telescope étendue. Figure 1 illustrates the wavelength dependence of the photon flux for blackbody temperatures corresponding to stars of spectral type G2, K5 and M5. The second panel shows the resulting the λ-dependence of the photon flux ratios relative to 5000 Å. The IR-to-visible brightness ratio increases rapidly towards the cooler stars. The improvement over the 4000 Å range is even greater due to the exponential decrease of the stellar flux towards the blue. Monitoring K and M stars at 1.6 μm (H-band) or 2.3 μm (K-band) instead of the 5000 Å region, would have the equivalent effect of using a much larger telescope.

2. Use of Telescope Time

Telescope time is of similar value as telescope size, in particular to programmes targeting large samples, small effects or long-term variability. High-resolution observations of bright IR sources are largely unaffected by air-scattered sunlight and sky variability (OH emission or thermal background). The monitoring programme can therefore make extended use of twilight and morning time as much as permitted by telescope operations.

3. Obscured Sources

The IR brightness argument, of course, applies even more to sources that are obscured by dust at visible wavelengths: The 'brightest' extrasolar system object on the sky (IRC +10216) is invisible in the optical but has a 10 μm magnitude of –7! Star formation is observed predominantly in the IR, and the Galactic Centre can be studied only in the IR (Eckart & Genzel, 1996). Large visual extinction will make only the brightest LMC targets accessible to high-resolution VLT observations. Yet, none of the limiting distance moduli are severely compromised if IR spectroscopy is employed. High-resolution IR surveys in the Magellanic Clouds will be possible and M31 is well within reach (Sneden et al., 1995).

4. Infrared Spectral Diagnostics

The IR features an enormous number of spectral lines: The 1– 5 μm spectrum of a cool giant (Hinkle et al., 1995) contains roughly 6000 lines, of which about 1500 are of atomic and 4500 of molecular origin. Nearly half of these lines occur in the near-IR (λ ≤ 2.5 μm). Solar-type stars (T_{eff} < 6500 K), in particular, have rich line spectra from an abundance of molecules. Most rotation-vibration lines of light molecules occur in the IR. Einstein coefficients A_{ij} for spontaneous emission are typically. 1–100 sec^{-1} (A_{ij} ~10^8 sec^{-1} for atomic resonance lines). The lines are frequently formed near LTE, and probe predominantly cooler regimes (allowing molecule formation) that may not be accessible to the high-temperature optical diagnostics.

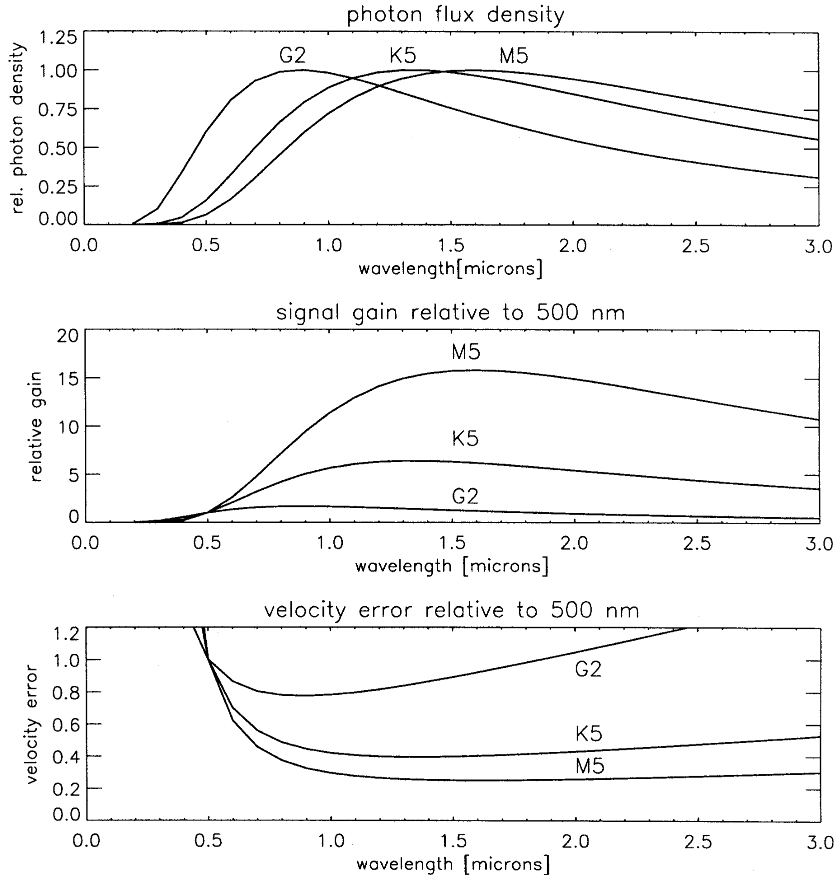

Figure 1: Upper panel: normalised photon flux density for blackbody temperatures corresponding to stellar spectral types G2, K5 and M5. Centre: wavelength-dependence of the photon flux, normalised to the flux at 500 nm for the three spectral types. The curves show the signal gain possible in the infrared for the cooler stars. The gain (vertical axis) is equivalent to an increase of the telescope area or a reduction of necessary integration times. Lower panel: wavelength-dependence of the corresponding velocity error, normalised to the error at λ = 500 nm on the same star.

The IR features a number of Zeeman-lines (1.56 μm Fe I, 2.23 μm Ti I, 12.32 μm Mg I). The ratio of σ and π-component splitting to the line widths for a given B-field increases linearly with λ and allows a more model-independent determination of field strengths in the IR (Saar, 1995).

The pure rotational (Δj = 2) quadrupole transitions in the vibrational ground state (v = 0) of molecular hydrogen, H_2, the most abundant constituent of the cool interstellar medium, occur in the infrared. Observable from the ground are several transitions at 3 μm – 5 μm, S(3) at 9.7 μm, S(2) at 12.28 μm and S(1) at 17.03 μm, the latter representing the lowest ortho-H_2 state, because of its statistical weight the most highly populated level in the coolest component of interstellar matter.

5. IR Spectroscopy: Why at a Very Large Telescope and at High Resolution?

IR spectroscopy fully exploits the collecting area (p D^2) gain of an 8-m over a smaller telescope, if the noise is independent of the telescope size. This holds for detector-limited faint-source observations in the near-IR, as well as for point-sources in the thermal IR, when the larger telescope's smaller diffraction limit and the use of an adaptive optics system keep the background étendue constant: $A\Omega$ p λ^2. In the best possible case, the dominating noise source is the observed object itself, the S/N p D is then solely due to the source photon statistics. This fundamental limit is familiar to optical observers; in the IR it is new for most targets. High-resolution spectroscopy, in particular, will benefit from the larger telescope size, as it is intrinsically handicapped by small signal levels.

Sensitivity gains greater than those due to the mirror size can result from instrument features, e.g. increased simultaneous spectral coverage or resolution. Usually these enhanced features are correlated with large instrument size, which could prohibit the implementation at low-emissivity foci of smaller telescopes.

In addition to the *information* contained in a high-resolution spectrum, there is a *sensitivity* increase for all unresolved spectral features through elimination of radiation not contributing to the signal (line photons) in both the source- and the background-limited cases. This gain associated with higher spectral resolution is equivalent to that of larger telescope size.

6. IR Spectroscopy: The Detector Array "Multiplex" Advantage

High-resolution (R P 100,000) astronomical IR spectroscopy was dominated by the Fourier transform spectrometer (FTS) when 'noise' was primarily caused by poor detectors, and simultaneous wavelength coverage resulted in a net efficiency gain. This "multiplex" advantage was lost with improving detectors to broadband radiation-noise. Frequently, bandpass-limiting filters ($\Delta\lambda$) were required to reduce the radiation background on the detector, at the expense of spectral coverage. With cryogenic grating monochromators used for post-dispersion and ultra-low noise detectors it became possible (Jennings et al., 1986) to narrow the bandpass $\Delta\lambda/\lambda$ for FTS observations to a small fraction of a narrow filter band, with the additional advantage of easy tunability. A postdispersed FTS using a detector array to recover a larger spectral range has been proposed for the VLT (Maillard, 1992). The strongest boost for the IR echelle, however, came with the arrival of truly large two-dimensional detectors. (Early monopolising of the detector array market by optical imaging aficionados has given the world the *pic*ture *el*ement, "pixel". Attempts to introduce the spectroscopic analogue, "spexel" have not been successful). The evolution of astronomical IR spectrometers in the last decade was guided by the rapid increase in the size and the noise reduction of semiconductor detector arrays. The appeal of low-noise IR arrays to spectroscopy lies in the possibility to distribute all spectral elements onto individual detectors. This reduces the radiation - noise bandwidth to its absolute minimum, i.e. that of a spectral resolution element, $\delta\lambda$. The resulting noise improvement p $(\Delta\lambda/\delta\lambda)^{1/2}$ easily exceeds an order of magnitude. The spectral coverage ($\Delta\lambda$) corresponds to the available number of detector elements in an array. With the recent introduction of InSb and HgCdTe 1k $\times$ 1k arrays, an IR echelle at R = 10^5 can now offer a spectral coverage ($\Delta\lambda$ / λ P N_{det} / R) in a single order equal to that of an FTS with a noise-limiting filter system. Large detector arrays grant the multiplex gain to dispersive instruments. The FTS, although closer to the 'perfect' spectrometer than any other instrument type is being superseded by the more sensitive echelle spectrograph (Ridgway & Hinkle 1992) at the very large telescopes.

Figure 2 illustrates the signal levels from astronomical sources compared to noise levels prevailing in a high-resolution IR spectrometer. The fundamental

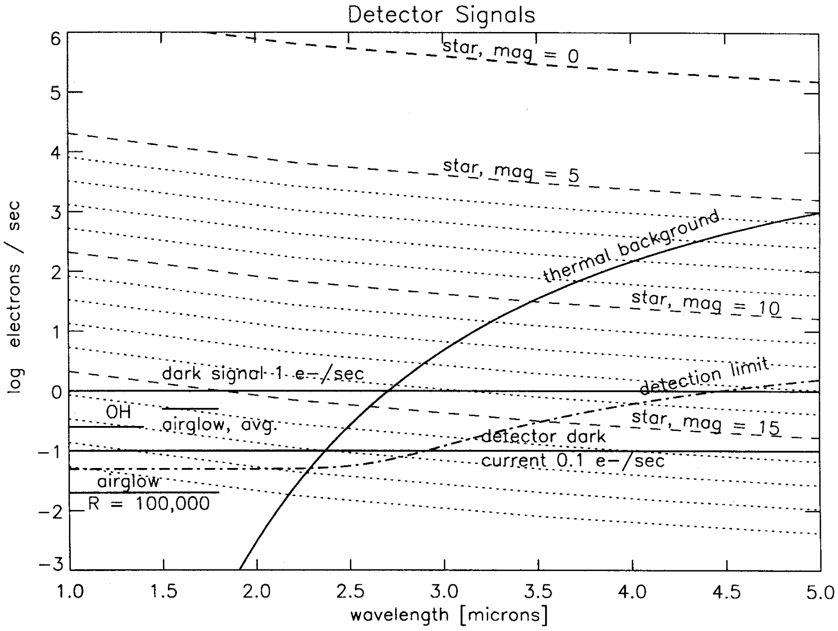

Figure 2: Detector signal levels (detected photons/sec) in comparison with the detector dark current (e^-/sec). Assumptions: Background temperature: 280 K, total emissivity 10%, total efficiency 10% (incl. atmosphere, telescope, detector Q.E.), R = 100,000, 0.1″/pixel, D_{Tel} = 8m, OH airglow values adopted from Maihara et al. (1993).

source-noise limit can be reached for many bright targets.

7. Exploiting the IR Advantage

Astronomy will benefit from IR echelle spectrographs in various ways. The VLT IR echelle will not only extend the number of observable objects considerably, but will offer capabilities not available otherwise. Sensitivity improvement can be aimed at fainter objects, higher spatial (extended sources), spectral and temporal resolution (or reduced integration times). Increased sensitivity will permit to extend studies from a few objects to a complete sample of an object class, access other, less luminous classes of objects, and to study previously unobservable phenomena in recognised but poorly-understood objects. Many extended sources have shown structure on small scales when observed with enhanced spatial resolution (e.g. auroral regions observed in H_3^+ on Jupiter). Studies of planets, stellar outflows, circumstellar disks, planetary nebulae, star-forming regions, etc. may benefit from the greater spatial resolution of the VLT echelle in the same way as, or – in combination with the spectral information – even more than pure imaging applications. The prospects for *solar-system* observations have been highlighted by Encrenaz (1994). The importance of high S/N, high-accuracy and high-resolution measurements on *bright* sources for astrophysics in general has recently been emphasised by several authors (Kurucz, 1992; Grevesse & Sauval, 1994; Dravins, 1994).

III. Science Priorities

1. Search for Extrasolar Planets: Infrared Radial Velocity Measurements

Recently, planetary companions have been identified to several solar-type stars, including a planet surprisingly close to 51Peg (cf. Mayor & Queloz, 1995). The hunt for extrasolar planets has concentrated on stellar reflex motions apparent in radial velocity (RV) variations, measured with optical high-resolution spectrographs (e.g. Hatzes, 1996). Until recently, the potential advantages of the IR could not be exploited because of a lack of instrumental sensitivity. Backed by the new technical capabilities, the IR now provides all qualities necessary for extrasolar planet searches:

• The extension of RV studies to the IR can constitute a quantitative improvement, equivalent to a substantial increase of the telescope collecting area.

• The extension of RV studies to the IR is essential, as complementary IR diagnostics may be needed to identify *stellar* causes of observed RV variations, which can be misinterpreted as reflex motions due to a planet.

The detection of extrasolar planets via RV measurements requires a precision in the range 1–10 m/sec. The reflex motion of the star increases linearly with the mass (⋆ sin i) of the planet and with the inverse square root of its distance from the star. For instance, Jupiter's effect on the Sun amounts to p 12 m/sec, (that of the Earth only p 0.1 m/sec). The rms error σ of RV measurements:

$$\sigma = \frac{c}{R * \frac{S}{N} * N_L^{1/2}} \qquad [2]$$

improves with the signal-to-noise S/N in resolved stellar lines, the resolving power R, and the number N_L of lines in the stellar spectrum. Numerical simulations have demonstrated (Hatzes & Cochran, 1992) that a precision of 8 m/sec can be obtained with R = 100,000, S/N = 300 and N_L = 5. Actually achieved precisions in the optical have been reported (Hatzes, 1996) in the range 3–25 m/sec.

In order to assess possible quantitative infrared advantages of planetary RV searches, it is necessary to consider the wavelength dependence of the achievable S/N ratios and of spectral line densities. Candidate stars for planetary searches are considerably brighter than the background at all wavelengths. For a given line density, the velocity error σ therefore scales with the λ-dependence of the detected source flux according to eq. [1] and Figure 1. The lower panel in Figure 1 illustrates the resulting RV errors for each of these spectral types, relative to that achievable at 5000 Å on the same stars. Obviously, the IR can offer dramatic improvements for the cooler stars.

The search for extrasolar planets is a prime example for a monitoring programme that would benefit greatly from extended use of the VLT during twilight and possibly early morning time.

Infrared Lines for Radial Velocity Studies and Calibration

The IR spectra of late-type stars feature strong spectral lines suitable for radial-velocity studies (Fig. 3). Several 'windows' can be recorded simultaneously with a cross-dispersed IR echelle spectrograph. The use of CO $\Delta v = 2$ lines at 2.3 µm to monitor the apparent velocity of integrated sunlight and the use of IR N_2O lines as highly accurate velocity standards for RV measurement have been demonstrated and described by Deming et al. (1987,1994). CO, a well-studied molecule, can also be used for calibration in stellar studies, in particular if Doppler-shifted stellar CO lines are measured against their telluric (laboratory) counterparts.

The Importance of Complementary IR Diagnostics

Arguments for including the IR in planetary searches follow from two possible causes for periodic variations in the apparent velocity of integrated starlight, that could be mistaken for planets: magnetically affected vertical gas motions and stellar spots.

The radial velocity of integrated sunlight has been monitored by different groups using different spectral diagnostics. Deming et al. (1987, 1994) have determined RV variations with a peak-to-peak amplitude of 28 m/sec over a p 11 year period using as main diagnostic ($\Delta v = 2$) ro-vibration CO lines. The effect is very similar to that of Jupiter the Sun. McMillan et al. (1993), using a Fabry-Pérot in the optical, find an upper limit of 4 m/sec over the same period. The discrepancy is far greater than the respective errors. Viewed from far away, our Sun would thus appear to have an extra planet or not, depending on which spectral diagnostic is used. An explanation of the correlation with the solar cycle, (Dravins, 1982, 1985), is the inhibition of vertical motion of gases affected by magnetic fields. Monitoring of IR Zeeman lines might help to distinguish magnetic field changes from reflex motions as a cause of observed velocity variations.

A large dark spot on a rotating stellar surface can cause a periodic shift of a spectral line's apparent position through a reduced contribution to the disk-integrated flux at the velocity of the spot's geometric location. Conversely, one can exploit spectral diagnostics characteristic for and originating *in* the spot. These can be spectral lines of molecules that are stable only at the low temperatures prevailing in cool spots: sunspots observations, for instance, reveal an enormous number of characteristic spectral lines (Wallace & Livingston, 1992). Another diagnostic are Zeeman-sensitive lines whose components are spectrally split by the field of a cool magnetic spot (e.g. Hewagama et al., 1993). A spot is identified as a 'planetary pretender' if the Doppler variation of the IR spot signature is opposite in phase to that of the 'regular' stellar diagnostics.

Fringe Benefits and other Applications of Planet-Search Techniques

The search for extrasolar planets automatically yields high-quality IR spectra of all stars included in a survey. Naturally, they can be exploited for a variety of scientific purposes. Spectra of candidate or other stars obtained with planetary search techniques, can examined for signatures of atmosphere dynamics or oscillations.

Planetary search tools can be applied to the suspected black hole in the Galactic Centre. Proper motions and velocity dispersion of the stars in the inner parsec of the galaxy have been measured to estimate the mass enclosed in the centre (Eckart & Genzel, 1996). The precise determination of the dynamic state and the mass/gravity distribution requires a measurement of the velocity *rate of change*. This is presently out of reach for proper motions, but in the range of RV techniques. Estimating the velocity variations of the inner late-type stars from the published centre distances and orbital periods yields numbers (10–100 m/sec/yr) similar to those achieved in RV planetary searches. RV

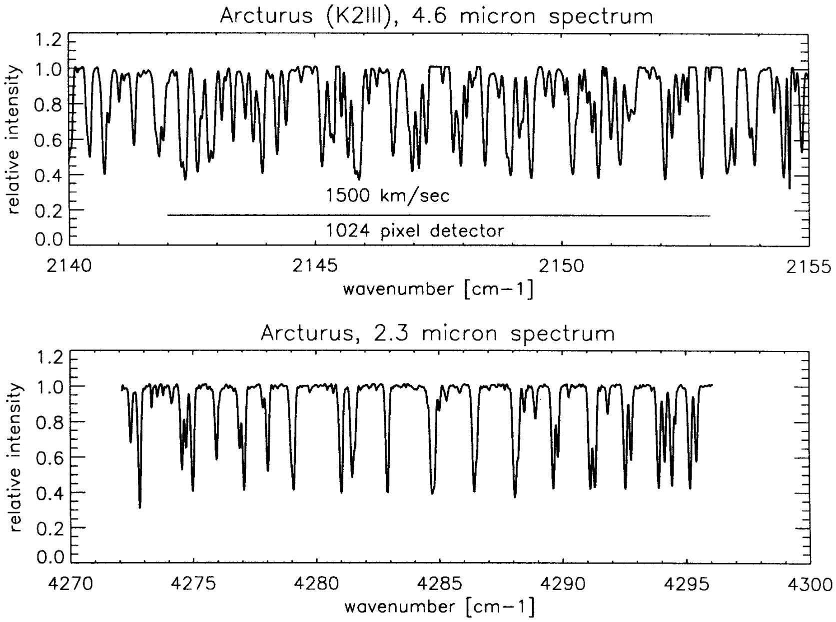

Fig 3. High-resolution (R >100000) spectra of αBoo (K2 III) from Hinkle et al (1995). The stellar spectra have been corrected for the atmospheric transmission. All absorption lines are of stellar origin and represent infrared transitions of carbon monoxide. Upper panel: fundamental (Δ v =1) lines in the M band; lower panel: first overtone (Δ v = 2) lines in the K-band. The horizontal bar indicates the range covered by a 1024 detector in a single order.

studies in the Galactic Centre have to be conducted in the IR, as the stars are totally obscured at visible wavelengths.

2. *Prospects for Direct Spectroscopic Detection of Extrasolar Planets*

The direct detection of an extrasolar planet requires the identification of its host's reflected starlight or its own infrared radiation. Both signatures are faint and contribute minutely to the stellar flux; in favourable cases as that of the Jupiter-like companion 0.05 AU from 51Peg (Mayor & Queloz, 1995), the intensity relative to the stellar (m_V=5) 'background' is p 5 10^{-5} (Δ mag =11), if Jupiter's size and albedo are assumed. An m_V P 16 object is difficult to detect in close proximity to a star: on one hand the reason for the 'brightness' of a planet, proximity prevents, on the other hand, a separation of the observable *images.* Alternatively, the *velocity* separation between star and planet is easily within current observational capabilities, even for relatively distant planets, although close planets have a higher detection probability because of their greater reflected and thermal 'brightness'.

The orbital motion of an extrasolar planet periodically Doppler shifts its entire spectrum relative to that of its host star. This global frequency modulation uniquely distinguishes the planetary spectrum and can unambiguously identify its contribution to the total observed spectrum. The amplitude of this velocity modulation yields directly the mass ratio (or the mass if the reflex motion of the star has been established previously) according to $m_s v_s + m_p v_p = 0$. Intensity variations in the planetary signature 90 degrees out of phase with the velocity can be attributed to the illumination phases. Their amplitude can be directly related to the inclination angle of the orbital plane.

The frequency modulation of the planetary spectrum holds the key to the main problem of faint signal detection: the bright stellar 'background' must be suppressed extremely accurately to extract the planetary part from the observed combined spectrum. Background subtraction at the p 10^{-4} – 10^{-5} level, usually prohibitive in ground-based astronomy, is tractable in this special case: the modulation operates against the stellar wavelengths with an amplitude that is large compared to the (p few km/sec) line widths. (A simplified view is that of an isolated planetary spectral line moving "on and off" a position in the stellar spectrum). All foreign effects, not showing the same large velocity amplitude and periodicity over the entire spectrum can in principle be eliminated. The problem of accuracy is reduced to that of overcoming the statistical noise of the stellar flux. A reduction of that noise can be achieved if a spatially occulting mask is used at the spectrograph entrance to (partially) suppress the stellar flux. This is most efficient at the greatest projected separation of planet and star, i.e. when the planet has the largest velocity differential.

High spectral resolution is mandatory, as in all high-background applications, to maximise the signal (line photons)-to-noise (stellar photons in a resolution element), but the relative measurement does not ask for the high absolute velocity accuracy of stellar reflex motion studies. The arguments for investigating cooler stars preferably in the IR follow those for reflex motion studies.

Recent model calculations by Bjoraker et al. (1996) predict the possibility of strong methane line emission in the 3 μm ν_3 - band in a heated atmosphere as that of 51PegP. A direct planetary detection and the characterisation via CH_4 bands should be within the reach of CRIRES at the VLT.

Uncovering Planetary Pretenders

The search for velocity-modulated planetary signatures in stellar spectra can be hampered by time-variable, periodic or random *stellar* effects with power at the orbital frequencies. Variability can be due to: stochastic shock waves, magnetic field variations, spots on rotating surfaces, etc. Planetary detection is primarily concerned with the *magnitude* of these disturbing effects. Understanding the *cause* of observed variations can be the subject for interesting studies in the respective fields. It is nevertheless important for planetary searches, as it helps eliminating stars with large 'side effects' as potential targets.

Again, the IR can provide spectral diagnostics that are particularly well tuned to these 'parasitic' effects, such as Zeeman lines for magnetic fields or molecular LTE lines diagnosing the altitude dependence of stellar atmosphere dynamics.

3. Other Examples of IR studies

IR spectroscopy at an 8-m telescope can be applied to hot stars (non-LTE H-lines, atmospheric structure, disks, mass transfer), but offers even greater benefits in the study of stars of spectral type F5 and cooler (e.g. Grevesse & Sauval, 1994). Their IR spectrum contains lines from virtually all light diatomic molecules, including CNO in various combinations. The transition originate from a large number of excitation states and can therefore diagnose a wide range of physical conditions and processes. Two problems in stellar physics which will benefit from the VLT IR echelle are addressed below.

Stellar Magnetic Fields

The understanding of stellar evolution and dynamic processes in stellar interiors and atmospheres is closely tied to the understanding of the role of magnetic (B-) fields. The direct measurement of stellar B-fields is based on the Zeeman effect, which is characterised by a linearly increasing separation of σ- and π-components relative to the line widths with wavelength. Unambiguous, i.e. model-independent B-field measurements on stars require full separation of the Zeeman components and can only be performed in the IR. The first magnetic-field measurements on an M dwarf flare star, AD Leo, were reported by Saar and Linsky (1985), who recorded the Zeeman-split profiles of two titanium lines near 2.2 μm. A large fraction (73%) of the stellar surface is covered with an average field of 3800 G. Their FTS spectrum of AD Leo required a 6-hour integration to obtain a S/N of 25. Available instrumentation had been pushed to its limits to record one example of a magnetic-field measurement. An update on stellar magnetic-field measurements and a review of first achievements with IR echelle spectrographs has been given by Saar (1995).

The most powerful magnetic field indicators known today are the high-Rydberg MgI 12.32 μm lines. Since their discovery (Goldman et al., 1980), identification (Chang & Noyes, 1983) and interpretation (Carlsson et al., 1992), they have revolutionised solar magnetic field studies (cf. reviews at IAU Symposium 154). Few attempts have been made to search for these lines in stars, all with prototype visitor instruments at large telescopes (e.g. Jennings et al., 1986). Integrations of several hours merely detected the lines in very bright but magnetically inactive red giant stars (α Ori, α Tau). Dwarf and main sequence stars, the prime targets for magnetic field studies will only become accessible with IR echelles at large telescopes.

Stellar Atmospheres

The ro-vibration lines of CO at 2.3 and 4.6 μm originate at photospheric and chromospheric altitudes in spectral type F5 and cooler stars. Formed near LTE, the lines are relatively easy to interpret. Pioneering studies on the Sun (Ayres & Testerman, 1981), and Arcturus (Heasley et al., 1978), and subsequent investigation of a few bright stars by Wiedemann et al. (1994) have revealed a serious conflict between the stellar models derived from UV/visible observations and the IR molecular line observations, which led to the postulation of extended, molecular cooling-dominated surface areas in coexistence with the classical chromospheres. The confirmation of this 'thermal bifurcation' scenario (Ayres, 1981) would have profound implications for the standard models (e.g. Kelch et al., 1978), which depend strongly on the spatial averaging properties of the species from which they are derived (high-excitation lines on the Wien-side of the Planck-curve). Dust formation, suspected to begin at the stellar surface-interstellar medium interface could be affected through the altered grain-destroying UV radiation spectrum or the very low temperatures created by CO- and SiO cooling catastrophes (Cuntz & Muchmore, 1994).

Stellar Oscillations and Atmosphere Dynamics

The solar 5-minute oscillations can be observed in the CO IR transitions with great sensitivity due to the large number of lines formed over a wide altitude range (Ayres & Brault, 1990) and their close coupling to the local kinetic temperatures (LTE line formation). Different oscillation modes are triggered in the – directly unobservable – interior and the convective zone of late-type stars, from where they propagate to the visible surface. Extrapolating to stellar research, time resolved observations can probe processes in the *stellar interior* relating to evolution, age, etc. Measurement of correlated temporal variations in Doppler-shifts and line intensities probe the *dynamics* of cool star atmospheres. Such measurements, using CO ($\Delta v = 1$) and ($\Delta v = 2$) lines (Ayres & Brault, 1990) and 12.3 μm MgI lines (Deming et al. 1988) with large FTS have contributed substantially to the understanding of the solar photosphere/chromosphere region. Other stars are out of reach for current telescope/instrumentation, but will be accessible with a cryogenic echelle at the VLT. The study of acoustic shock waves in slowly rotating, i.e. magnetically inactive, stars (e.g. Cuntz et al., 1994) would contribute in a major way to the understanding of the elusive heating processes leading to the widely observed but poorly explained chromospheres in late-type stars (cf. *Mechanisms of Chromospheric & Coronal Heating*, eds. Ulmschneider, Priest & Rosner [Springer: 1991]). In this case, the sensitivity of the cryo-echelle permitting stellar observations is *fundamental*, since in the Sun – usually the primary case study for late-type stars – dissipation of magnetic (in addition to acoustic) energy accounts for substantial non-radiative energy input into the upper atmosphere and does not permit the identification of the individual causes of the observed structures. Again, few attempts to study oscillations of IR lines in cool stars with adequate time resolution have been undertaken in the past because of the lack of instrumental sensitivity.

IV. Observational Capabilities at the VLT

1. Instrument Concept

CRIRES is the IR echelle spectrograph in the revised VLT Instrumentation Plan. Its concept emphasises high resolving power ($R = 10^5$), high IR sensitivity and large spectral coverage. CRIRES is a cryogenic spectrometer utilising only reflective optics except for

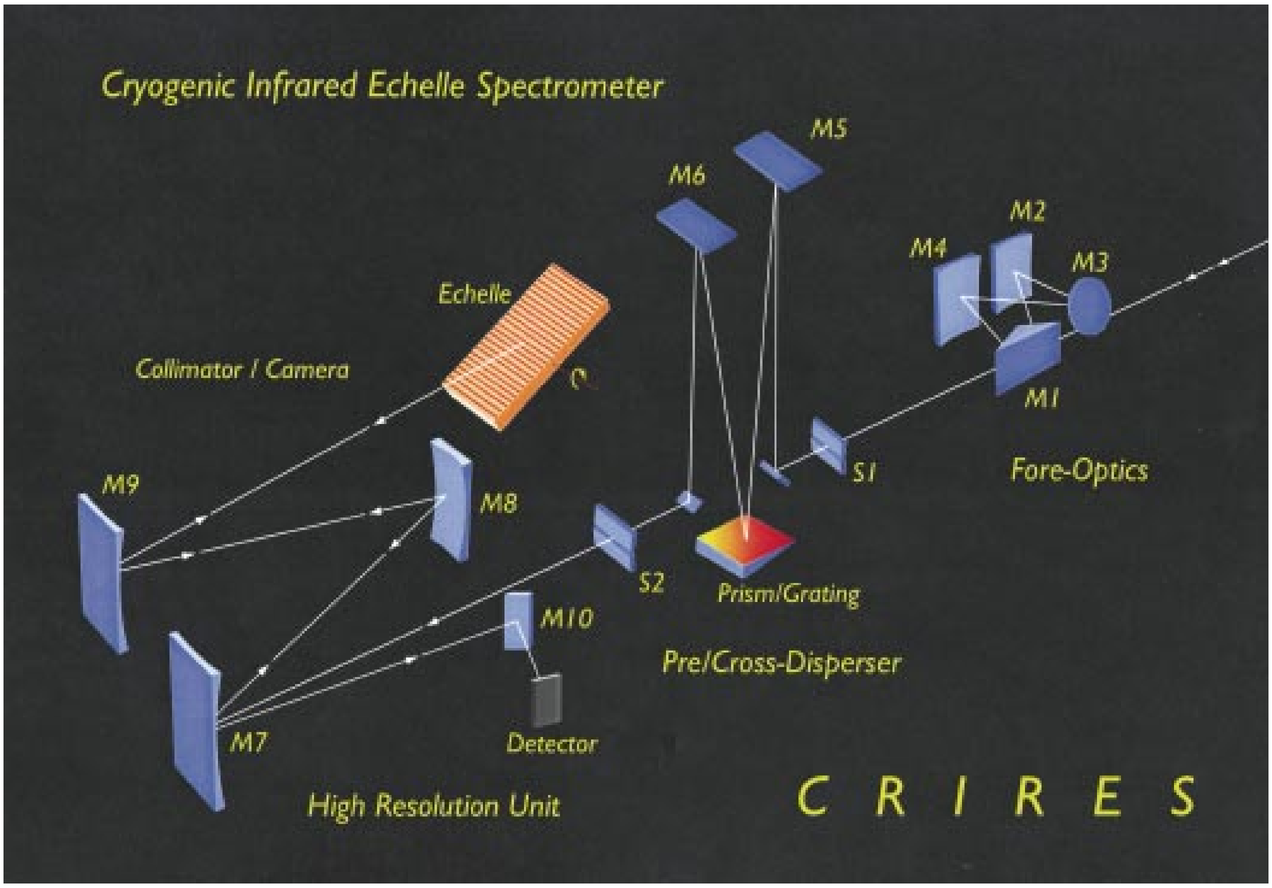

Figure 4: CRIRES, schematic of the optical layout.

the entrance window and the pre/cross-dispersing elements. The operating range extends from 1–5 μm. The non-thermal IR ($\lambda \leq 2$ μm) has been fully integrated in the concept as a range of immense scientific importance, containing spectral diagnostics such as the HeI 10830 Å line, CN bands in the J-band, CO $\Delta v=3$ lines and bandheads, and neutral metal lines in the H-band (1.6 μm).

The envisaged CRIRES would extend most of the UVES capabilities into the IR.

Due to the tight stability requirements, the Nasmyth platform with a low-emissivity focus is the natural location for the IR echelle spectrograph. The resolving power of 10^5 can be realised with a single 40-cm echelle, yielding a resolution-slit product of $R\Theta = 20{,}000$ at an 8-m telescope. Observations of fainter point sources with a 0.2 arcsec slit require low-order adaptive correction for light concentration. A curvature-sensing AO system external to the instrument appears to yield the best overall performance. The increase of the background in the thermal IR would be only marginal, even irrelevant for bright-source observations. The reflection losses due to the extra optics are negligible compared to the reduction of slit losses.

The primary instrument mode will produce crossdispersed echelle spectra. A long-slit mode is envisaged, subject to optical field and mechanical constraints. The necessity for field-de-rotation will depend on the final slit length and its astronomical implications. No de-rotator is foreseen in the instrument. The task can be accomplished by the optical train of the AO system.

2. Instrument Description

The following description refers to the 3-D drawing (Figure 4). A more detailed description will be given in a forthcoming report. The instrument will be housed in a vacuum tank for operation at cryogenic temperatures. Optical system and radiation shields are cooled to 60–80 K. The detector operating temperature will be in the 20–30 K range. Functionally, the instrument can be divided into: adaptive optics unit, calibration unit, fore-optics, pre/crossdisperser and high-resolution section:

The calibration unit provides for flux calibration, detector flatfielding, and wavelength calibration of the echelle. It includes a gas cell for precision velocity measurements. The fore-optics section incorporates a cold pupil stop to eliminate all light not passing via the telescope secondary. A source image is formed at the entrance slit of the predisperser, which determines the spectral resolution of the echelle and acts as the main field stop. A small camera views the field image reflected off the predisperser entrance slit. Alternatively, the wavefront sensor for the AO system may be positioned here. This solution would eliminate the potential problem of uncompensated flexure between AO wavefront sensor and spectrograph slit.

The basic crossdispersed modes for all of the wavelength bands instrument will be realised by shallow gratings mounted interchangeably in the predisperser section. This concept retains the option for single-order observations with optimal parasitic light suppression, and the possibility to simultaneously record a low-resolution spectrum off the polished predisperser exit slit. An alternative design places the crossdisperser in the echelle section, as customary in optical spectrographs. This concept has not been proven for an IR spectrograph, however, and needs to be investigated further.

The beam expanding from the predisperser exit slit into the high-resolution section is collimated to illuminate the large echelle. Tilt-tuning of the echelle centres the desired wavelength on the detector. The dispersed light is returned through the 3-mirror collimator to the detector array(s). A small diverter mirror must probably be used to separate the spectrum from the entrance slit. The f/7 entrance and exit beam produces the required plate scale of 0.1 arcsec/pixel, with two detector elements sampling the nominal 0.2 arcsec entrance slit. A sampling finer than two pixels per resolution element can be obtained by scanning the grating in steps corresponding to fractions of a pixel.

3. Performance

Sensitivity and S/N

Figure 2 shows the contributions to the detector signal which determine the noise and the detection limits given in Table 1. A useful definition of 'sensitivity' must refer to the different conditions under which observations are carried out. Faint-source limiting magnitudes, largely determined by instrument properties are given in Table 1. Signal-to-noise ratios, relevant for small effects in bright' (Table 2) sources, are listed in Table 3.

With a read-noise expected in the 10 e^- range, the faint limits are dictated by the dark current (< 1 e^- /sec/px) in the J, H (outside of strong OH airglow lines) and K bands and by the thermal background radiation (telescope and atmosphere) at the longer wavelengths. The S/N increases as the square root of the integration time. In the faint source limit, the S/N increases linearly with the signal.

Table 2 shows the stellar magnitudes at which the flux from the source begins to dominate the noise. The S/N increases as the square root of the signal in the fundamental bright source limit. To illustrate the system efficiency, Table 3 lists the integration times required to achieve a S/N of 100 on a 5th and a 10th magnitude star at all wavelengths.

TABLE 1: Limiting magnitudes for S/N = 3 in 1 hour.

λ (µm)	1.2	1.6	2.2	3.3	4.2	4.7
mag	18	17.5	17	15	13.5	12.5

Assumptions: Dark signal (incl. detector current, stray light) 1 e^-/sec, total emissivity .1, total efficiency 10% (incl. atmospheric and telescope transmission, instrument efficiency, detector Q.E.), accumulation of > 100 e^- per exposure to overcome read noise.

TABLE 2: Stellar magnitudes where point source observations become source-noise limited.

λ (µm)	1.2	1.6	2.2	3.3	4.2	4.7
mag	16	15	14	10	7	5

TABLE 3: Integration times required for S/N = 100 on a 5th and a 10th mag star.

λ (µm)	1.2	1.6	2.2	3.3	4.2	4.7
T[sec], mag = 5	<1	1	2	2	3	5
T[sec], mag = 10	50	100	160	350	6,000	15,000

V. Conclusion

"We trust that in the final vote, committees and directors will favour high resolution, because even though most astronomers don't use it, they know as we know that astrophysics comes out of high-resolution observations" (S. Ridgway, Conclusion of an invited review talk at the ESO Workshop 'High-Resolution Spectroscopy with the VLT' 1992).

References

Ayres, T.R. 1981, *Ap.J.* **244**, 1064.
Ayres, T.R. & Testerman, L. 1981, *Ap.J.* **245**, 1124.
Ayres, T.R. & Brault, J. 1990, *Ap.J.* **363**, 705.
Bjoraker, G & Deming, D. 1996, private communication.
Carlsson, M. , Ruttren, R.J. & Shchukina, N.G. 1992, *A&A* **253**, 567.
Chang, E. S. & Noyes, R.W. 1983 *Ap.J.* **275**, L11.
Cuntz, M. & Muchmore, D.O. 1994 *Ap.J.* **433**, 303.
Cuntz, M., Rammacher, W. & Ulmschneider, P. 1994, *ApJ.* **432**,690.
Deming, L.D. & Plymate, C. 1994 *Ap.J.* **426**, 382.
Deming et al 1987, *ApJ.* **316**,771.
Deming, L. D. , Boyle R.J. , Jennings, D.E. & Wiedemann G. 1988, *Ap.J.* **333**, 978.
Dravins, 1982 ARA&A 20,61 and 1985, IAU Coll. 88, Stellar Radial Velocities.
Dravins, D. 1994, in The impact of long-term monitoring on variable star research, (eds. de Groot & Sterken), Kluwer Acad. Publishers.
Eckart, A. & Genzel, R. 1996, *Nature*, Vol. **383**, 415.
Encrenaz, T., 1994, *The Messenger*, No. **75**, 12.
Goldman, A. et al. 1980 *, New Atlas of IR Solar Spectra* Vol. **2**, Dept. of Physics, Univ. of Denver.
Grevesse, N. & Sauval, A.J. 1994 in *Molecular opacities in the stellar environment*, (ed. U.G. Jørgensen), IAU Coll. 146,
Hatzes, A. 1996, Report to ESO Working Group on Extrasolar Planets.
Hatzes, A.P. & Cochran, W.D. 1992, in Proceedings of ESO Workshop on High Resolution Spectroscopy with the VLT (ed. M.-H. Ulrich).
Heasley, J.N., Ridgway, S.T., Carbon, D.F., Milkey, R.W. & Hall, D.N.B. 1978, *Ap.J.* **219**,970.
Hewagama, T., L.D. Deming, D.E. Jennings, V. Osherovich, G. Wiedemann, D. Zipoy, D.L. Mickey, & H. Garcia 1993, *Ap.J.* Suppl, **86**.
Hinkle, K.H , Wallace L. & Livingston, W. 1995, *Arcturus Atlas*, Astron. Soc. of the Pacific, San Francisco.
Jennings, D.E., Deming, L. D., Wiedemann, G. & Keady, J. J., 1986, *ApJ.* **310**, L39.
Kelch, W.L., Linsky, J.L., Basri, G.S., Chiu, H. , Chang, S., Maran, S.P. & Furenlid, I. 1978, *Ap.J.* **220**, 962.
Kurucz, R.L. 1992, *Rev. Mexicana Astron. Astrof.* **23**, 187.
McMillan et al 1993, *ApJ.* **403**, 801.
Maihara, T., Iwamuro, F., Hall, D.N.B., Cowie, L.L., Tokunaga, A.T. & Pickles, A.J. SPIE, 1993, Vol. **1946**, 581.
Maillard, J.-P. 1992 in Proceedings of ESO Workshop on High Resolution Spectroscopy with the VLT (ed. M.-H. Ulrich).
Mayor, M & Queloz, D. 1995, *Nature*, Vol. **378**, 23.
Moorwood, A.F.M. & Wiedemann, G. 1992, in Proceedings of ESO Workshop on High Resolution Spectroscopy with the VLT (ed. M.-H. Ulrich).
Ridgway, S. & Hinkle, K 1992, in Proceedings of ESO Workshop on High Resolution Spectroscopy with the VLT (ed. M.-H. Ulrich).
Saar, S.H. & Linsky, J.L. 1985 *Ap.J.* **299**, L47.
Saar, S. 1995, in Stellar Surface Structure, IAU Symp. 176.
Sneden, C. et al 1995, *PASP* **107**,997.
Wallace L. & Livingston, W. 1992, *An Atlas of a Dark Sunspot Umbral Spectrum from 1.16 to 5.1 µm*, KPNO/NSO Technical Report.
Wiedemann, G., Ayres, T.R. , Saar S.H. & Jennings, D.E. 1994 *Ap.J.* 423.
Wynn-Williams C.G. & Becklin, E.E. 1987 (eds.) Infrared Astronomy with Arrays, eds., Univ. of Hawaii, Hilo.

Günter Wiedemann
e-mail: gwiedema@eso.org

REPORTS FROM OBSERVERS

Star Formation in NGC 6611 with ADONIS and Hubble

D. CURRIE, K. KISSELL, ED SHAYA, P. AVIZONIS AND D. DOWLING, University of Maryland
D. BONACCINI, ESO

New details of the star-formation process have been revealed by a co-ordinated use of the ADONIS system on the 3.6-metre telescope at La Silla, in combination with data from the WFPC2 Camera of the Hubble Space Telescope. In this very preliminary report, we illustrate some of the unique capabilities of the ADONIS system for high-resolution near-infrared observations of the stellar formation process.

The observations address NGC 6611 (also known as M16 or as the Eagle Nebula). This is a dense molecular cloud in which a small cluster of high-mass stars has recently formed. The very high ultraviolet flux emitted by these early-type stars has dispersed or "photo-eroded" surrounding regions of the molecular cloud. Variations in the density of the gas and dust of the cloud have resulted in an uneven irregular erosion, forming the "elephant trunks" seen in the ground-based image shown in Figure 1. Investigation of the details of the resulting structure gives a measure of the resistance of the cloud to the photo-erosion process, which, in turn, is a measure of the density of the various regions of the cloud. While other properties, such as the magnetic field and local temperature, may also affect the rate of erosion, this may be one of the most direct methods of measuring the density profile about pre-protostellar objects.

These data were taken by Douglas Currie with Kenneth Kissell of the University of Maryland and Domenico Bonaccini of ESO. The generous support of the La Silla 3.6-m telescope team was also determinant. This preliminary image processing has been conducted by Ed Shaya, Petras Avizonis, and Dan Dowling of the University of Maryland. The analysis of these data will be conducted by this group, in collaboration with other members on the WPFC2 IDT team (i.e., Jeff Hester, Paul Scowen and others) and other individuals at the University of Maryland. The observations described here were conducted in early May, 1996 on the 3.6-metre telescope at La Silla using the ADONIS adaptive optics system and the SHARP II NICMOS Camera.

The scientific objectives of these observations are to provide observational data for the understanding of star-formation processes. These three areas of particular interest to us and the targets of our succeeding analyses consist of:

Figure 1: M16 Nebula (North to the top). A ground-based image of the nebula obtained by David Malin illustrates the context of our observations of M16. Observationally, M16 consists of a cluster of early-type, very luminous, very massive young stars and an HII region containing "elephant trunks" or "columns". The early-type stars have photo-eroded most of the molecular cloud leaving behind the structures in the HII region. Fluctuations in density in the original molecular cloud caused irregularities in the photo-erosion process. In particular, on the large scale, the "elephant trunks" pointing north-west, i.e., towards the hot stars, are the result of large-scale density fluctuations which have shielded portions of the molecular cloud from photo-erosion. On the smaller scale, which is our area of interest, we will see "bumps" and "pimples" caused by the smaller density variations. We believe that this is due to the excess material in self-gravitating pre-protostellar regions. The solid outline indicates the extent of the WFPC2 image.

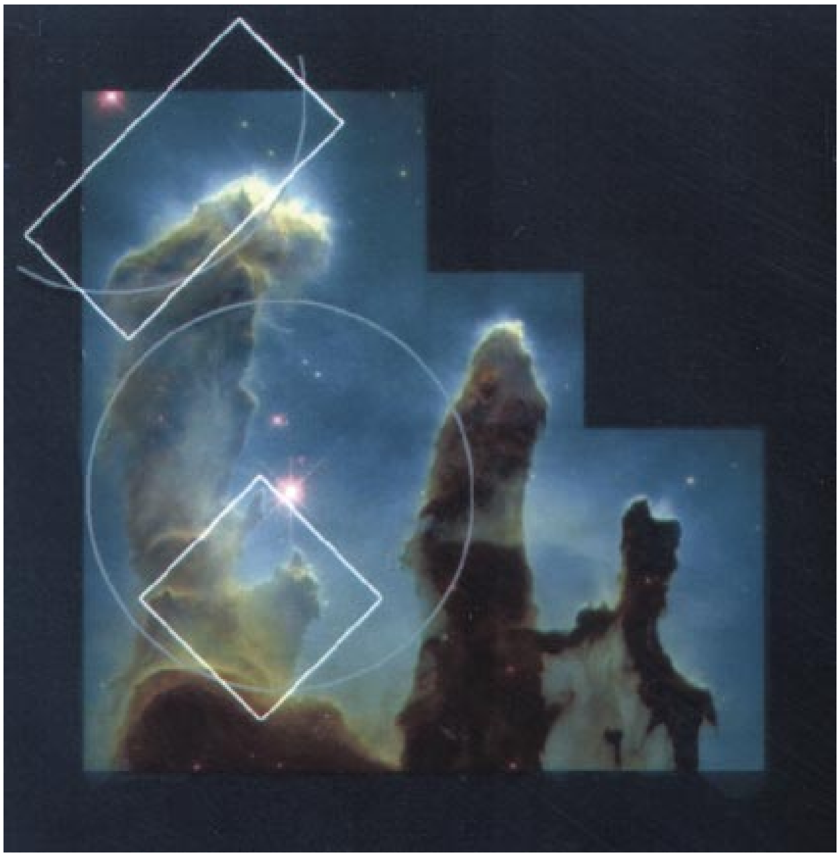

Figure 2: WFPC2 emission-line image of the central portion of the HII region of M16. North is on the upper left. This was obtained on the WFPC2 of the Hubble Space Telescope on 22 April 1995 (Hester et al., 1996) and is a colour composite in which the red image is in the ionised sulphur [SII] filter, the green image is Hα and the blue image is doubly ionised oxygen [OIII]. This colour sequence is in order of the energy of ionisation. The solid outlines illustrate the boundary of the regions mapped using the ADONIS System on the 3.6-metre telescope at La Silla. The upper region (denoted the "TIP") explores the top of Column III and the region above the column. The lower region, denoted "367", is located near Walker Star #367. The gray circles indicate the outer limits of the ADONIS field of view due to the optical mount for a beam splitter in the ADONIS optical system.

developed initially by Walker, et al. (1988), by Chini et al. (1990), and by Hillenbrand et al. (1993). In each case, the primary limitations have been resolution (with overlap of objects due to the extreme crowding), and limiting magnitude in various bands. The combination of the increased resolution and the deeper exposures of the ADONIS data, and the capabilities of Hubble, should permit a significant extension of the analysis of Hillenbrand.

(1) Density Profiles of Dust and Gas as a Function of the Stage of Stellar Formation

The dimensions of the features revealed in the Hubble data yield information related to the density profile of the in-falling dust and gas. For example, we can obtain a "characteristic size" related to the current stage of the formation process for a given object. The ESO data should allow us to place an object within the normal classification schemes for star formation, i.e., from the classes described by Hillenbrand to the very early class described, for example, by André (1995).

(2) Direct Evidence of Pre-Main Sequence Objects for the Fainter Components of M16

M16 has long been an interesting region in the search for "pre-main sequence" objects. Such work has been

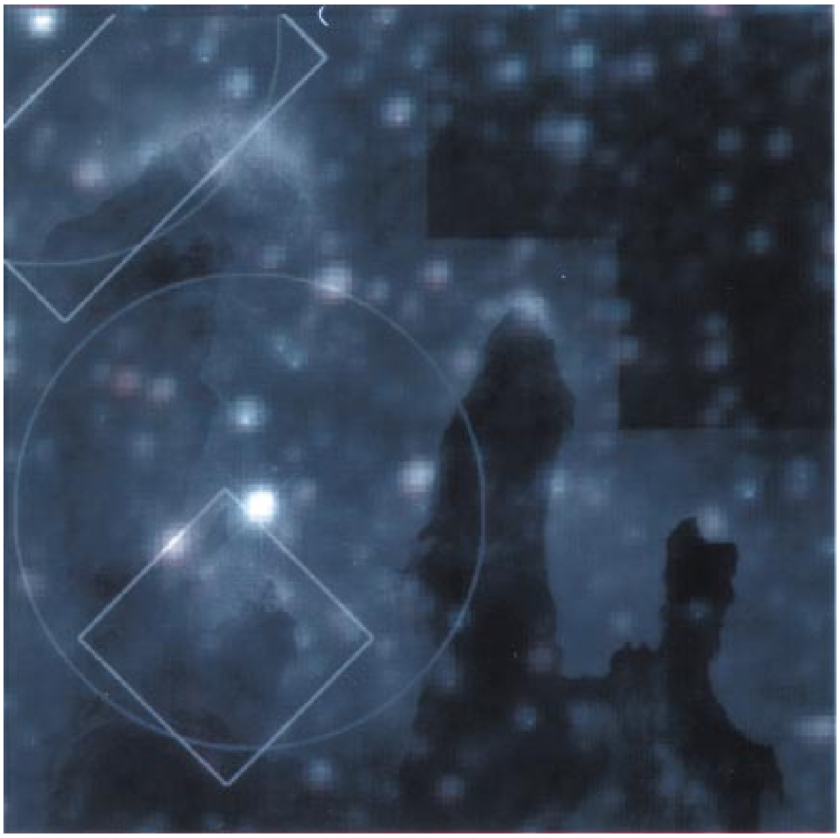

Figure 3: Infrared Structure of the WFPC2 area. North is on the upper left. This figure illustrates the general context of the Hubble Space Telescope observations, as illustrated by recent ground-based observations in H and K bands (Hillenbrand et al., 1993). The published version of the Hillenbrand data covers 225 square minutes to a limiting magnitude of about 14. Figure 2 shows only the portion which directly corresponds to our Hubble image. This image is a colour composite using the J and K magnitudes as the blue and red images. The white "ghost" image is the same region in the filter for Hα emission from our WFPC2 observations. Thus the white "cores" of the stars come from the Hubble data. The regions which were observed at La Silla in J, H, and K bands are indicated by the rectangular outlines.

Adaptive Optics at ESO is Delivering Exciting Science

Figure 1: Adonis K-band 10-sec-exposure image of a point source obtained at the 3.6-m telescope on La Silla (top). The look-up table is power 1/4th in order to highlight the low level features. The corresponding uncorrected 10-sec-exposure image is shown at the bottom.

Adonis is the ADaptive Optics Near Infrared System that ESO is regularly offering since December 1994 on the La Silla 3.6-m telescope. The instrument has been built by the Observatoire de Paris-Meudon as a follow-up of the previous ComeOn+ system. It is equipped with Sharp II and Comic IR cameras, to cover the range 1–5 μm. They have respectively been built by the Max-Planck-Institut für Extraterrestrische Physik in Garching and a team from Observatoire de Meudon and Observatoire de Grenoble in France. Foreoptics allows for polarimetry, Fabry-Perot Spectroscopic imaging with resolving powers R = 900 and 2500 in K-band, and by the time you will read this article also coronography. For a detailed description see our web pages on www.eso.org.

Observations with Adaptive Optics is still a virgin territory in astronomy, with plenty of fruits to pick. Many observers have already used it and an updated publication list is kept in the Web. Adonis is so far regularly oversubscribed by more than a factor 2. We often see excited scientists leaving La Silla with their data, and we encourage them to publish in The Messenger *reports on their preliminary results. This will help new observers and encourage healthy competition.*

If you are planning to observe with Adaptive Optics for the first time, some preparation to find the best tricks to observe your own object is necessary. Especially the data calibration, both spatial and photometric, requires good planning of the observing nights. ESO is trying to help with web pages at the www.eso.org site, which will act more and more as user manual and tips recorder on line, as well as with technical support during your proposal preparation.

For the data processing, ESO has come up with a dedicated software package called Eclipse, which has a pipeline, number crunching approach. The goal is that the observer checks his/her data possibly during the observing run itself, in order to better focus on the scientific targets he/she is getting. Thanks to a collaboration with Dr. J. Christou from the Starfire Optical Range [NM-USA], we will attach to Eclipse powerful iterative deconvolution software tailored to adaptive optics data.

Domenico Bonaccini,
dbonacci@eso.org

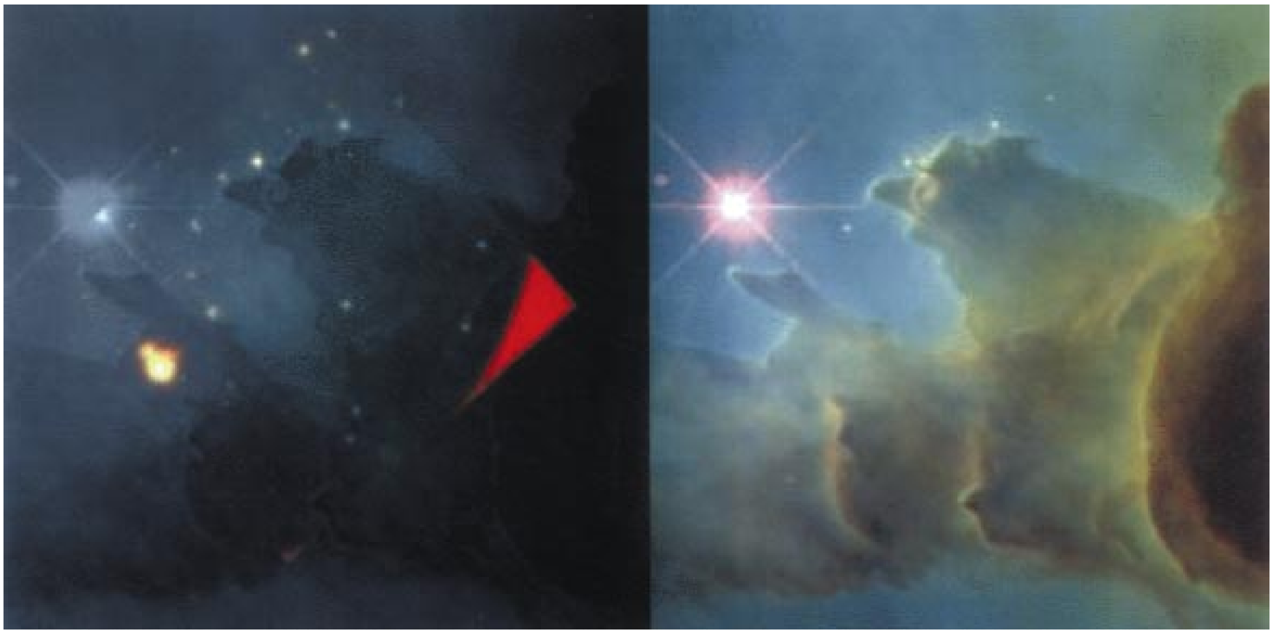

Figure 4: ADONIS observation of Region 367. North is to the bottom left. This picture is rotated by ~90° counterclockwise when compared to Figs. 2 and 3. This region near Walker Star #367 is the primary target region of interest for our M16 observations at La Silla (left). The images in the colour composite consist of the red for K, green for J, and blue for H band observations. The white background image (the "ghost" image) is the Hα data from our WFPC2 observations. This region has a large number of bumps where the photo-erosion process is slowed by positive density fluctuations of different sizes. These specific areas are discussed later. The ADONIS image is 37″ by 37″ which represents four pointings of the 25.6 × 25.6 arcsecond FoV of the SHARP II Camera. The resolution (before image deconvolution) is about 280 mas FWHM for the K-band. This is within a factor of two of that which can be achieved in the visible on the Hubble Space Telescope. The red region at the edge of the left image is the annular mount which holds the beam-splitter, the red colour illustrates the low (300 K) temperature of the emission of this room-temperature object. The high-resolution information obtained by the dual use of Hubble and ADONIS allows a unique probe into the star-forming region. Multiple systems are now resolved.

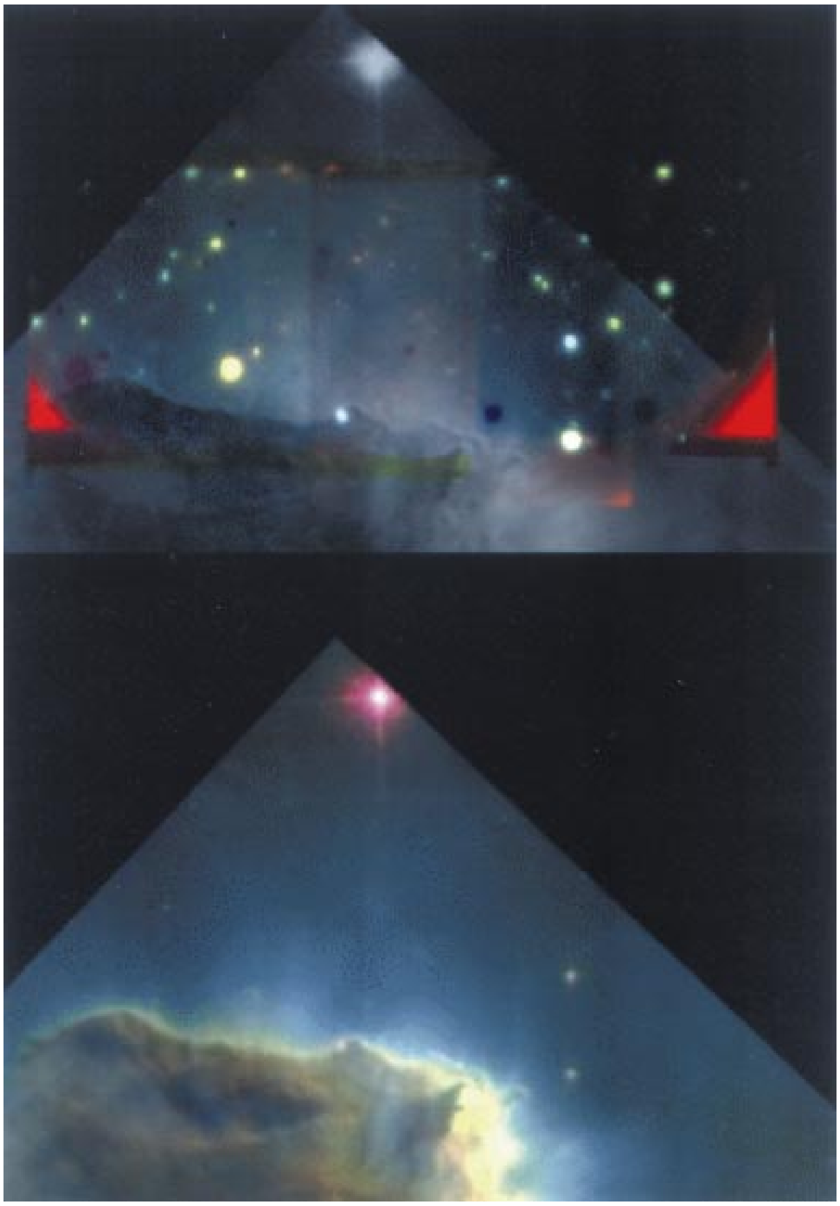

Figure 5: ADONIS observations of TIP (top). North is up. This figure illustrates the region around the "TIP" of Column III. As in Figure 4, this figure is composed of both WFPC2 and ADONIS observations. The region contains a number of protrusions of different sizes and very high activity due to the proximity to the blue stars.
Many of the objects detected in the ADONIS are above and outside of the molecular cloud of the tip, indicating that they are not directly associated with the column.
The outline of this image is 60″ by 32″ which consists of the data from six individual pointings in K band and four pointings in H band and J band. The resolution is about 280 mas (FWHM). This image has the same colour combinations as described for Figure 4.

(3) Investigation of the Very Red Source 367 B

About 10″ from Walker Star 367, there is a very strong infrared source which does not appear in our V filter data. This appears to be a double star which is buried within the column. This may be a star imbedded indeed within the column. Its colours, and the measures of extinction will reveal much about the star, and the internal structure of the column.

Because far-infrared data are needed in order to distinguish the early stage of the individual star-formation regions, the programme at the University of Maryland is currently using data which we have obtained using Hubble WFPC2 data, 350-micron data from Caltech Submillimeter Observatory using the GSFC bolometer array, and the millimetre interferometric observations obtained with the Berkeley-Illinois-Maryland (BIMA) array in addition to the data from the ADONIS observations at ESO.

Figure 2 illustrates the regions observed at La Silla in the context of our recent WPFC2 observations, and Figure 3 shows the context with respect to the existing near infrared observations.

Figures 4 and 5 show the WFPC2 observations at the bottom and the ESO data at the top. At present, the ESO data, with its infrared sensitivity, show far more objects than are visible in the Hubble data.

It is critical to obtain the best resolution in order to understand the extended nature of the objects. To this end, we are using the Lucy algorithm for the deconvolution. This can remove the extended, one-arcsecond skirt of the Adaptive Optics PSF due to the correction residuals, as illustrated in Figure 6. The presence in adaptive optics corrected images of an extended halo around the central high-resolution object is typical. This has been observed and its cause is well understood. It is due to uncorrected higher spatial frequencies, and in some cases to deformable mirror "actuator print-through", whose regular pattern makes four secondary peaks in the PSF. Astronomers who are looking for faint structures underneath this skirt, will have to familiarise themselves with deconvolution, as well as take care that enough SNR is present in the observed object and structure.

A major objective in our high-resolution observations using the ADONIS system has been to identify the relation between the morphology seen in our images from the Hubble Space Telescope and the conventional knowledge concerning the process of star formation as known through observations in the infrared wavelength region. Historically, as shown in the process of obtaining successively higher resolution observations of NGC 6611 (e.g. the successive works of Walker, Chini, and Hillenbrand), the understanding of the physics depends sharply upon the ability to resolve fine features and separate multiple star systems. We now present some of the preliminary results in addressing this relationship. In particular, in this section, we will address three specific features indicated by the morphology of our Hubble Space Telescope images.

The "stalk" star (also known as EGG 041, Hester et. al., 1996) which is indicated as "C" in Figure 7 suggests a density concentration which is resistant to the photo-erosion process, resulting in a sharp protrusion. This is seen as a point source in the visible and a strong, co-located point source in the J, H, and K band. Thus this object appears to be a YSO. However other morphologically interesting features have not, in general, displayed an infrared component. The feature "A" (also known as EGG 039), for example, appears to be a strong density fluctuation with a relatively small characteristic size of a few hundred AU. There is an infrared source (B) which is located relatively close to A and which has, in the past, been tentatively identified with A. However, the ADONIS data, with their high resolution and suitability for precise astrometry, indicate that this source is most probably a background source. The morphological feature, A, is located approximately 1 arcsecond from the infrared source, B, but is not aligned with the latter. It is unlikely that the infrared source is the uncovered generator of the density fluctuation. Thus it appears that B is a background source and that we do not have, at our current limiting magnitude, a source which appears to be contained in the morphology feature A.

The other area of interest lies above the tip of the large column (Fig. 8). At the top of the column, there are many "fingers" i.e. features which have an extent of approximately 1000 AU in cross dimension and several thousand AU in length. They are then followed by a stem which is bent by approximately 90° and is typically a few thousand AU in extent and attached to the body of the column. These "fingers" are not associated with K-band sources, at our current limiting magnitude. However, one of these objects indicated by "C" in Figure 8 (also known as EGG 001), has been of particular interest. This appears to be an older or more eroded finger. It shows the typical finger structure of Sulphur II emission on the boundary. This eroded finger has two infrared sources, A and B which are located in the vicinity of C. The fainter source B is located more than an arcsecond from the morphology feature. It is also not "in line", so it cannot be the exposed source of the density enhancement which has been "excavated". Source A is located within the morphology feature. However it is located at the trailing end of the finger (with respect to the eroding source) and is significantly asymmetrical with respect to the central axis of C. Thus it likewise does not appear to be associated with C. Most likely, both infrared sources are background objects. The final determination of the status of these objects will result from detailed colour studies of comparing A and B with nearby sources and, perhaps, an evaluation of the silicate absorption feature.

Preliminary Conclusions

The primary scientific conclusions which can be addressed at this time are: (1) the columns appear to be extremely dense (greater than 20 magnitudes of visual extinction over a major part of their area), and (2) the density enhancements identified by the HST images do not contain protostars with a 2-micron signature (at our current level of sensitivity). Most of the stars (seen in the regions which are not obscured by the columns) are background stars in the gal-

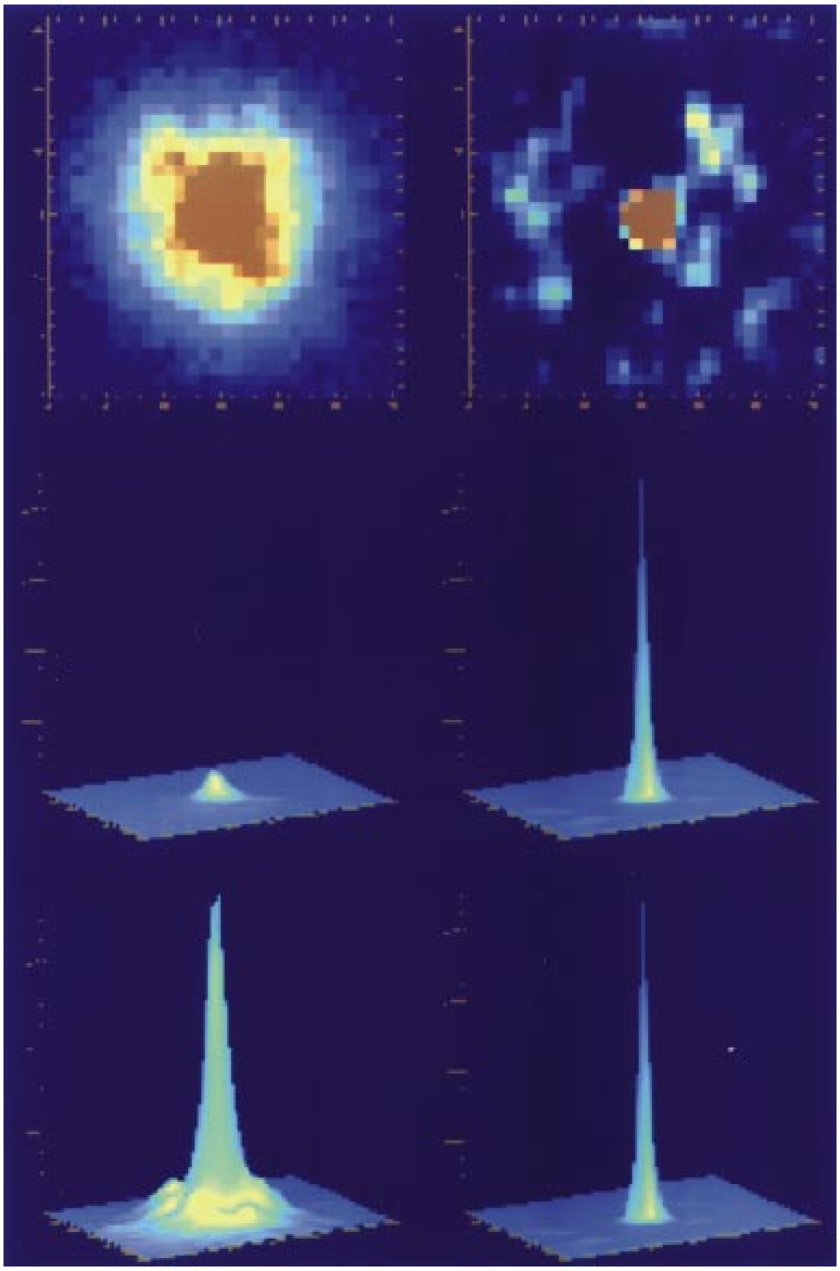

Figure 6: Image Deconvolution in K band: In order to utilise fully the higher frequency components available in the ADONIS data, we need to perform an image deconvolution and/or image reconstruction. For the present data, we use our Lucy-Richardson procedures developed for the Hubble Space Telescope modified for adaptive optics images (Currie et al., 1995). This will allow an improved understanding and identification of the extended and double sources. The top left figure is the image of a (nominally) point source in our K band data set, 27″ from the WFS reference star. The reference star has m_V = 11.26 and B–V = 0.45. The small patch is 3″ square, and the FWHM of the image from ADONIS is 0.28″ at this offset distance. Due to field anisoplanatism, we see indeed a lowering of the PSF Strehl Ratio to about 8%. This same image is shown in a three-dimensional surface representation in the centre-left and lower left images. The deconvolved images are shown along the right side. In this case, the FWHM of the deconvolved image is 0.13″. The centre image pair is normalised to illustrate the improvement obtained in the Strehl ratio (about a factor of 12, one third of the gain coming from the reduction of the width of the core and the remainder coming from the redistribution of the energy in the extended base of the image) The bottom image pair is normalised to illustrate the narrowing of the peak and the extended structure at the base of the ADONIS image. The wings out to about 1″ are normal for an adaptive optics system. One sees that there are specific features associated with the ADONIS class of AO system. The sub-peaks are probably due to print-through from the regular pattern of actuators in the deformable mirror. This same feature can be seen in the Starfire Optical Range (NM) data described in a earlier publications (Christou et al., 1995 ; Currie et al., 1995). To date we have performed a spatially independent deconvolution but later expect to evaluate the spatially dependent effects and then use our full algorithm.

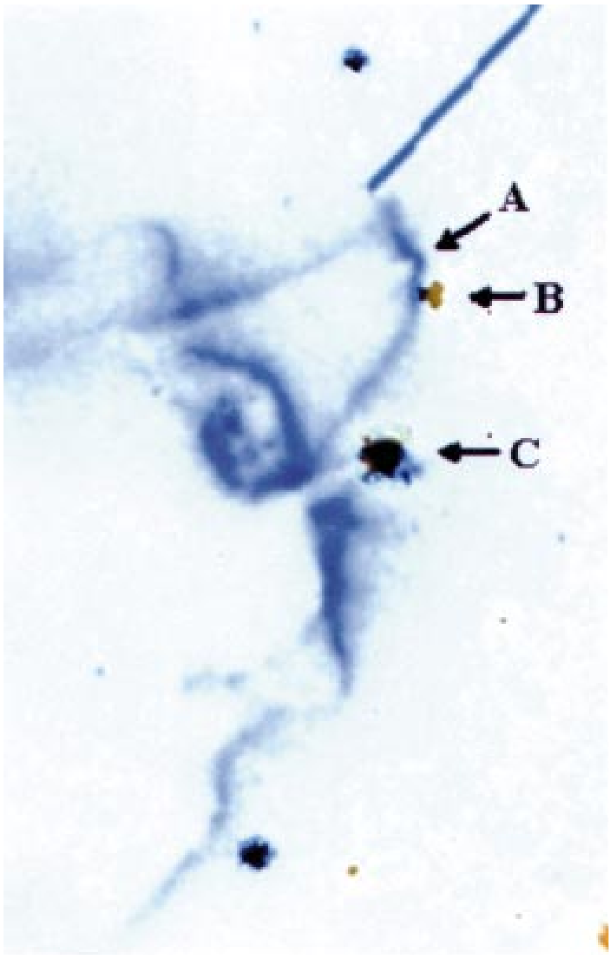

Figure 7: This image is a superposition of the K-band picture obtained using the SHARP II Camera and the ADONIS system on the 3.6-metre telescope at ESO (in red) with the HST image, obtained in the Sul-phur II emission using the F673N filter, displayed in blue. North is up. It is an enlargement of the upper right square inset of Figure 2 near Walker 367. The spatial registration of the two images was obtained by aligning about 15 stars (mostly outside this field of view). The agreement in the positions of these 15 alignment stars is of the order 0.1 arcsecond, over the entire ESO field of view, covering 35 by 35 arcseconds. This internal agreement among the reference stars is more accurate, by a factor of at least 5 times, than the location offsets which are discussed in the text.

axy, with significant extinction. From an Adaptive-Optics technology point of view, we have illustrated the potential for a large improvement in the PSF (or Strehl ratio) across the observed field from the use of deconvolution procedures.

It is clear that deconvolution techniques will contribute considerably to the astrophysical throughput of Adaptive Optics. Iterative deconvolution capabilities are being added to the ESO eclipse pipeline processing software, to be used routinely on Adonis data.

References

1. André, P. Low-Mass Protostars and Protostellar Stages. *Astrophysics and Space Science*, vol. **24**, p. 29, 1995.
2. Chini, R. and Wargau, W.F. Abnormal Extinction and Pre-Main Sequence Stars in M16. *Astronomy and Astrophysics*, vol. **227**, p. 213, 1990.
3. Hillenbrand, Lynne A., Massey, Philip, Strom, Stephen E. and Merrill, K. Michael. NGC 6611: A Cluster Caught in the Act. *The Astronomical Journal*, vol. **106**, no. 5, p. 1906–1946, 1993.
4. Walker, H. J. and Wolstencroft, R.D. Cool Circumstellar Matter around Nearby Main-Sequence Stars. *The Astronomical Society of the Pacific*, vol. **100**, p. 1509–1521, 1988.
5. Hester, J. Jeff, Scowen, Paul A., Sankrit, Ravi, Lauer, Tod R., Ajhar, Edward A., Baum, William A., Code, Arthur, Currie, Douglas G., Danielson, G. Edward, Ewald, Shawn P., Faber, Sandra M., Grillmair, Carl J., Groth, Edward J., Holtzman, Jon A., Hunter, Deidre A., Kristian, Jerome, Light, Robert M., Lynds, C. Roger, Monet, David G., O'Neil, Earl J. Jr., Shaya, Edward J., Seidelmann, Kenneth P. and Wesphal, James A. "Hubble Space Telescope WFPC2 Imaging of M16: Photo-evaporation and Emerging Young Stellar Objects." *The Astronomical Journal*, Volume **111**, No. 6, 1996.
6. Currie, Douglas G., Avizonis, Petras V., Dowling, Daniel M., Kissell, Kenneth E., O'Leary, Dianne P., Nagy, James G., and Fugate, Robert Q. "Approaches for Image Processing Supporting Adaptive Optics". 1996. In Proceedings (edited by M. Cullum), Topical Meeting on Adaptive Optics, October 2–6, 1995, Garching bei München, Germany, by the European Southern Observatory, p. 299–304.
7. Christou, J.C., Ellerbroek, B., Fugate, B.Q., Bonaccini, D. and Stanga, R. "Rayleigh Beacon Adaptive Optics Imaging of ADS 9731: Measurements of the Isoplanatic Field of View" , 1995, *ApJ*, **450**, 369–379.

Domenico Bonaccini,
dbonacci@eso.

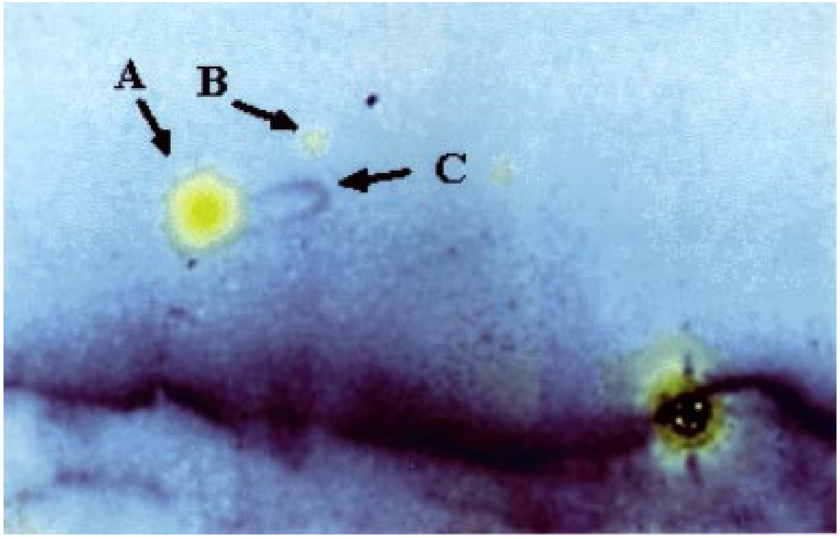

Figure 8: This is a magnified region located above the tip of the largest column in our HST image (see Figs. 2 and 5 – top). North is up. The picture is a superposition of Sharp II K-band and HST images, with the red and blue components as indicated in Figure 7. The astrometric alignment was performed using our centroiding algorithms in order to translate, rotate and rescale the images, as in the above figure. Once again, the agreement in the positions of the 7 reference stars is of the order of 0.1 arcsecond.

On the Shape of the Point Spread Function at the NTT + SUSI

R. FALOMO, Osservatorio Astronomico di Padova, Italy

The actual shape of the Point Spread Function (PSF) is of great importance for several applications. It affects both the spatial resolution and the signal-to-noise ratio of the observations. For a ground-based telescope, the observed PSF shape is in general a combination of instrument and atmospheric effects, with the latter usually dominant during average seeing conditions. Radial brightness profiles of stellar images were already studied more than 20 years ago by King (1971) over a range of several magnitudes using photographic plates. It was found that the PSF has a core (that is commonly described by a Gaussian profile) and a wide wing that produces an extended *halo* around star images (see also Racine, 1996, for further discussion).

A good knowledge of the PSF shape and of its possible variations within the field and with time is crucial when observations at the limit of the instrument capabilities are considered. In this note a quantitative estimate of the difference in instrument performances as a function of PSF changes, based on observations collected at the NTT, is reported.

In the course of a programme aimed at studying faint nebulosities around quasars and BL Lac objects (in collaboration with M.-H. Ulrich) we have obtained several images with the NTT + SUSI (pixel scale 0.13″/pixel) during different sky conditions. The telescope was used in remote control from Garching in January 1996 and the seeing ranged from 0.5 to 1.2 arcsec. In each CCD frame we studied the shape of stars of different magnitude and location in the field. For each object we secured one short (p 2 minutes integration) and one long (p 20–30 minutes). No significant trend of star shape was found by comparing short- and long-exposure images, indicating that guiding and tracking were good. From the analysis of the images obtained in sub-arcsec seeing, the shape of the stars was found to be slightly elliptical (ellipticity ε P 0.05 to 0.1) with only a marginal dependence on the position in the field.

The radial brightness profiles of the star images were derived from the azimuthal averaging of fluxes, and for each frame a combined profile was produced by merging stars of different magnitudes. We also used saturated stars to extend the profile over several magnitudes after checking that the region of the profile in common with that on non-saturated stars was in good agreement. In spite of small differences of ellipticities of the star images, the azimuthally averaged radial profiles of stars in the same frame are rather similar.

Figure 1a shows a comparison of the PSF profiles obtained during different seeing conditions from various CCD frames. Profiles are normalised to the same peak flux. Seeing values are estimated from the FWHM of the core of non-saturated star images. In Figure 1b the same profiles are reproduced after normalisation to the total flux. This yields a direct idea of how the same point-like object is observed under different seeing conditions. In particular, the large (p 2 mag) difference in the peak flux from 0.5 to 1.2 arcsec seeing is evident. Also a significant difference is present in the extended wing whose surface brightness changes by p 1.5 mag in the same seeing interval (0.5 to 1.2 arcsec). While the variation in the inner part of the PSF influences mainly the spatial resolution and the capability of detecting isolated faint sources, the rise in the wing of the PSF as seeing degrades is a limiting factor when studying features close to bright point-like sources. This is the case for instance in studying host galaxies of quasars and BL Lacs.

The relatively large surface brightness of the PSF halo tends to hide the presence of a real nebulosity (the host galaxy) around the quasar. On the other hand, a poor evaluation of the shape of the PSF may lead one to derive an erroneous contribution of the host galaxy or

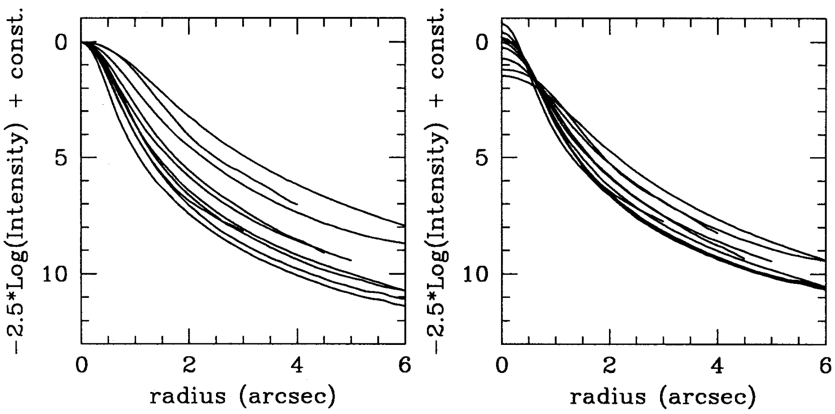

Figure 1: Comparison of radial surface brightness profiles of stars observed with the NTT + SUSI (R filter) under different seeing conditions (FWHM = 0.5 to 1.5 arcsec). The profiles are normalised to the peak flux (a) and to the total flux (b).

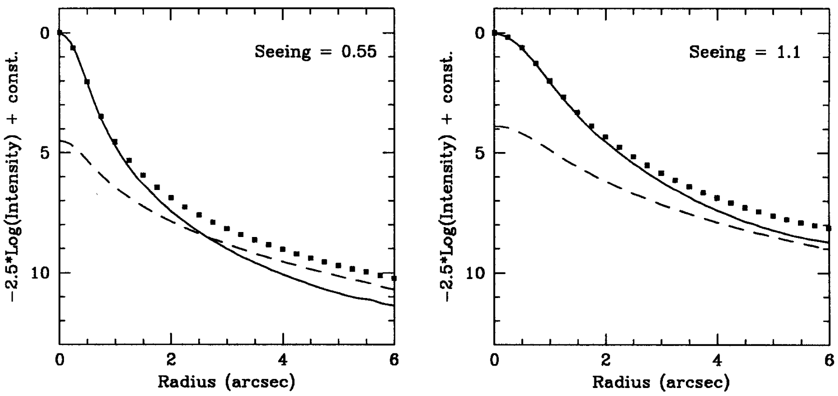

Figure 2: (a): A simulated observation of a quasar (filled squares) through 0.55″ seeing hosted by an elliptical galaxy (dashed line) of effective radius 10 kpc at z = 0.3 and contributing 10% to the flux of the point source (solid line). (b) Same as (a) but for 1.1″ seeing.

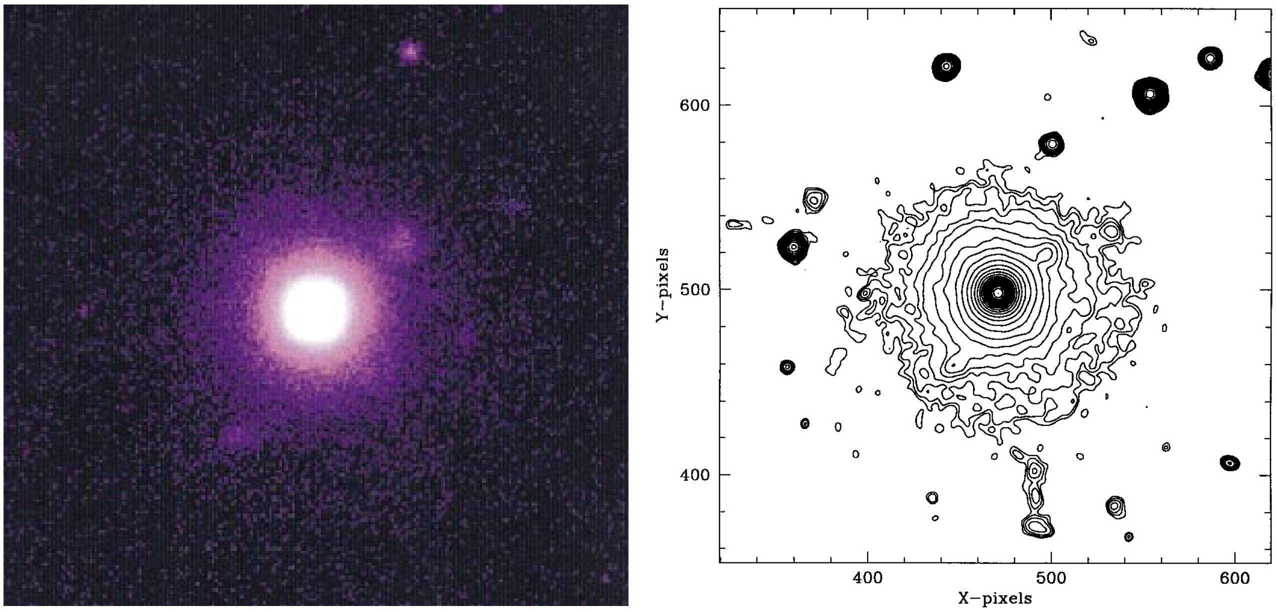

Figure 3: (a): R-band image of the Flat Spectrum Radio Quasar PKS 0736+01 obtained with the NTT + SUSI. The field shown is 25 arcsec on the side with North to the top and East to the left. (b): Contour plot of the field: faintest magnitude is 25.5 per square arcsec and spacing between isophotes is 0.4 mag.

even to find unreal nebulosities if the PSF wing is underestimated. In Figure 2a, b the radial brightness profile of a quasar nucleus is superposed on that of an elliptical host galaxy (effective radius = 10 kpc at redshift = 0.3) of total magnitude 10% of the quasar luminosity after convolution with a PSF corresponding to 0.55 and 1.1 arcsec seeing. The ratio of 10% is roughly the relative ratio found from HST observations for low-redshift quasars observed by Bachall et al. (1997).

With p 0.5 arcsec seeing, the emission from the host galaxy begins to be detectable at p 1 arcsec and becomes greater than the PSF wing beyond p 3 arcsec. If the seeing is 1.1 arcsec, the same object is marginally resolved and the contribution of the galaxy remains below the PSF emission. In the real cases, one has to account for the S/N of the data that should be adequate to study surface brightness emission down to 25–26 mag/square arcsec. This can be obtained with NTT + SUSI in the red with exposures of less than 1 hour during dark time.

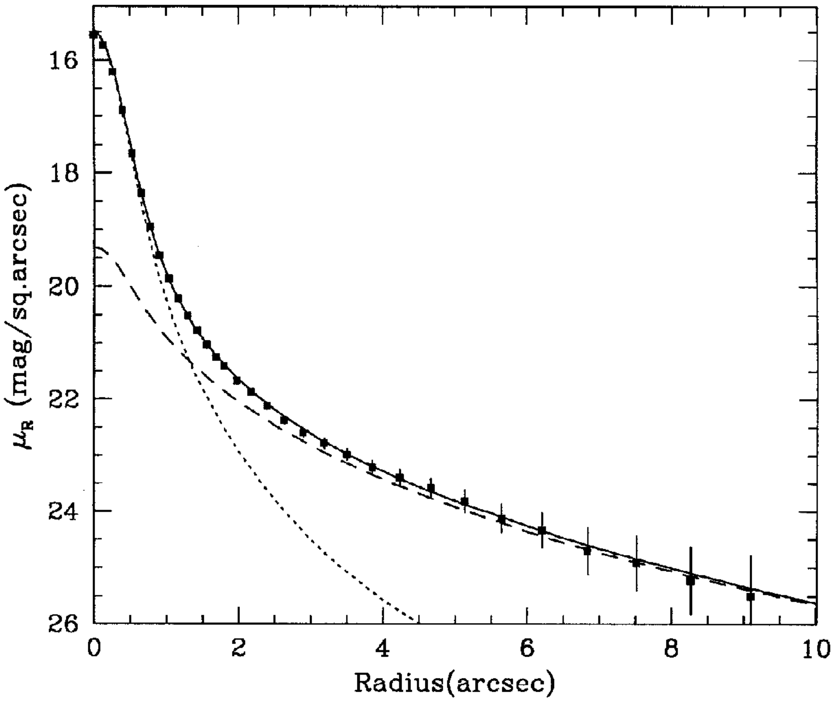

Figure 4: Radial surface brightness profile of the quasar PKS 0736+01 (filled squares) together with the best fit model (solid line). The point source is modelled by a scaled PSF (dotted line) while the host galaxy (dashed line) is given by an $r^{1/4}$ law convolved with the PSF.

In Figure 3 is reported an example of such an observation secured during the 1996 January run with the NTT + SUSI and R filter. The image shows the flat spectrum radio quasar PKS 0736+01 (*z* = 0.19) as well as two close resolved companions that are embedded in the nebulosity of the object. The radial luminosity profile (see Fig. 4) is very well represented by an elliptical galaxy with a bright point source in the nucleus. It is found that the galaxy has MR = –23.5 and effective radius of p 15 kpc ($H_0 = 50$, $q_0 = 0$). It is interesting to compare the observed shape of the PSF obtained during sub-arcsec conditions with that of HST. Figure 5 shows the comparison between NTT PSF with 0.55 arcsec seeing and HST + WFPC2 (F814W filter, PC1 detector) PSF as derived from TinyTim (Krist, 1996) model (no scattered light included). The curves are normalised to have the same total flux. While the region within p 1 arcsec from the nucleus is clearly better investigated with HST, at larger radii the contributions of the extended wing of the two PSFs are rather similar. The final comparison needs of course to account for different apertures of the telescopes, plate scale and detector performances. This may tend to favour HST data to investigate regions close to the nucleus and ground-based data for the external regions. A combination of the two would yield the optimal characterisation of the host properties.

In both cases, a good modelling of the PSF is a fundamental step for the application of techniques of image analysis as PSF subtraction, deconvolution and co-addition of images with different PSFs. Although there are some limitations (mainly due to the reliability of the models), PSF modelling yields noise-free comparison images that can be easily matched to the observed images. While for HST images a suitable model (e.g. TinyTim) is available (but there are some limitations as the lack of the scattered light contribution); for ground-based data this task is clearly more compelling given the strong seeing dependence of the PSF. From the observed shape of our NTT + SUSI star images it is found that a Moffat function, with β P 2.1 and FWHM that matches the seeing, is a good model down to p 10 magnitudes below the peak flux. Beyond this level, there appears to be an excess of the observed PSF with respect to the Moffat model. Although this model could work properly for image deconvolutions and co-additions, when accurate PSF subtraction is involved (as is the case of poorly resolved faint objects) the Moffat model may not be adequate.

References

Bahcall et al., 1997 *Ap.J*, in press.
King, I, 1971, *PASP*, **83**, 199.
Krist, J. 1996, The TinyTim User's Manual.
Racine, R., 1996, *PASP,* **108**,699.

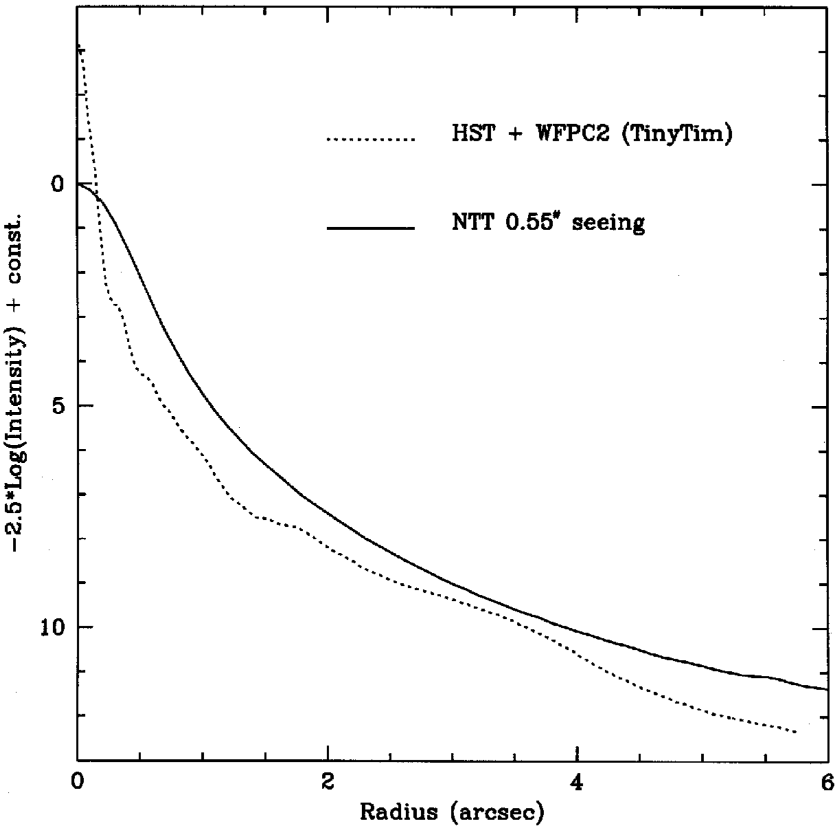

Figure 5: Comparison of NTT + SUSI observed PSF (seeing 0.55″) with HST + WFPC2 TinyTim model of PSF.

Quasar Hosts

A WORKSHOP JOINTLY ORGANISED BY ESO AND IAC

P. Crane and I. Perez-Fournon

The idea that the nuclei of normal galaxies are the hosts of the tremendously luminous sources known as quasars has been around for some time. New instruments and observational techniques have opened a view into the close environment of quasars and allowed us to explore their neighbourhoods and neighbours in unprecedented detail. The ESO/IAC workshop on Quasar Hosts was organised to discuss these developments and their implications. A main objective of the workshop was to explore the nature of the close environments of quasars as well as the relationship between quasars and their somewhat less lofty cousins; Active Galactic Nuclei and BL Lac objects.

This workshop was the first formal scientific contact between ESO and the Instituto de Astrofísica de Canarias (IAC) scientific communities on a topic of mutual scientific interest. The attendees represented most of the researchers active in this field from both communities as well as from outside the ESO and IAC communities.

The workshop venue was the very attractive Conference Centre of the Cabildo Insular de Tenerife in Puerto de la Cruz. Although some people accompanying participants complained about the weather, scientific and technical discussions occupied the full attention of the attendees. The topic, the venue, and the company served well to focus the attention on the objectives of the workshop. The details of the organisation were managed in excellent fashion by the staff at the IAC.

The plenary sessions of the meeting were scheduled over three full days from 24 to 26 September with a round-table discussion and summary on the morning of 27 September. In fact, the final discussion was extremely lively. So much that the local organisers had to shift the venue from the Conference Centre to the bus for the trip to the Observatorio del Teide.

The most exciting development presented at the workshop was the quality and diversity of the new data that are or are becoming available. Of course the results from HST were foremost in many people's minds. They were not disappointed. However, adaptive-optics systems are coming into operation and although the results are sparse so far, the promise is great. This will be especially true in the near-IR where the detector technology has made great advances. Indeed, there were several reports of NIR imaging of quasars, and their hosts were reported even without adaptive optics. To add to everyone's anticipation, several speakers presented results from ISO that were in a preliminary stage of analysis, but were clearly of high quality and promise.

Many attendees were attracted to the meeting by the idea of, or at least hearing tales of, naked quasars. This was not to be, although at least one speaker facetiously thought they might be found locally. These turned out not to be quasars and the images will not appear in the proceedings. It seems that to within the limits of current methods, all quasars are well surrounded by relatively normal

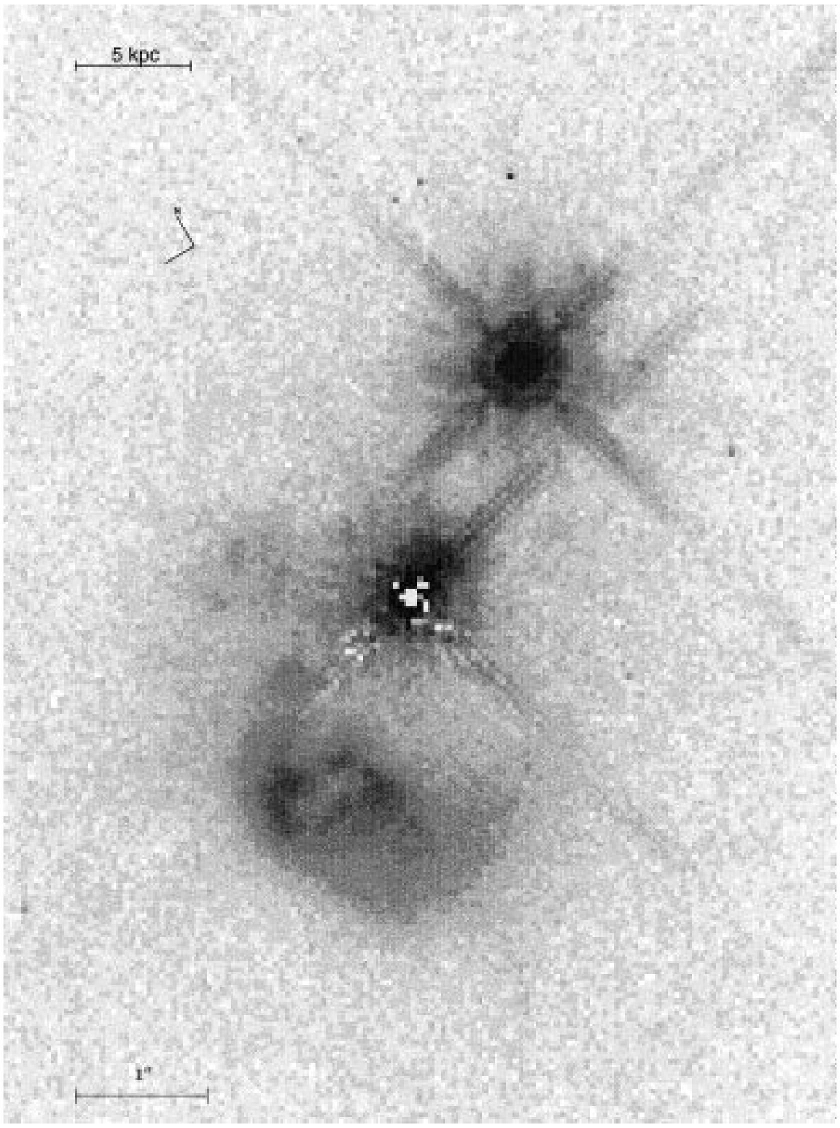

Figure 1: IRAS 04505–2958 is an infrared ultraluminous source which is also an optical QSO (i.e. by the criteria of Véron-Cetty and Véron in their catalogue). The figure shows two bright components separated by 1.6 arcsec, northernmost of which is known to be a foreground G star. Note the ring-like feature 1.5 arcsec south-east of the nucleus and a second clear "blob" 1 arcsec east of the nucleus with four or more other distinct but less luminous blobs beside it.
We interpret the image as a violent interaction between two galaxies, one of which at least was a spiral. The ring may be the ring galaxy left behind when one galaxy plunges vertically through the plane of a spiral. The prominent blob could be the displaced nucleus of the ring galaxy, the lesser blobs sites of star formation. The projected distance between the QSO and the centre of the ring is p 5 kpc ($H_0 = 75$) so that if the interacting galaxies collided at no more than 500 km/s, the one passed through the plane of the other less than 10^8 years ago.
Courtesy Peter Boyce, Department of Physics and Astronomy, University of Wales, Cardiff, UK.

galaxies of a wide variety of types and luminosities.

The relationship between active galaxies, ultra-luminous IRAS galaxies, quasars, and quasar hosts occupied many speakers, and much of the talk during the coffee breaks. Although there was no definitive scenario blessed by the participants, there were clear lines for further research to be followed up. Evidently, it was the connection between the new observational potentials and the possibility to further our understanding of the origin and evolution of nuclear activity that made this meeting so timely.

Philippe Crane
e-mail: pcrane@eso.org

ESO Libraries: Enhanced Services on the WWW

U. GROTHKOPF, ESO

These are exciting times for librarians. Never before have library services changed so quickly as they do now, and never before have library users requested access to such a variety of information resources within a minimum of time. Even more, our users want the important resources to be presented in an easily understandable way without having to read extended manuals, and, of course, they want them to be accessible from their desktops.

The World Wide Web (WWW) plays a major role in this scenario. It provides easy access to a large number of useful databases and other electronic resources (but note that the most comprehensive bibliography in astronomy and astrophysics still is only available on paper!) For libraries, the Web represents both a great challenge and a wonderful opportunity: We librarians need to know where to find the requested information, how to cope with the variety of access procedures currently used, and how to make sure electronic publications will be retrievable after many years despite their seemingly ephemeral nature. But we also have an extremely flexible tool at hand that allows us to present our services in an organised, clearly laid out way. The homepage has become the business card of a library.

When we designed the ESO Libraries homepage (http://www.eso.org/libraries/eso-libraries.html, Fig. 1) in early 1995, we had two kinds of users in mind: those who wish to find their own way to information resources should find links to the most important internal resources as well as external sites; those who prefer to just send their enquiries and requests to us must be able to do so from everywhere and at any time. The main options on our homepage were changed very little since then, but ease of access to some of the services has been improved. The following is a brief description of new or recently enhanced ESO Libraries services on the Web. Most of them can be reached from the Libraries Catalog and Databases page at URL http://www.eso.org/libraries/esocat.html. Should you wish to obtain more detailed information or have

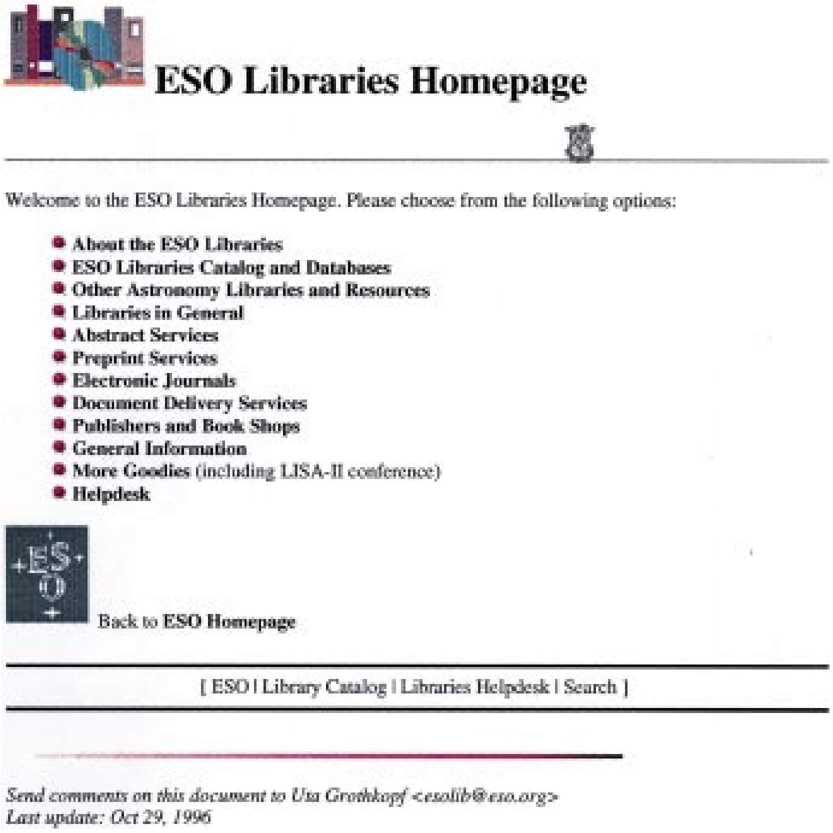

Figure 1: The ESO Libraries World Wide Web homepage.

questions regarding these and other services, please contact the librarians (esolib@eso.org).

1. World Wide Web Version of the Library Catalog

1.1 WebCat

The ESO Libraries catalog has been available on the Internet for three years and can be accessed by telnet. Since October 1996, ESO is among the first organisations to offer the library catalog through a World Wide Web interface. The WebCat is available at URL http://www.eso.org/libraries/webcat.html. It can also be reached via the libraries' homepage ESO Libraries Catalog and Databases / ESO Libraries Catalog and finally on the WebCat icon. In addition, it is directly accessible by clicking on the Library Catalog option on the top or bottom index bar on any ESO Libraries Web page.

1.2 IAU Thesaurus Terms Added to Catalog Records

The IAU Thesaurus was compiled for the International Astronomical Union, Commission 5 (Documentation) by R.M. and R.R. Shobbrook [1]. Its primary aim is to standardise the terminology used in astronomy by means of controlled vocabulary.

During the past summer, IAU Thesaurus terms were added to catalog records for astronomy books. All records to which the same thesaurus term was assigned can be found easily by clicking on the hypertext link in the WebCat. For an even more complete search, cross references from the initial search term will find catalog records that contain related, broader or narrower thesaurus terms.

2. Preprints Received in the ESO Library Garching

The library in Garching receives an average of 200 preprints per month from other astronomical institutes world-wide. Authors' names, titles, and issuing institutes are included in the preprints database which has been WAIS-indexed, so that search results will be displayed according to their relevance. Based on retrieved preprints, users can now complete their search by choosing from various options: links to the ADS Abstract Service and to the STEPsheet database

Figure 2: Publications of the ESO users community. The Web interface provides links to the ADS Abstract Service, the ESO preprint database and the SISSA electronic preprint archive. ▼

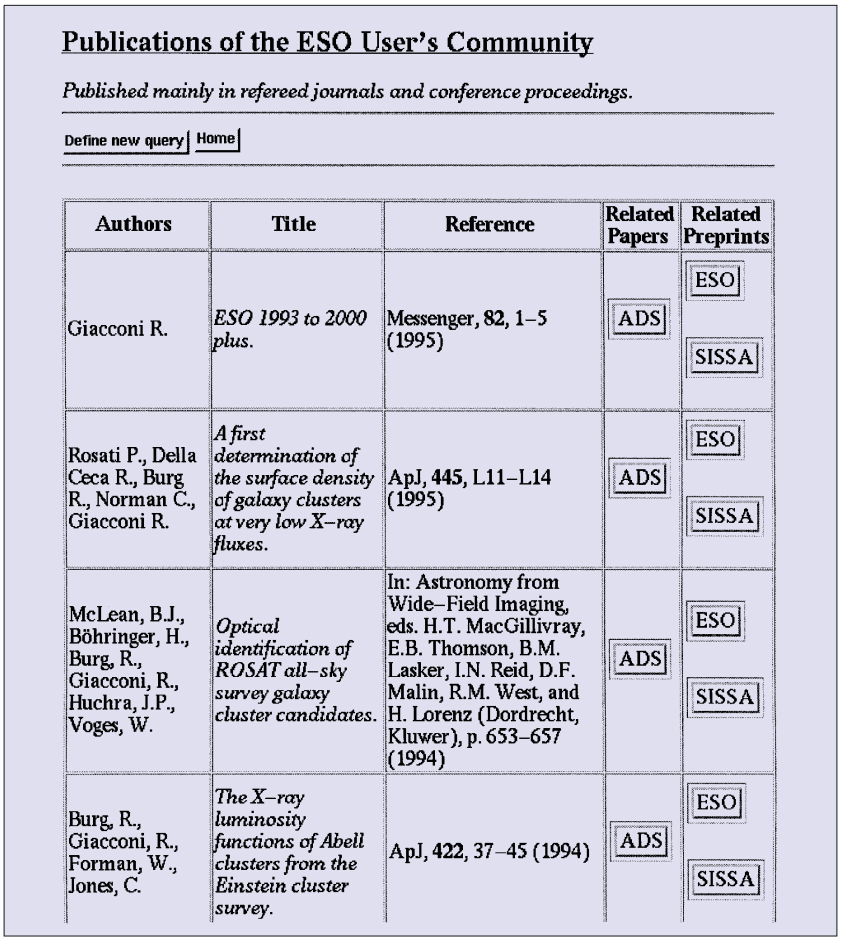

Publications of the ESO User's Community

Published mainly in refereed journals and conference proceedings.

Define new query | Home

Authors	Title	Reference	Related Papers	Related Preprints
Giacconi R.	*ESO 1993 to 2000 plus.*	Messenger, **82**, 1–5 (1995)	ADS	ESO SISSA
Rosati P., Della Ceca R., Burg R., Norman C., Giacconi R.	*A first determination of the surface density of galaxy clusters at very low X–ray fluxes.*	ApJ, **445**, L11–L14 (1995)	ADS	ESO SISSA
McLean, B.J., Böhringer, H., Burg, R., Giacconi, R., Huchra, J.P., Voges, W.	*Optical identification of ROSAT all–sky survey galaxy cluster candidates.*	In: Astronomy from Wide–Field Imaging, eds. H.T. MacGillivray, E.B. Thomson, B.M. Lasker, I.N. Reid, D.F. Malin, R.M. West, and H. Lorenz (Dordrecht, Kluwer), p. 653–657 (1994)	ADS	ESO SISSA
Burg, R., Giacconi, R., Forman, W., Jones, C.	*The X–ray luminosity functions of Abell clusters from the Einstein cluster survey.*	ApJ, **422**, 37–45 (1994)	ADS	ESO SISSA

(the preprints database of the STScI Library to which bibliographic details are added upon publication of a preprint) allow them to check whether a paper has been published in the meantime. The ESO preprints database can be queried again in order to find other preprints of interest. Finally, the SISSA electronic preprint server in Trieste, Italy, a mirror site of the Los Alamos National Laboratory's e-print archive, can be accessed and searched for related preprints.

3. Publications of the ESO User's Community

The bibliography of publications of the ESO user's community contains papers by ESO staff members and visiting astronomers if they refer to data obtained with ESO telescopes. A query form supports searches for authors, titles, and publication years. Hyperlinks are provided to the ADS Abstract Service from where the abstract of the paper as well as related publications may be retrieved, to the ESO Libraries' preprint database in order to find titles of currently unpublished papers, and to the SISSA electronic preprint server (Fig. 2). Astronomers might find these new features especially useful when preparing observing proposals.

4. Access to Electronic Journals

As publishers are moving more and more towards electronic publishing, some of the astronomical journals will be made available in electronic form, be it exclusively or in addition to the paper version. The ESO Libraries provide access to on-line versions from the Electronic Journals WWW page at URL http://www.eso.org/libraries/electronic.html. In addition, electronic addresses of journals are included in the library catalog. From early next year onwards, URLs will not only be displayed in the WebCat, but will be active links to the corresponding site. Double clicking on the underlined address will then take users directly into the electronic journal.

Acknowledgements

Our sincere thanks go to ESO's Webmaster Michael Naumann who worked tirelessly on these enhancements in especially stressful times.

References

[1] Shobbrook, R.M. and R.R. Shobbrook: The Astronomy Thesaurus. Version 1.1. Comp. for the International Astronomical Union, Commission 5. Epping: Anglo-Australian Observatory, 1993.

Uta Grothkopf
e-mail: ugrothko@eso.org

ANNOUNCEMENTS

IN MEMORIAM

Gerhard Bachmann

24.5.1931 – 9.12.1996

With deep regret we have to inform the ESO Community of the passing of Mr. Bachmann.

Mr. Bachmann served as Head of Administration of ESO from December 1972 until May 1996.

He contributed greatly to the creation and development of an administrative and political framework for European research in Astronomy, in particular in the ESO member states.

We are deeply grateful for his work.

Dr. Peter Creola
President of the Council

Prof. Riccardo Giacconi
Director General

New ESO Preprints

September–November 1996

Scientific Preprints

1185. P.A. Mazzali et al.: The properties of the peculiar type Ia SN 1991bg. II. The amount of ^{56}Ni and the total ejecta mass determined from spectrum synthesis and energetics considerations. *M.N.R.A.S.*
1186. R.E.S. Clegg, P.J. Storey, J.R. Walsh, L. Neale: Measurement of the ^{12}C/^{13}C ratio in Planetary Nebulae. *M.N.R.A.S.*
1187. L. Achmad, H.J.G.L.M. Lamers, L. Pasquini: Radiation driven wind models for A, F and G supergiants. *AA*.
1188. P. Martin and J. Belley: Nebular gas abundances and mixing processes in the ringed galaxy NGC 4736. *AA*.
1189. M. Villar-Martín and L. Binette: Ca depletion and the presence of dust in large scale nebulosities in radio galaxies (II). *AA*.
1190. S.G. Djorgovski et al.: Dynamical correlations for globular clusters in M31. *ApJ*.
1191. D. Minniti et al.: An unusual brightening of the eclipsing binary star AKO 9 in the globular cluster 47 Tucanae observed with HST. *ApJ*. Letters.
1192. J.Th. van Loon et al.: Mass losing AGB stars in the LMC. To appear in Proc. Of IAU Symp. 177: *The Carbon Star Phenomenon*, 27–31 May 1966, Antalya (Turkey), ed. R.F. Wing, Kluwer AP.
1193. L. Masperi and S. Savaglio: Comparison of stars and decaying neutrinos as additional sources of intergalactic UV background. *AA*.
1194. G. Mathys et al.: The mean magnetic field modulus of Ap stars. *AA*.
1195. P. Fouqué and W.P. Gieren: An improved calibration of Cepheid visual and infrared brightness relations from accurate angular diameter measurements of cool giants and supergiants. *AA*.
1196. G. Meylan and D.C. Heggie: Internal dynamics of globular clusters. *AA Review*.
1197. S. Cristiani et al.: The clustering properties of the Lyman-α clouds. *M.N.R.A.S.*

Scientific Preprints

71. P. Dierickx et al.: The VLT primary mirrors: mirror production and measured performance.
72. The Early Universe with the VLT. Contributions on VLT instrumentation. To be published in the Proceedings of the ESO Workshop "The Early Universe with the VLT", ed. J. Bergeron, Springer Verlag, in press.

Personnel Movements

International Staff

(1 October – 31 December 1996)

ARRIVALS

EUROPE

BONNEAU, Jean-Michel (F), Finance Controller
DEVILLARD, Nicolas (F), Astronomical Data Reduction Specialist

GRAY, Peter (AUS), Integration Manager
MOHAMMADZADEH, Ali (N), CCD Specialist
SOKAR, Barbara (D), Draughtswoman
HOOK, Isobel (GB), Fellow
DENISE, Christophe (F), Computer Simulation Analyst
SCODEGGIO, Marco (I), Fellow
VERNET, Joël (F), Student

CHILE

MOLITON, Renaud (USA), Coopérant, La Silla
TIEFTRUNK, Achim (D), SEST Fellow

DEPARTURES

EUROPE

DE ROOS, Rinze (NL), Operation Technician
GÜNTHER, Peter (DK), Accounting Assistant
BÖHM, Torsten (D), Fellow

The ESO Director General Receives Award

The region of Puglia, Italy, conferred their award "Targhe d'Oro della Regione Puglia" to prominent Italians living in Germany.
Among the seven distinguished personalities receiving the award in 1996 is Professor Riccardo Giacconi.
The seven recipients this year are Claudio Abbado (Music), Giancarlo Biamino (Medicine), Riccardo Giacconi (Science and Technology), Salvo Ricci Mazzolini (Journalism), Bruno Sacco (Design), Giovanni Trapattoni (Sport) and Giuseppe Vita (Industry).

Written-Off Computer Equipment Available at ESO Headquarters

The following items, in good condition for further use, have recently been written off at ESO-Garching and are immediately available for scientific institutes at a small nominal fee or even free of charge, on the condition that

– a request is presented to ESO, Contracts and Procurement (Mrs. E. Kunstein-Hackbarth, Tel. 0049-89-320 06-204; Fax: 0049-89-320 73 27) until February 28, 1997;

– agreements are taken on the terms and conditions of delivery.

Assignment will be made mainly by taking into account the order of presentation of the formal request.

E. Kunstein-Hackbarth

Item No.	Description	Serial number	Order date
1	Kennedy tape drive model 9400	504-1254	1985
2	Dylon magnetic tape coupler		1985
3	HP1000 A400 computer	2850F00156	1989
4	HP disc drive model 7914	2504E02251	1985
5	HP disc drive model 7937	2920E15658	1989
6	HP disc drive model 7937	2720A05552	1987
7	Kennedy tape drive model 9400	504-1239	1985
8	Tek Xpress X-terminal (broken)		1990
9	Equinox PBX for RS 232 connections		1985
10	Solbourne model 5E/800i	P0101199	1991
11	Transtec model GDT6225	3303992	1987

MESSENGER INDEX 1995–1996 (Nos. 79–86)

SUBJECT INDEX

SL-9/Jupiter Encounter

Reports from Observers

Other Astronomical News

Announcements

AUTHOR INDEX

A

B

C

D

E

F

G

ESO, the European Southern Observatory, was created in 1962 to . . . establish and operate an astronomical observatory in the southern hemisphere, equipped with powerful instruments, with the aim of furthering and organising collaboration in astronomy . . . It is supported by eight countries: Belgium, Denmark, France, Germany, Italy, the Netherlands, Sweden and Switzerland. It operates the La Silla observatory in the Atacama desert, 600 km north of Santiago de Chile, at 2,400 m altitude, where fourteen optical telescopes with diameters up to 3.6 m and a 15-m submillimetre radio telescope (SEST) are now in operation. The 3.5-m New Technology Telescope (NTT) became operational in 1990, and a giant telescope (VLT = Very Large Telescope), consisting of four 8.2-m telescopes (equivalent aperture = 16 m) is under construction. It is being erected on Paranal, a 2,600 m high mountain in northern Chile, approximately 130 km south of Antofagasta. Eight hundred scientists make proposals each year for the use of the telescopes at La Silla. The ESO Headquarters are located in Garching, near Munich, Germany. It is the scientific, technical and administrative centre of ESO where technical development programmes are carried out to provide the La Silla observatory with the most advanced instruments. There are also extensive facilities which enable the scientists to analyse their data. In Europe ESO employs about 200 international Staff members, Fellows and Associates; at La Silla about 50 and, in addition, 150 local Staff members.

The ESO MESSENGER is published four times a year: normally in March, June, September and December. ESO also publishes Conference Proceedings Preprints, Technical Notes and other material connected to its activities. Press Releases inform the media about particular events. For further information, contact the ESO Information Service at the following address:

EUROPEAN
SOUTHERN OBSERVATORY
Karl-Schwarzschild-Str. 2
D-85748 Garching bei München
Germany
Tel. (089) 320 06-0
Telex 5-28282-0 eo d
Telefax (089) 3202362
ips@eso.org (internet)
ESO::IPS (decnet)

The ESO Messenger:
Editor: Marie-Hélène Demoulin
Technical editor: Kurt Kjär

Printed by
Druckbetriebe Lettner KG
Georgenstr. 84
D-80799 München
Germany

ISSN 0722-6691

Contents